# Transient merging of two Rhine flow regimes from climate change

Erwin Rottler

Cumulative dissertation

submitted for obtaining the degree
"Doctor of Natural Sciences" (Dr. rer. nat.)
in the research discipline Geoecology

Institute of Environmental Science and Geography
Faculty of Science
University of Potsdam

March 2021

First supervisor:
Prof. Dr. Axel Bronstert

Second supervisor:
Dr. Gerd Bürger

Mentor:
Dr. Theresa Blume

First reviewer:
Prof. Dr. Axel Bronstert

Second reviewer:
Prof. Dr. Gerd Bürger

Independent reviewer:
Prof. Dr. Kerstin Stahl

Examination board members:
Prof. Dr. Axel Bronstert
Dr. Gerd Bürger
Prof. Dr. Kerstin Stahl
Prof. Dr. Oliver Korup
Prof. Dr. Jens Tronicke
Prof. Dr. Bruno Merz

Published online on the
Publication Server of the University of Potsdam:
https://doi.org/10.25932/publishup-51766
https://nbn-resolving.org/urn:nbn:de:kobv:517-opus4-517665

# Declaration of originality

I, Erwin Rottler, hereby declare that, to the best of my knowledge, this work does not bear resemblance to any other work in whole or in part and has been completed by myself. I did not use any other sources and means than specified. Furthermore, this work has not been previously submitted to any university. All sources have been referred to and this work gives adequate credit to others for their work. I, in no way, claim to have created this information myself.

| | |
|---|---|
| Location and Date | Erwin Rottler |

# Summary

River flooding poses a threat to numerous cities and communities all over the world. The detection, quantification and attribution of changes in flood characteristics is key to assess changes in flood hazard and help affected societies to timely mitigate and adapt to emerging risks. The Rhine River is one of the major European rivers and numerous large cities reside at its shores. Runoff from several large tributaries superimposes in the main channel shaping the complex from regime. Rainfall, snowmelt as well as ice-melt are important runoff components. The main objective of this thesis is the investigation of a possible transient merging of nival and pluvial Rhine flood regimes under global warming. Rising temperatures cause snowmelt to occur earlier in the year and rainfall to be more intense. The superposition of snowmelt-induced floods originating from the Alps with more intense rainfall-induced runoff from pluvial-type tributaries might create a new flood type with potentially disastrous consequences.

To introduce the topic of changing hydrological flow regimes, an interactive web application that enables the investigation of runoff timing and runoff seasonality observed at river gauges all over the world is presented. The exploration and comparison of a great diversity of river gauges in the Rhine River Basin and beyond indicates that river systems around the world undergo fundamental changes. In hazard and risk research, the provision of background as well as real-time information to residents and decision-makers in an easy accessible way is of great importance. Future studies need to further harness the potential of scientifically engineered online tools to improve the communication of information related to hazards and risks.

A next step is the development of a cascading sequence of analytical tools to investigate long-term changes in hydro-climatic time series. The combination of quantile sampling with moving average trend statistics and empirical mode decomposition allows for the extraction of high resolution signals and the identification of mechanisms driving changes in river runoff. Results point out that the construction and operation of large reservoirs in the Alps is an important factor redistributing runoff from summer to winter and hint at more (intense)

rainfall in recent decades, particularly during winter, in turn increasing high runoff quantiles. The development and application of the analytical sequence represents a further step in the scientific quest to disentangling natural variability, climate change signals and direct human impacts.

The in-depth analysis of in situ snow measurements and the simulations of the Alpine snow cover using a physically-based snow model enable the quantification of changes in snowmelt in the sub-basin upstream gauge Basel. Results confirm previous investigations indicating that rising temperatures result in a decrease in maximum melt rates. Extending these findings to a catchment perspective, a threefold effect of rising temperatures can be identified: snowmelt becomes weaker, occurs earlier and forms at higher elevations. Furthermore, results indicate that due to the wide range of elevations in the basin, snowmelt does not occur simultaneously at all elevation, but elevation bands melt together in blocks. The beginning and end of the release of meltwater seem to be determined by the passage of warm air masses, and the respective elevation range affected by accompanying temperatures and snow availability. Following those findings, a hypothesis describing elevation-dependent compensation effects in snowmelt is introduced: In a warmer world with similar sequences of weather conditions, snowmelt is moved upward to higher elevations, i.e., the block of elevation bands providing most water to the snowmelt-induced runoff is located at higher elevations. The movement upward the elevation range makes snowmelt in individual elevation bands occur earlier. The timing of the snowmelt-induced runoff, however, stays the same. Meltwater from higher elevations, at least partly, replaces meltwater from elevations below.

The insights on past and present changes in river runoff, snow covers and underlying mechanisms form the basis of investigations of potential future changes in Rhine River runoff. The mesoscale Hydrological Model (mHM) forced with an ensemble of climate projection scenarios is used to analyse future changes in streamflow, snowmelt, precipitation and evapotranspiration at 1.5, 2.0 and 3.0 °C global warming. Simulation results suggest that future changes in flood characteristics in the Rhine River Basin are controlled by increased precipitation amounts on the one hand, and reduced snowmelt on the other hand. Rising temperatures deplete seasonal snowpacks. At no time during the year, a warming climate results in an increase in the risk of snowmelt-driven flooding. Counterbalancing effects between snowmelt and precipitation often result in only little and transient changes in streamflow peaks. Although, investigations point at changes in both rainfall and snowmelt-driven runoff, there are no indications of a transient merging of nival and pluvial Rhine flood regimes due to climate warming. Flooding in the main tributaries of the Rhine, such as the Moselle River, as well as the High Rhine is controlled by both precipitation and snowmelt.

Caution has to be exercised labelling sub-basins such as the Moselle catchment as purely pluvial-type or the Rhine River Basin at Basel as purely nival-type. Results indicate that this (over-) simplifications can entail misleading assumptions with regard to flood-generating mechanisms and changes in flood hazard. In the framework of this thesis, some progress has been made in detecting, quantifying and attributing past, present and future changes in Rhine flow/flood characteristics. However, further studies are necessary to pin down future changes in the flood genesis of Rhine floods, particularly very rare events.

# Kurzfassung

Überflutungen durch Flusshochwasser stellen für zahlreiche Städte und Gemeinden auf der ganzen Welt eine große Gefahr dar. Die Detektion, Quantifizierung und Attribuierung sich verändernder Hochwassereigenschaften ist wichtig, um Änderungen in der Gefahrenlage zu bewerten und Anrainerstaaten die Möglichkeit zur Abschwächung und Anpassung an das Hochwasserrisiko zu geben. Der Rhein ist einer der großen Flüsse Europas und zahlreiche Städte liegen an seinen Ufern. Sich überlagernde Abflüsse aus den großen Zuflüssen prägen das komplexe Abflussregime des Rheins. Sowohl Regen, Schneeschmelze als auch Eisschmelze sind wichtige Abflusskomponenten. Vorrangiges Ziel dieser Arbeit ist die Untersuchung der Möglichkeit einer durch den Klimawandel verursachten vorübergehenden Überlagerung von nivalen und pluvial Hochwasserereignissen im Rheingebiet. Steigende Temperaturen können zu einer früheren Schneeschmelze und intensivieren Niederschlägen führen. Die Überlagerung von durch Schneeschmelze angetriebenen Spitzenabflüssen aus den Alpen mit intensiveren Hochwasserereignissen aus den pluvialen Zuflüssen, könnte zur Bildung eines neuen Hochwassertyps mit möglicherweise katastrophalen Folgen führen.

Eine interaktive Web-Anwendung, die es ermöglicht, Zeitpunkt und Saisonalität von Abfluss auf der ganzen Welt zu untersuchen, führt in die Thematik sich verändernder hydrologischer Abflussregime ein. Die Untersuchungen und der Vergleich von unterschiedlichsten Abflusspegeln im Rheingebiet und darüber hinaus weißen darauf hin, dass sich Flusssysteme auf der ganzen Welt im Wandel befinden. In der Gefahren- und Risikoforschung ist die Bereitstellung von Hintergrundinformationen und Informationen zu aktuellen Entwicklungen für Anwohner und Entscheidungsträger auf leicht zugängliche Weise von großer Bedeutung. Zukünftige Studien sollten sich das Potential wissenschaftlicher Web-Anwendungen, um die Kommunikation in Bezug auf Naturgefahren und -risiken zu verbessern, verstärkt zu Nutze machen.

Nächster Schritt ist die Entwicklung einer kaskadierenden Sequenz analytischer Methoden, um langfristige Änderungen in hydro-klimatoligischen Zeitrei-

hen zu detektieren. Eine Kombination aus Quantil-Berechnungen, Statistiken basierend auf gleitenden Mittelwerten und empirischer Bandzerlegung ermöglicht die Extraktion hochaufgelöster Signale und die Identifizierungen zu Grunde liegender Antriebsmechanismen. Die Ergebnisse der Analysen zeigen, dass der Bau und Betrieb von großen Stauseen zur Gewinnung von Wasserkraft zu einer Umverteilung von Wasser vom Sommer in den Winter führt. Zudem weisen die Ergebnisse auf (mehr) intensivere Niederschläge hin, die wiederum hohe Abflussquantile intensivieren. Die Entwicklung und Anwendung der analytischen Sequenz stellt einen weiteren Schritt in dem wissenschaftlichen Bestreben, natürliche Klimavariabilität, Signale des Klimawandels und direkte anthropogene Einflüsse zu entwirren, dar.

Die detaillierte Untersuchung von Schneemessungen und die Simulation der alpinen Schneedecke mittels physikalisch-basiertem Schneemodell, ermöglicht die Quantifizierung von Änderungen in der Schneeschmelze im Rheingebiet oberhalb von Basel. Steigenden Temperaturen verringern nicht nur hohe Schmelzraten, ein Dreifach-Effekt kann identifiziert werden: Schneeschmelze wird schwächer, findet früher statt und formiert sich in höhere Lagen. Auf Grund der großen Höhenunterschiede im Gebiet, findet die Schneeschmelze nicht gleichzeitig in allen Höhenlagen statt. Simulationen weisen darauf hin, dass Höhenbänder zusammen in Blöcken schmelzen. Der Beginn und das Ende eines Schmelzereignisses scheint durch vorbeiziehende warme Luftmassen und die betroffenen Höhenlagen durch zugehörige Temperaturen und die Schneeverfügbarkeit bestimmt zu werden. Basieren auf diesen Erkenntnissen, wird eine Hypothese, die höhenabhängige Kompensationseffekte in der Schneeschmelze beschreibt, vorgestellt: In einem wärmeren Klima mit einer gleichbleibenden Abfolge von Witterungsbedingungen, findet die Schneeschmelze in höheren Lagen statt, d.h., der Block an Höhenbändern, der den Hauptbestandteil des Schmelzwassers freigibt, ist nach oben verschoben. Die Verschiebung in höhere Lagen führt dazu, dass die Schneeschmelze in einzelnen Höhenbändern früher kommt, der Zeitpunkt des Schmelzereignisses jedoch unverändert bleibt. Schmelzwasser aus höheren Lagen ersetzt, zumindest teilweise, Schmelzwasser aus tieferen Lagen.

Die Erkenntnisse über historische und gegenwärtige Änderungen im Abfluss, der Schneedecke und zu Grunde liegenden Mechanismen bilden die Grundlage der Untersuchungen möglicher zukünftiger Änderungen im Abfluss des Rheins. Das für die Mesoskala entwickelte hydrologisiche Modell mHM wird mit einem Ensemble aus Klimaszenarien angetrieben und projizierte Änderungen im Abfluss, der Schneeschmelze, im Niederschlag und der Evapotranspiration bei 1.5, 2.0 und 3.0 °C Erwärmung untersucht. Ergebnisse der hydrologischen Simulationen zeigen, dass künftige Änderungen der Hochwassereigenschaften im Rheingebiet durch zunehmenden Niederschlagsmengen und abnehmende Schneeschmelze

bestimmt werden. Steigende Temperaturen verringern saisonale Schneedecken. Zu keinem Zeitpunkt im Jahr führen höhere Temperaturen zu einer Zunahme des Hochwasserrisikos durch die Schneeschmelze. Kompensationseffekte zwischen Schneeschmelze und Niederschlag resultieren oftmals in geringe und nur vorübergehende Erhöhungen von Spitzenabflüssen.

Obwohl Untersuchungen auf Veränderungen sowohl in der Schneeschmelze als auch im Niederschlag hinweisen, finden sich keine Hinweise auf eine durch den Klimawandel verursachte vorübergehende Überlagerung von nivalen und pluvialen Hochwasserregimen im Rheingebiet. Hochwasserereignisse in den Hauptzuflüssen, wie zu Beispiel der Mosel, und dem Hochrhein werden sowohl durch Niederschläge als auch Schneeschmelze kontrolliert. Vorsicht muss geübt werden, wenn Teilgebiete, wie das Einzugsgebiet der Mosel als rein pluvial oder das Rheingebiet oberhalb von Basel als rein nival gesehen werden. Die Ergebnisse zeigen, dass diese (zu starke) Vereinfachung zu irreführenden Annahmen bezüglich möglicher Änderungen von Hochwasser verursachender Mechanismen und Hochwassergefahr führen können. Diese Doktorarbeit ist ein Schritt vorwärts im wissenschaftlichen Streben die Detektion, Quantifizierung und Attribuierung vergangener und zukünftiger Veränderungen in den Abfluss- und Hochwasserregimen des Rheins zu verbessern. Weitere Untersuchungen sind nötig, um zukünftige Veränderungen in der Hochwassergenese sehr seltener Hochwasserereignisse einzuschätzen.

# Acknowledgements

I thank my supervisors and colleagues for their support. Whatever challenge there was, I was able count on their backing, encouragement and guidance. The completion of this thesis only was possible through the continuous support of colleagues from the chair of hydrology and climatology, University of Potsdam and the research training group NatRiskChange. Furthermore, I want to thank colleagues from the University of Innsbruck, who accommodated me during my research stay and took me to field trips in the Alps. I also want to thank colleagues from the Department of Computational Hydrosystems, UFZ Leipzig for their patience and support with regard to the simulations with mHM. None of the work would have been possible without the backing from my family and friends. Thank you!

# Contents

# List of Figures

# List of Tables

# List of frequently used abbreviations

| | |
|---|---|
| **AMO** | Atlantic Multidecadal Oscillation |
| **aTS** | Adaptive Time Step Scheme |
| **CEEMDAN** | Complete Ensemble Empirical Mode Decomposition with Additive Noise |
| **D** | Discharge |
| **DDS** | Dynamically Dimensioned Search algorithm |
| **DOY** | Day of the Year |
| **ECHSE** | Eco-Hydrological Simulation Environment |
| **EDK** | External Drift Kriging |
| **E-OBS** | Daily gridded Observational Data sets in Europe |
| **EMD** | Empirical Model Decomposition |
| **EEMD** | Ensemble Empirical Model Decomposition |
| **ET** | Evapotranspiration |
| $ET_{loss}$ | Estimated evapotranspiration loss |
| $ET_{max10}$ | 10-day evapotranspiration maxima |
| **GCM** | Global Climate Model |
| **GRDC** | Global Runoff Data Centre |
| **IMF** | Intrinsic Mode Functions |
| **ISI-MIP** | The Inter-Sectoral Impact Model Intercomparison Project |
| **IQR** | Interquantile range |
| **KGE** | Kling-Gupta-Efficiency |
| **LAI** | Leaf Area Index |
| **MeteoSwiss** | Federal Office of Meteorology and Climatology of Switzerland |
| **mHM** | Mesoscale Hydrologic Model |
| **MK** | Mann-Kendall trend test |
| **M-max14** | Magnitude 14-day snowmelt maximum of elevation band |
| **M-max14** | Magnitude 14-day snowmelt maximum on catchment scale |
| **MPR** | Multiscale Parameter Regionalization |
| **mRM** | Multiscale Routing Model |
| **MODIS** | Moderate Resolution Imaging Spectroradiometer |
| **MQ** | Mean Runoff |

| | |
|---|---|
| **NAO** | North Atlantic Oscillation |
| **NRMSE** | Normalised Root Mean Square Error |
| **NSE** | Nash-Sutcliffe Efficiency |
| **P** | Precipitation |
| **PBIAS** | Percentage Bias |
| $P_{max5}$ | 5-day precipitation maxima |
| **PSO** | Partilce Swarm Optimization |
| $P_{solid}$ | Solid fraction of precipitation |
| **R** | Radiation |
| **RCP** | Representative Concentration Pathway |
| **RoS** | Rain on Snow |
| **RQ** | Research question |
| **SD** | Snow Depth |
| $S_{elev}$ | Average elevation of snowmelt |
| $S_{frac}$ | Estimated contribution of snowmelt to streamflow |
| **SLF** | Institute for Snow and Avalanche Research |
| $S_{max10}$ | 10-day snowmelt maxima |
| **SWE** | Snow Water Equivalent |
| **T** | Temperature |
| **T-max14** | Timing 14-day snowmelt maximum of elevation band |
| **T-max14** | Timing 14-day snowmelt maximum on catchment scale |
| **TST** | Theil-Sen trend estimator |
| **WSL** | Swiss Federal Institute for Forest, Snow and Landscape Research |
| **QDAY** | Quantiles on a daily basis |
| **QMOV** | Quantiles from and within a 30 day moving window |
| **QYEA** | Quantiles estimated on annual level |

# 1 Introduction

## 1.1 Motivation

### 1.1.1 Natural hazards and risks

Natural disasters are a constant threat to communities around the world. On a regular basis, climate-related or geophysical disasters cause enormous economic losses and injure, displace and even kill people (CRED & UNISDR, 2018). Commonly, natural disasters are classified according to the underlying type of hazard, whereby a natural hazard is defined as "an unexpected and/or uncontrollable natural event of unusual magnitude that might threaten people" (Bokwa, 2013). The compilation of data on the occurrence and impact of natural disasters usually goes along with the distinction of hydrological (e.g., floods or wave action), meteorological (e.g., storms or extreme precipitation) and geophysical (e.g., earthquakes or vulcanic activity) disasters (CRED & UNISDR, 2018). One crucial aspect with regard to loss prevention, is the correct assessment of the risk posed by natural hazards. Risk is "the possibility of suffering harm from a hazard" (Eastman et al., 1997) and is defined as a function of hazard probability, the exposed values and their vulnerability (e.g., Crichton, 1999; Peduzzi et al., 2001; Schneiderbauer and Ehrlich, 2004), whereby the components of the risk equation are not static, but can change over time. For example, climatic changes have the potential to alter the frequency and intensity of the hazard, the expansion of settlements can increase the number of exposed values and the installation of protective constructions can lower the vulnerability. Taking the transient nature of the risk components into account, the risk is then calculated by integrating over the range of relevant hazard levels (h):

$$Risk(t) = \int Hazard(h,t) \cdot Exposure(h,t) \cdot Vulnerability(h,t)\ \mathrm{d}h. \tag{1.1}$$

This equations is widely accepted and used in hazard and risk research (e.g.,

Schneiderbauer and Ehrlich, 2004; Kron, 2005; Merz et al., 2010). It underlines the fact, that changes in risk can be due to changes in various factors ranging from changes in hazard intensity to the capacity of communities to recover from a crisis (Schneiderbauer and Ehrlich, 2004; UNDRR, 2019). Hazard and risk research aims at a better understanding of all three risk components. Recent advances in risk research include the development of probabilistic and fully scalable damage models (Sieg et al., 2019; Schoppa et al., 2020), the compilation of consistent event inventories (Veh et al., 2018, 2019), the advancements of radar-based precipitation nowcasting (Ayzel et al., 2019, 2020; Costa Tomaz de Souza et al., 2020), the reliable estimation of the distribution of extreme precipitation (Ulrich et al., 2020), the application of novel measures to understand complex systems (Wendi et al., 2019), the usage of complex networks to track extreme rainfall (Ozturk et al., 2018), the assessment of flood synchrony on the continental scale (Kemter et al., 2020), the usage of hydrological models to assess projected changes in floods, droughts and water availability (Didovets et al., 2019; Mtilatila et al., 2020) and the investigation of the dynamics of human behaviour in response to flooding (Bubeck et al., 2020).

### 1.1.2 Riverine flooding

The analysis conducted in the framework of this doctoral thesis addresses changes in the hazard component of the risk equation. The focus is on changes in timing and magnitudes of floods of complex river systems. River floods are among the most frequent and costly types of natural disasters (UNDRR, 2019). In recent decades, several large floods occurred in Europe. In August 2002, record breaking rainfall amounts and intensities caused the Elbe River to burst its banks and damage the historical cities of Prague and Dresden (Ulbrich et al., 2003; Kreibich et al., 2005; Kundzewicz et al., 2005). In Germany, direct losses amounted to more than 9 billion EUR (Mechler and Weichselgartner, 2003; Kreibich et al., 2005). Only a few years later, in June 2013, high antecedent moisture and an atmospheric blocking situation triggered widespread flooding in central Europe, particularly in the Elbe and the Upper Danube Basins (Blöschl et al., 2013; Thieken et al., 2016). In January 1995, saturated soils and centennial rainfall events triggered several flood surges in the Moselle River, which where one of the main drivers of the extreme flooding in the Lower Rhine, particularly in the city of Cologne (Ulbrich and Fink, 1995). Cologne, together with other cities along the Rhine, such as Koblenz or Bonn, had been flooded only less than two years earlier during Christmas 1993 (Fink et al., 1996; Kundzewicz et al., 2013).

Presented examples of flood disasters demonstrate that the understanding of mechanisms generating floods is crucial to assess flood risk and protect cities and communities along the river banks. One key challenge in flood hazard research is

the detection, quantification and attribution of historic and future changes in flood regimes. Recent studies investigating river runoff in Switzerland (Horton et al., 2006; Addor et al., 2014; Brunner et al., 2019b; Muelchi et al., 2020), the United States (Lins and Slack, 1999; Villarini and Smith, 2010; Brunner et al., 2020a), and Norway (Vormoor et al., 2015, 2016) all indicate that changes in flow/flood regimes are ongoing and will continue to change in the future. Studies for Europe point at the importance of a profound understanding of spatial patterns of flood seasonality characteristics and underlying flood-driving mechanisms (Hall and Blöschl, 2018; Berghuijs et al., 2019). The analysis of peak discharges recorded in Europe between 1960–2010 inter alia hint at changes in the timing (Blöschl et al., 2017), magnitude (Blöschl et al., 2019) and the spatial extent (Kemter et al., 2020) of floods. Climatic changes are expected to further alter peak flow characteristics in Europe (e.g., Alfieri et al., 2015; Thober et al., 2018).

### 1.1.3 The Rhine River Basin

The Rhine River is an important waterway in Europe and numerous large cities (e.g., Basel or Cologne) reside at its shores (Fig. 1.1 b). It's basin spans across numerous country boarders and landscapes. In the South, the Rhine River Basin encompasses parts of the European Alps and snowmelt and ice-melt are important runoff contributors (Stahl et al., 2016). Catchments dominated by the build-up and melt of seasonal snow covers commonly are classified as nival. Nival runoff regimes are characterised by low discharge during winter when precipitation is solid and accumulated in temporary snow packs and by high runoff values during snowmelt season. The fact that the Rhine Basin upstream gauge Basel represents approximately 20 % of the catchment area of the Rhine River, but delivers nearly half of its discharge, points at the importance of the Alps as "water tower" (Viviroli et al., 2007). On its way downstream to the delta region and the North Sea, the Rhine River receives water from numerous tributaries draining low mountain ranges and low land areas. Major tributaries, such as the Main River or the Moselle River, often are referred to as pluvial-type rivers. A pluvial flow regime is dominated by rainfall-driven runoff and discharge is high during winter and low during summer. In the main channel of the Rhine River, pluvial and nival waters from the different sub-basins superimpose and create a complex flow regime. Climatic changes are expected to alter runoff characteristic of both pluvial and nival flow regimes in the Rhine River Basin (e.g., Middelkoop et al., 2001; Pfister et al., 2004; Menzel et al., 2006; Bosshard et al., 2014; Kundzewicz et al., 2018). Due to the inestimable socio-economic value of the Rhine River, a comprehensive understanding of future nival and pluvial flow/flood characteristics is of great importance.

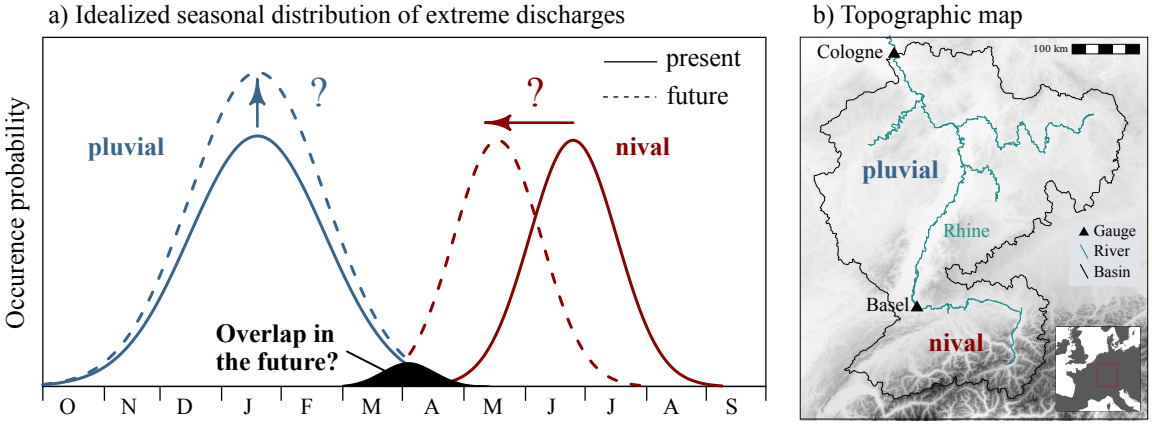


***Figure 1.1:*** *Transient merging of Rhine flow regimes under climate change.*

### 1.1.4 Detection and quantification of runoff changes

Numerous studies have been conducted to detect and quantify changes in river runoff. Based on the underlying data type, two groups of investigations can be distinguished: 1) studies based on observational data and 2) analyses using hydrological model simulations. When investigating discharge recordings, major benefits in attributing changes can be gained by performing a multi-variable analysis and including additional information on temperature, snowmelt or precipitation (Kormann et al., 2015; Vormoor et al., 2016; Skålevåg and Vormoor, 2021). Information on additional variables also is the key to determine and distinguish flood generating processes (Berghuijs et al., 2019). Studies investigating changes in flood characteristics often analyse the timing and magnitude of annual streamflow maxima (e.g., Blöschl et al., 2017, 2019; Kemter et al., 2020) or runoff peaks above a certain threshold (peak-over-threshold method) (e.g., Petrow and Merz, 2009; Bačová-Mitková and Onderka, 2010; Vormoor et al., 2016). However, studies based on observational data often are limited by the spatial and temporal coverage of the data. A sufficient length of a time series is necessary to perform a meaningful trend analysis. A high density of observational stations is crucial, inter alia, to address spatial variability. Furthermore, observational data needs to undergo thorough quality checks and the application of homogenisation techniques is required to ensure that no non-climatic features affect the recordings (Moberg et al., 2006; Li-Juan and Zhong-Wei, 2012). In addition, the installation and maintenance of ground observation networks often is costly and labour-intensive, particularly at remote locations.

In order to address limited data availability and to gain additional insights into hydrological systems, hydrological models can be used to simulate river runoff. Hydrological simulations foster hydrological process understanding and help to

close existing knowledge gaps. Numerous different hydrological models were developed over the last decades and are in use today. Hydrological models can be classified using different criteria. Taking a look at the level of physical principles implemented, physically-based (white box), conceptual (grey box) and empirical (black box) models can be distinguished. Hydrological models can be used to simulate specific events (event-based) or in a continuous manner. Parameters can be either spatially distributed or lumped (Jajarmizadeh et al., 2012; Devia et al., 2015). One key advantage using hydrological models is the ability to investigate both historic and future hydrological conditions. Scenario-based simulations provide vital information on impacts of climatic changes on the hydrological cycle (e.g., Alfieri et al., 2015; Vormoor et al., 2015; Thober et al., 2018; Di Sante et al., 2021). Ideally, multiple climate and hydrological models are used within a multi-ensemble modelling chain (e.g., Samaniego et al., 2019).

## 1.2 Objectives and structure

The overarching aim of this thesis, as stated in the title, is the investigation of a possible transient merging of Rhine flow/flood regimes under global warming (Fig. 1.1 and 1.2). In the present climate, nival floods are seasonally separated from rainfall-triggered floods, and the risk of nival and pluvial types occurring together is negligible. However, continued global warming might cause snowmelt to occur earlier in the year and rainfall to be more intense. The superposition of snowmelt-induced floods originating from the Alps with (more intense) rainfall-induced runoff from pluvial-type tributaries might create a new flood type with potentially disastrous consequences. In view of this overarching aim, five specific research questions (RQs) are formulated:

1. What are the main drivers of changes in runoff timing and seasonality?
2. Which analytical and visualisation techniques are suitable to detect and present changes in river runoff?
3. How do higher temperatures affect snowmelt event characteristics?
4. Do precipitation events intensify?
5. What factors control future changes in Rhine River flood seasonality?

Four studies have been conducted to tackle these questions (Fig. 1.3). To detect, quantify and present changes in hydrological flow regimes, an interactive

web app that enables the investigation of runoff timing and runoff seasonality observed at river gauges all over the world is developed and presented (Chapter 2). A cascading sequence of analytical tools to extract high resolution signals of long-term changes in hydro-climatological data forms the basis of investigations presented in Chapter 3. Detailed insights into changes in seasonal snow covers due to rising temperatures are obtained simulating Alpine snow packs (Chapter 4). Future changes in flood characteristics in the Rhine River are investigated forcing a hydrological model with an ensemble of climate projection scenarios (Chapter 5).

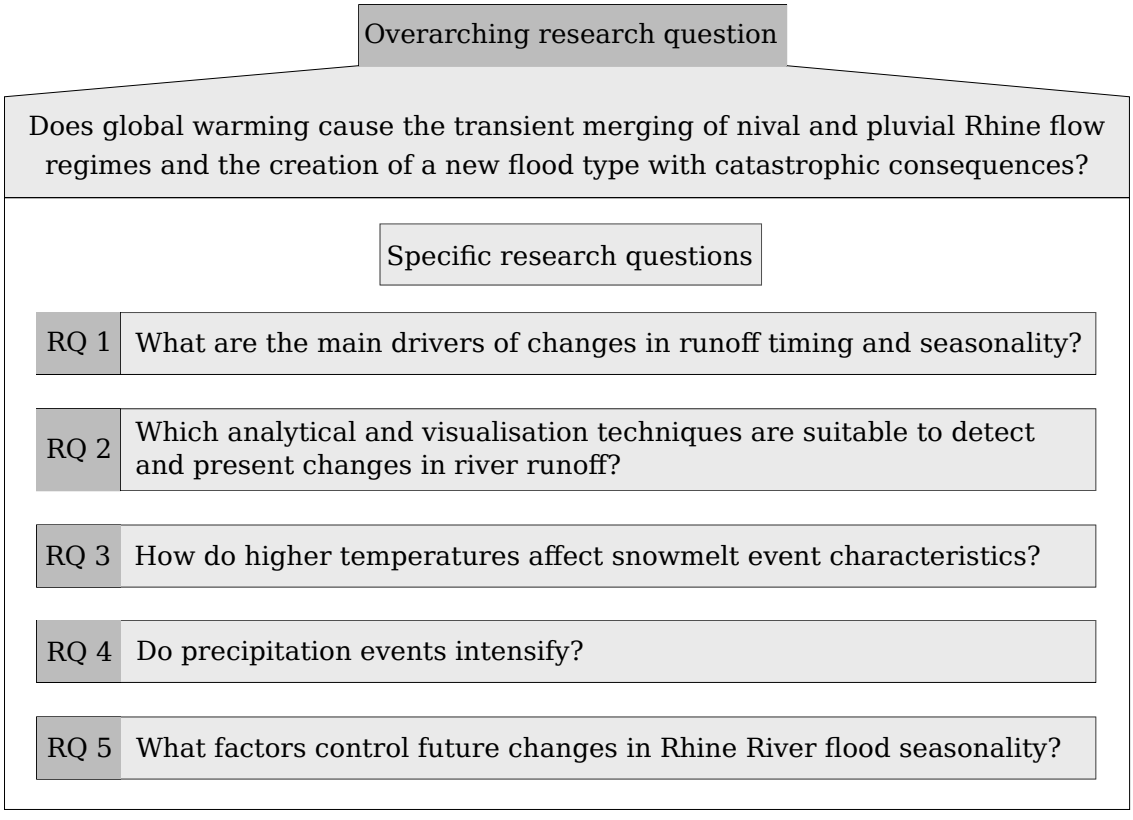


***Figure 1.2:*** *Overview on overarching and specific research questions.*

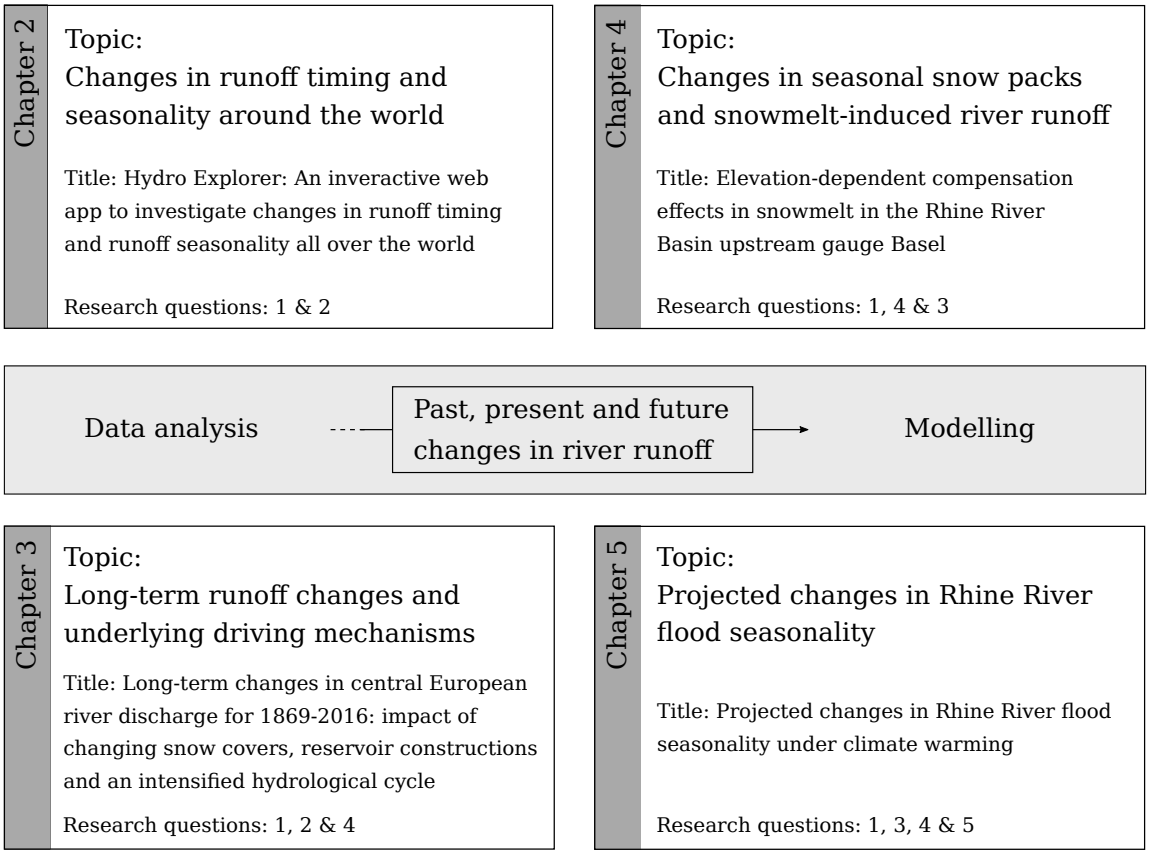


***Figure 1.3:*** *Scheme of the structure of the main part of the doctoral thesis.*

### 1.2.1 Changes in runoff timing and seasonality around the world

Discharge of many rivers, including the Rhine River, is measured at a large number of gauging stations. However, it still remains rather difficult to access the data and to quantify possible changes. As important as the detection of changes, is the presentation of results in an easy accessible way for parties in- and outside the scientific community. The main objective of investigations presented in chapter 2 is the development of an interactive web application that enables the investigation of discharge time series with regard to changes in runoff timing and runoff seasonality in the Rhine River Basin and beyond. The aim is to provide an interactive application that can be used to explore, learn, teach, and communicate changes in river runoff, ensure easy accessibility and re-usability, allow for testing of parameter sensitivity, and enable a straightforward comparison between analytical tools, river gauges, regions, and time frames.

### 1.2.2 Long-term runoff changes and underlying driving mechanisms

The next step is the development of a cascading sequence of analytical tools to investigate long-term changes in daily resolution hydro-climatic time series. The combination of quantile sampling with moving average trend statistics and empirical mode decomposition allows for the extraction of high resolution signals and the identification of mechanisms driving changes in river runoff. The sequence of analytical tools is applied to discharge data recorded along rivers with nival, pluvial and mixed flow regimes as well as temperature and precipitation covering the time frame 1869–2016. The main objective of investigations presented in chapter 3 is the assessment of the long-term impact of changes in snow cover, changes in precipitation and anthropogenic modifications of the river network on river runoff.

### 1.2.3 Changes in seasonal snow packs and snowmelt-induced river runoff

Changes in seasonal snow packs due to rising temperatures represent a key aspect of the hypothesis of a transient merging of nival and pluvial flow regimes in the Rhine River Basin. Hence, detailed investigations of changes in Alpine snow packs are requisite to address this open research question. The analysis of in situ snow measurements and snow simulations using a physically-based snow model provide additional insights into changes in seasonal snow covers. The main objectives of analysis presented in chapter 4 is the quantification of changes in timing, magnitude and elevation of snowmelt in the sub-basin upstream gauge Basel and a better understanding on how changes in snowmelt translate into changes in river runoff.

### 1.2.4 Projected changes in Rhine River flood seasonality

The insights on past and present changes in river runoff, snow covers and underlying mechanisms acquired in previous chapters form the basis of investigations of potential future changes in Rhine River runoff. The mesoscale Hydrological Model (mHM) forced with an ensemble of climate projection scenarios is used to analyse future changes in streamflow, snowmelt, precipitation and evapotranspiration at 1.5, 2.0 and 3.0 °C warming. The main objective in chapter 5 is the investigation future conditions of nival, pluvial and mixed hydrological regimes in Rhine River Basin.

## 1.3 Author contribution

The main part of this thesis consists of four research articles, which have been published, or are submitted and are intended to be published in international peer-reviewed journals. The manuscript layouts have been adjusted to the formatting of this thesis, yet main text and figures remain as published/submitted, except for the summarising key points, which where adjusted in the framework of this thesis. Specific author contributions of the four articles are as follows:

**Chapter 2**: ER and AB designed the study. ER wrote the software code and set up the Shiny server. Under the lead of ER, all authors contributed to the development of the analytical tools and the user interface of the web app. ER wrote the original draft of the paper with input from all co-authors. With the support of KV, ER revised the manuscript during peer-review.

**Chapter 3**: ER developed the cascading sequence of analytical tools, conducted the analysis and wrote the manuscript. TF, GB and AB provided guidance in the process of data analysis and preparation of the original draft of the manuscript. With the assistance of all co-authors, ER revised the manuscript during peer-review.

**Chapter 4**: ER, KV and AB designed the study. ER conducted the snow simulations and the data analysis. All authors interpreted and discussed the results. ER wrote the original draft of the manuscript with input from all co-authors. With support from all co-authors, ER revised the manuscript during peer-review.

**Chapter 5**: AB and GB drafted the hypothesis of a transient merging of Rhine flow regimes. AB, GB and ER designed the study. ER conducted the hydrological simulations and analysed model results. All co-authors provided guidance during model set-up, model simulations and the analysis of simulation results. All authors interpreted and discussed results. With input from all co-authors, ER wrote the original draft of the manuscript and revised the manuscript during peer-review.

In addition to the above mentioned manuscripts, the author also participated in the following publications, which are not included in the thesis:

**Erwin Rottler**, Christoph Kormann, Till Francke and Axel Bronstert: Elevation-dependent warming in the Swiss Alps 1981–2017: Features, forcings and feedbacks. *International Journal of Climatology*, 39: 2556– 2568. `https://doi.org/10.1002/joc.5970`, 2019.

Kristin Vogel, Tobias Sieg, Bernhard Fiedler, Tomas Moran, Madlen Peter, **Erwin Rottler**, Georg Veh and Axel Bronstert: Natural Hazards in transition. *Earths's Future. submitted*.

# 2 | Hydro Explorer: An interactive web app to investigate changes in runoff timing and runoff seasonality all over the world

Published as: Erwin Rottler, Klaus Vormoor, Till Francke and Axel Bronstert: Hydro Explorer: An interactive web app to investigate changes in runoff timing and runoff seasonality all over the world. *River Research and Applications*, 1-11, https://doi.org/10.1002/rra.3772, 2021.

**Key points:**

- Historic changes in runoff seasonality and runoff timing
- Development of the interactive web app *Hydro Explorer*
- Investigation of >7000 discharge time series
- Quick comparison of gauges, regions, methods and time frames

## Abstract

Climatic changes and anthropogenic modifications of the river basin or river network have the potential to fundamentally alter river runoff. In the framework of this study, we aim to analyse and present historic changes in runoff timing and runoff seasonality observed at river gauges all over the world. In this regard, we develop the *Hydro Explorer*, an interactive web app, which enables the investigation of >7000 daily resolution discharge time series from the Global Runoff Data Centre (GRDC). The interactive nature of the developed web app allows for a quick comparison of gauges, regions, methods, and time frames. We

illustrate the available analytical tools by investigating changes in runoff timing and runoff seasonality in the Rhine River Basin. Since we provide the source code of the application, existing analytical approaches can be modified, new methods added, and the tool framework can be re-used to visualise other data sets.

## 2.1 Introduction

Rivers are important lifelines nourishing communities along their shores. Their waters inter alia are used for drinking, irrigation, energy production, industry and transportation. Any change in the total amount or seasonal distribution of water potentially has serious consequences. Human livelihood often is directly linked to the water level. Hence, it is crucial to detect changes in river runoff and identify underlying driving mechanisms. Discharge is measured at a large number of gauging stations all over the world. However, it often remains rather difficult to access the data and to quantify possible changes. In addition, as important as the detection of changes, is the presentation of results in an easily accessible way for parties in- and outside the scientific community. This is particularly difficult for larger data sets covering multiple river basins on different continents.

In recent years, the potential of interactive web tools to share information is increasingly recognised and used by the scientific community. Scientifically engineered online tools support a very broad spectrum of objectives including data distribution (Moghadas et al., 2019), the analysis of data (McMurdie and Holmes, 2014; Brendel et al., 2019), drought monitoring (Zink et al., 2016), teaching statistics (Doi et al., 2016), data mining (Dunning et al., 2017) or the evaluation and selection of climate model ensembles (Parding et al., 2020). Often, the open-source programming language R and the R package 'Shiny' are used to develop interactive web content. R fosters open and reproducible science and software is ideally suited to be re-used, customised and refined (Slater et al., 2019).

In this perspective, the main object of this study is the development of the *Hydro Explorer*, an interactive Shiny web application that enables the investigation of runoff time series from all over the world in terms of changes in runoff timing and runoff seasonality. Changes in timing or the seasonal distribution of runoff are excellent indicators of impacts of climate change or modifications of the river network or watershed (Stewart et al., 2004; Kormann et al., 2015; Schwartz et al., 2017; Rottler et al., 2020; Brunner et al., 2020a). We aim to provide an interactive tool that can be used in- and outside the scientific community to explore, learn, teach and communicate topics related to streamflow, ensure easy accessibility and re-usability, allow the testing of parameter sensitivity of analytical tools and enable a straightforward comparison between analytical tools, river gauges, regions and

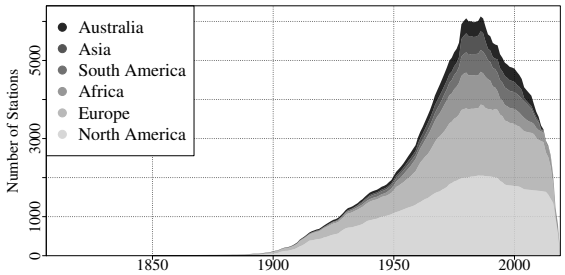


***Figure 2.1:*** *Availability of GRDC daily resolution discharge time series by year and continent (status as of May 2019).*

time frames. Here, we present the analytical tools available and illustrate the functionality of the web application by investigating selected gauging station from the Rhine River Basin in Central Europe.

## 2.2 Runoff data

In the framework of this study, we focus on the global runoff data set from the Global Runoff Data Centre (GRDC). GRDC was established in 1988 and is operating under the patronage of the World Meteorological Organization (WMO) to foster research on global and climate change. Their unique collection of discharge time series comprises daily resolution runoff data from more than 7000 gauging stations from all over the world and represents a key data set for hydrological research. The length of the stored discharge series varies and ranges from a couple of years to more than 200 years. Most time series are available for Europe and North America (Fig. 2.1). Updates to GRDC come with delays and frequencies vary among contributing agencies. Therefore, fewer observations are available in recent years. The daily resolution discharge data used in the following analysis was provided by GRDC May 2019.

## 2.3 Architecture and implementation

The web app was implemented based on the R package 'Shiny', which offers a framework for web application development in R (Chang et al., 2019; Slater et al., 2019). The core of the *Hydro Explorer* consists of the typical two-file structure of a Shiny web app (Fig. 2.2). One R-file defines the layout and the appearance of the web app (ui.R) and another one contains all computational instructions (server.R). The *Hydro Explorer* is part of the R package 'meltimr'. The open-source R package 'meltimr' including detailed instructions how to install and test the

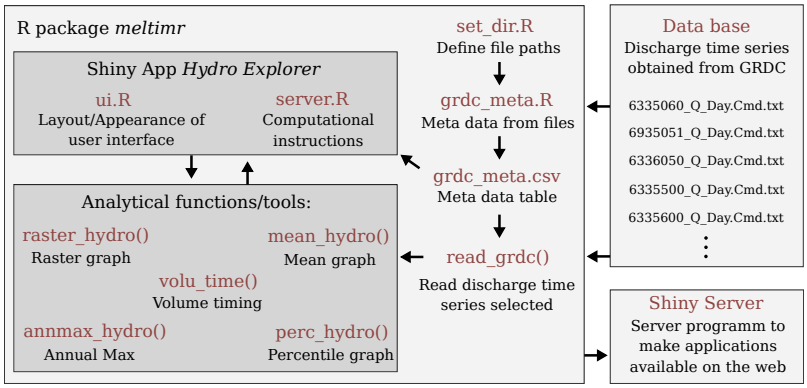


***Figure 2.2:*** *Architecture and implementation of the Shiny web application Hydro Explorer.*

functionality is available at https://github.com/ERottler/meltimr. All functions the *Hydro Explorer* needs are incorporated in this R package. We chose this set-up to enable easy sharing and installation of the programme code. Existing tools can be easily modified and new analytical approaches added. All analytical tools also can be used outside the web app environment.

As a first step in order to use the web app, a table containing meta information about all discharge time series located in the data folder (e.g. station name, gauge location and file path) needs to be compiled (Fig. 2.2). This only has to be done once, before the first start of the web app (see file grdc_meta.R). The GRDC discharge data is imported in a later step following the interaction with the user interface. The separation of the data base from the web app enables the re-use of the web app with a different set of GRDC runoff data, facilitates the incorporation of additional data sources and keeps required working memory at a minimum. To host the web app online, the installation of a shiny web server is necessary. An example instance of the *Hydro Explorer* is available at: http://natriskchange.ad.umwelt.uni-potsdam.de:3838/HydroExplorer/. Resources needed to host the web app are low. A web server with one central processing unit (CPU) and one gigabyte (GB) of working memory is sufficient, but may need to be extended if larger traffic, i.e., multiple parallel users, are expected.

## 2.4 Analytical tools

In the following, we present the selection of analytical tools available within the *Hydro Explorer*. The presented tools enable the investigation of daily resolution discharge time series with regard to changes in runoff timing and runoff seasonality. Fig. 2.3 presents the user interface of the *Hydro Explorer*. Fig. 2.4 depicts the

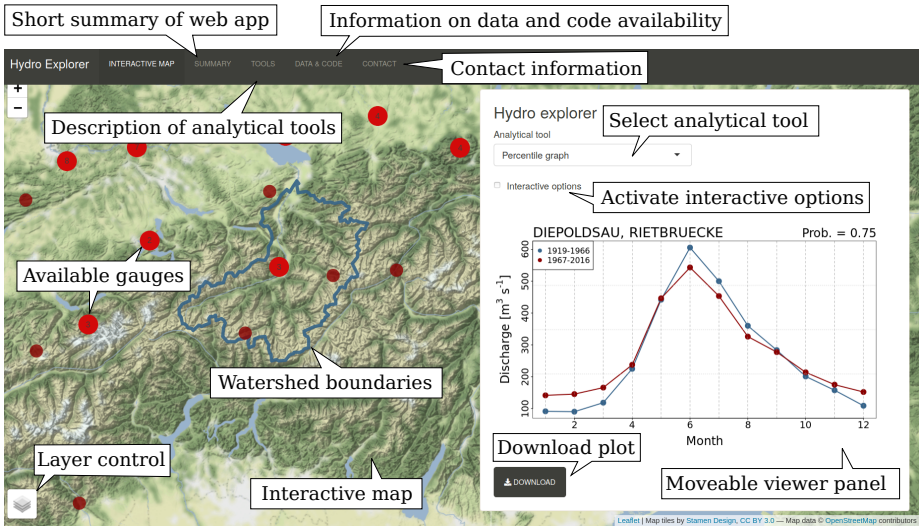


***Figure 2.3:*** *User interface of the Hydro Explorer with call-outs giving information about the individual components.*

analytical tools and plot types.

### 2.4.1 Raster graph

A raster graph is a three-dimensional surface plot, where the x-axis is the day of the year, the y-axis the individual years and the z-axis the daily value of the investigated variable (e.g streamflow, temperature or snow depth). The visualisation of the data using raster graphs provides a quick first insight into the dynamics and processes controlling investigated variable at the selected site (Koehler, 2004; Strandhagen et al., 2006). This visualisation tool enables the display of inter- and intra-annual variability in one single figure. A similar visualisation technique is used in Kormann et al. (2015) to display intra-annnual and elevation-dependent signals in trends in alpine hydro-climatological data. Within the web app, the time frame displayed and the start day of the (hydrological) year (e.g. 1. October or 1. November) can be selected.

### 2.4.2 Mean graph

Mean annual cycles (or mean annual hydrographs) provide a very good first insight into runoff seasonality, e.g. due to the build-up and melt of seasonal snow packs. The *Mean graph* tool displays mean annual cycles for two selected time frames. Vertical lines mark days of the year of the annual maximum value. The time lag between the days of maximum runoff of the two selected time frames

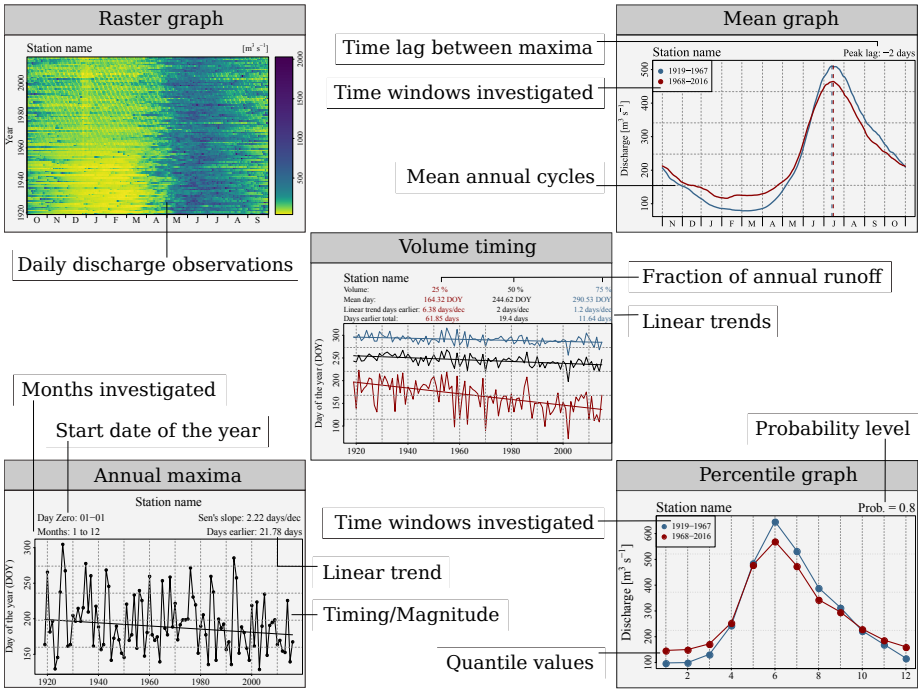


***Figure 2.4:*** *Analytical tools and plot types available within the Hydro Explorer.*

is noted top right (Fig. 2.4). The two time frames compared can be varied. In addition, a moving average window can be applied to the time series and its impact on the annual cycles studied.

### 2.4.3 Volume timing

A frequently applied approach to investigate the timing of (snowmelt) runoff, is the determination of the day of the year (DOY) a certain fraction of the total annual volume passes a discharge gauging station (e.g. Stewart et al., 2004, 2005; Maurer et al., 2007; Déry et al., 2009). The *Volume timing* tool displays the DOYs when 25/50/75 % of the total annual runoff were recorded. On top of the panel, mean DOY and a Theil-Sen estimate of the linear trend are noted for each volume fraction (Theil, 1950; Sen, 1968; Bronaugh and Werner, 2013). The start day of the year (e.g. 1.October or 1.November) can be modified interactively within the web app. Furthermore, the time frame investigated can be varied.

### 2.4.4 Annual maxima

The investigation of annual runoff maxima represents a common approach to assess changes in flood characteristics (e.g. Petrow and Merz, 2009; Hall and Blöschl, 2018; Kemter et al., 2020). *Annual Max* enables the investigation of changes in timing and magnitudes of runoff maxima. Within the *Hydro Explorer*, the annual maxima characteristic of interest can be selected via a drop-down menu choosing 'Day of the year' or 'Magnitude'. Furthermore, the investigation of monthly maxima is possible ('Trend monthly maxima'). Linear trend estimates based on the Theil-Sen approach are noted top right. Within the web app, the start day of the year can be modified and the determination of maximum values for selected months of the year (e.g. seasonal) conducted.

### 2.4.5 Percentile graph

The *Percentile graph* enables the investigation of changes in quantile values over time. Changes in low, mean and high flows can be investigated. Quantile values are estimated on a monthly level based on all daily values of a month. In a 50-year time window, for example, quantile values for January are based on 50 times 31 values. Quantiles are estimated empirically based on type 8 of the function 'quantile' in the R environment, as recommended by Hyndman and Fan (1996). Two plot options are available: 'Line plot' and 'Image plot'. For the selection 'Line plot', quantiles values of individual probability levels (e.g. 0.75 or 0.90) for two selected time frames are compared. The 'Image plot' option shows the difference in quantile values between the two selected time frames for all probability levels, i.e. 0.01 - 0.99 sorted along the y-axis.

### 2.4.6 Further options

River gauging stations can be filtered according to data availability and location (see option *Filter stations*). Furthermore, watershed boundaries derived based on the HydroSHEDS drainage network (Lehner, 2012) can be visualised via the layer control on the bottom left (Fig. 2.3). A short summary, a description of the analytical tools, information about the data and code availability and contact information also are included into the web app (Fig. 2.3).

## 2.5 Example of use

In the following, we illustrate the functionality of the analytical tools using examples from the Rhine River Basin (Fig. 2.5 and Tab. 2.1). The Rhine River

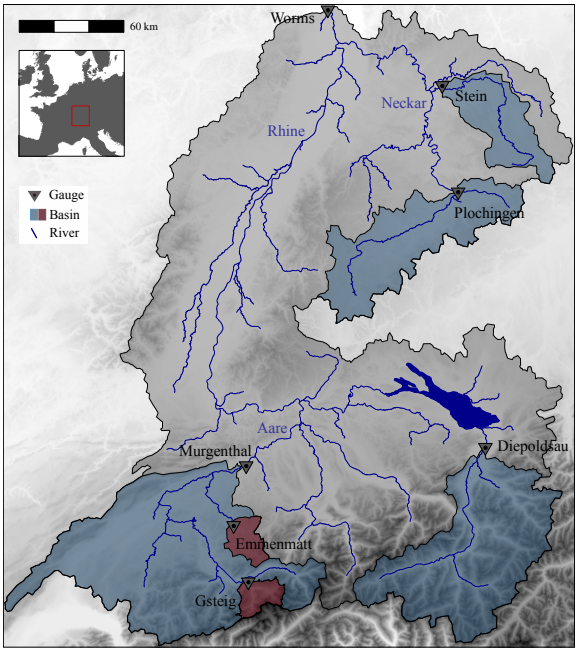


***Figure 2.5:*** *Topographic map of the Rhine River Basin until gauge Worms with selected gauges and sub-basins used to illustrated the functionalities of the Hydro Explorer.*

stretches from the European Alps in the south to the North Sea and is the second largest river in Central Europe (Middelkoop et al., 2001; Belz et al., 2007; Stahl et al., 2016). Snow and glacier melt dominate runoff in the Alpine part of the basin, rainfall-runoff processes dominate the runoff regimes of important tributaries such as Neckar, Moselle and Main. The Middle and Lower Rhine River is characterised by a complex flow regime (Belz et al., 2007; Stahl et al., 2016). Time frame investigated, i.e., 1919 to 2016, corresponds to the maximum common time period of selected river gauges.

### 2.5.1 Raster graph

We use the raster graph tool to investigate the runoff seasonality at the two Swiss gauges Diepoldsau and Gsteig (Fig. 2.5). Gauge Diepoldsau is located at the Alpine Rhine just upstream Lake Constance, Gsteig gauging station is located in the southern part of the Aare River. In the Alpine Rhine Basin, numerous large reservoir lakes for hydropower have been constructed since the 1960s (Wildenhahn and Klaholz, 1996; Bosshard et al., 2013). There are no large reservoir lakes for hydropower production upstream gauge Gsteig. At both gauges, the raster graphs hint at a strong runoff seasonality with low/high runoff during winter/summer

***Table 2.1:*** *River gauges selected: Station name, associated river, location (WGS 84), catchment area, mean runoff (MQ).*

| Name | River | Latitude | Longitude | Area [km²] | MQ [m³/s] |
|---|---|---|---|---|---|
| Diepoldsau | Rhine | 47.383 | 9.6409 | $6.19 \cdot 10^3$ | 230.36 |
| Gsteig | Lutschine | 46.664 | 7.8715 | $3.79 \cdot 10^2$ | 18.89 |
| Murgenthal | Aare | 47.267 | 7.8306 | $1.01 \cdot 10^4$ | 285.78 |
| Emmenmatt | Emme | 46.955 | 7.7488 | $4.43 \cdot 10^2$ | 11.85 |
| Plochingen | Neckar | 48.707 | 9.4190 | $4.00 \cdot 10^3$ | 46.95 |
| Stein | Kocher | 49.258 | 9.2871 | $1.93 \cdot 10^3$ | 22.20 |

(Fig.2.6 a and b). River runoff at gauges Diepoldsau and Gsteig seems to be dominated by the build up and melt of a seasonal alpine snow cover. Furthermore, a diagonal pattern is imprinted at gauge Diepoldsau since the 1960s. This is a typical signal of high-head hydropower generation with reservoir lakes (e.g., Meile et al., 2011; Pérez Ciria et al., 2019; Rottler et al., 2020). Along with higher energy consumption and hydropower production, more runoff is recorded during the week compared to the weekend. As the days of the weeks shift over time, a diagonal pattern shows up in the raster graph. The example presented shows that the visualisation of discharge time series as raster graph is well suitable to get a first quick insight into important runoff characteristics.

### 2.5.2 Volume timing

We also use the two Swiss gauges Diepoldsau and Gsteig to illustrate the functionality of the analytical tool *Volume timing*. At gauge Diepoldsau, the timing of the annual runoff fractions shifts towards the beginning of the hydrological year (Fig. 2.6 c). The first 25 % of discharge are recorded more than 60 days earlier. The DOY recording the centre of volume, i.e., 50 % of the annual runoff, occurs almost 20 days earlier. We attribute detected changes at gauge Diepoldsau mainly to the construction and operation of reservoirs, as hydropower production using large reservoir lakes redistributes runoff from summer to winter (Verbunt et al., 2005; Belz et al., 2007; Bosshard et al., 2013). In contrast, for gauge Gsteig, which has no large reservoir lakes for hydropower production upstream, linear trend estimates hint at little to no changes in the timing of runoff fractions (Fig.2.6 d). The investigation of annual runoff fractions (e.g. centre of volume) can give a good insight into changes in the seasonal redistribution of water. However, caution has to be exercised interpreting changes, as the sensitivity of this indicator can vary across the year and be influenced by other flow components (Whitfield, 2013).

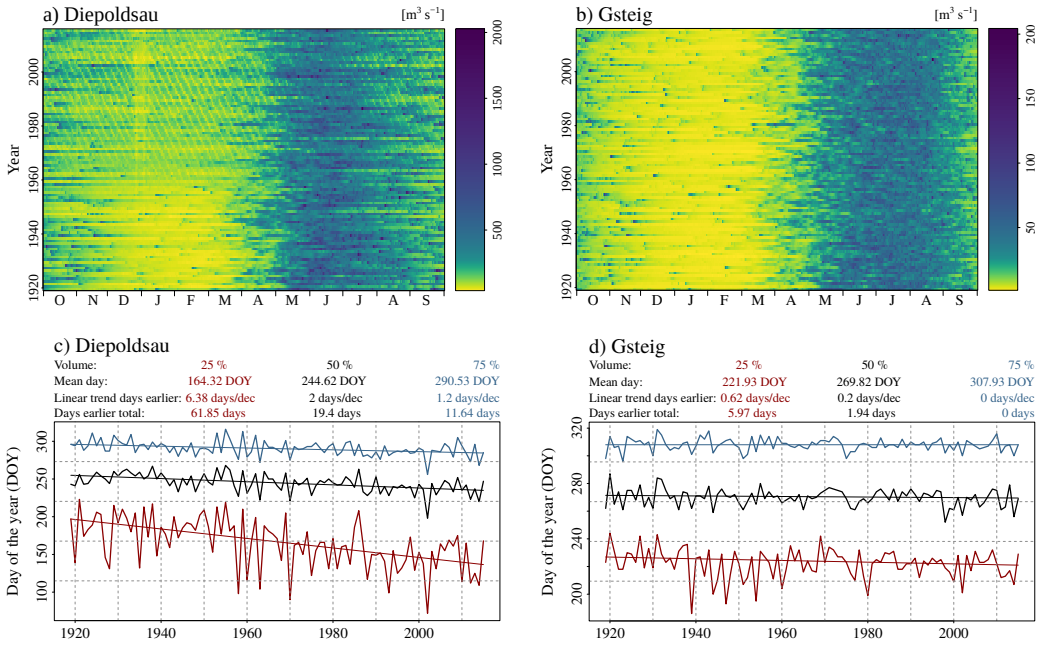


***Figure 2.6:*** *Raster graphs and changes in timing of annual runoff fractions for discharge measured at gauges Diepoldsau (a and b) and Gsteig (c and d) for the time frame 1919-2016.*

### 2.5.3 Annual maxima

In order to introduce the analytical tool *Annual Max*, we investigate the timing of runoff maxima observed at gauge Diepoldsau and Gsteig. We compare changes in the timing of annual runoff maxima (determined between January and December) with changes in the timing of runoff maxima determined between January to August. The variation of months included into the quantification of runoff maxima can help to assess the robustness of trends in the timing of runoff maxima and supports the attribution of detected signals. In the example presented, we exclude months at the end of the year (September to December), where snowmelt only plays a marginal role for runoff generation. The resulting shorter period (Januar to August) includes all important changes related to snowmelt. The comparison of the two periods allows for assessing signal robustness and the potential impact of an earlier snowmelt-runoff timing on the trends in the timing of annual runoff maxima.

The analysis of annual runoff maxima (January to December) at gauge Diepoldsau indicates that annual peak values occur about three weeks earlier in recent years compared to the beginning of the time frame investigated (Fig. 2.7 a). However, when only taking the months January to August into account, no shift forward in time can be detected (Fig. 2.7 b). The attribution of an earlier annual

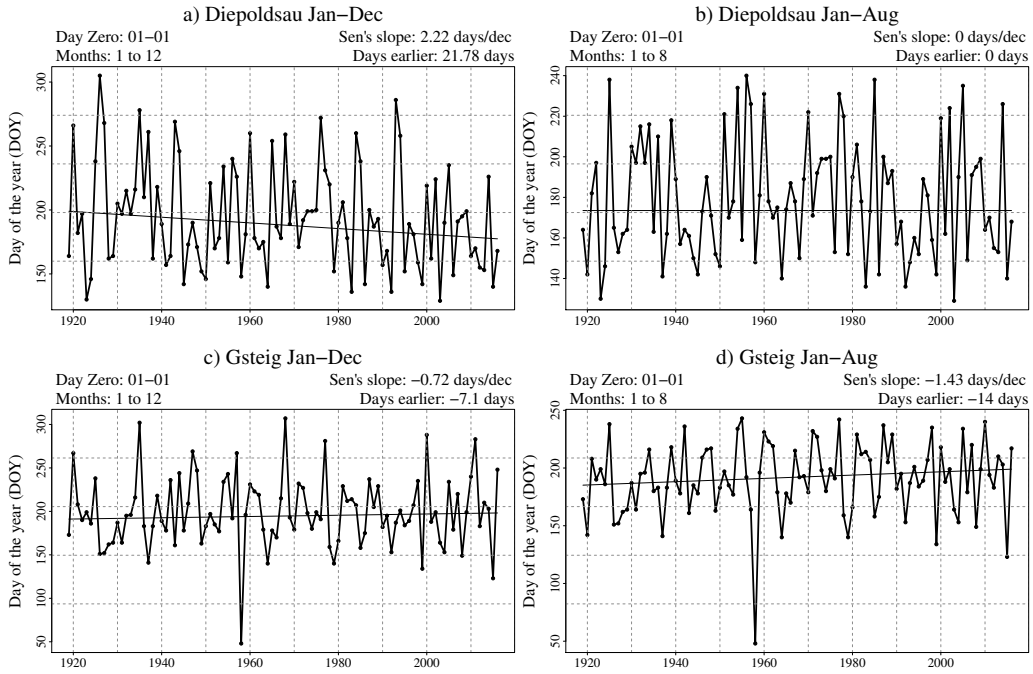


***Figure 2.7:*** *Changes in timing of annual runoff maxima for gauge Diepoldsau taking all months into account (a) and only values from January to August (b). Time frame investigated: 1919-2016.*

peak flow timing at gauge Diepoldsau (Fig. 2.7 a) to an earlier onset of snowmelt does not seem to be tenable. At gauge Gsteig, runoff peaks show the tendency to occur later in the year in more recent decades (Fig. 2.7 c). This tendency is enhanced when only taking the months January to August into account (Fig. 2.7 d). Our results point at the sensitivity of trends in the timing of peak discharges to the months included into the analysis. At both gauges, snowmelt seems to dominate runoff. However, the exclusion of months outside the snowmelt season from the analysis strongly affects the trend in timing of runoff peaks. This underlines that linear trends in runoff timing should always be interpreted with respect to the choices made for the analysis (i.e. selection of time frames, seasons, and stations).

### 2.5.4 Percentile graph

In order to illustrate the functionality of the analytical tool *Percentile graph*, we calculate runoff quantiles for gauges Murgenthal and Emmenmatt. Gauge Murgenthal is located in the South-East of the Rhine Basin at the Aare River. At gauge Emmenmatt, runoff of the Emme River, a tributary of the Aare River, is measured

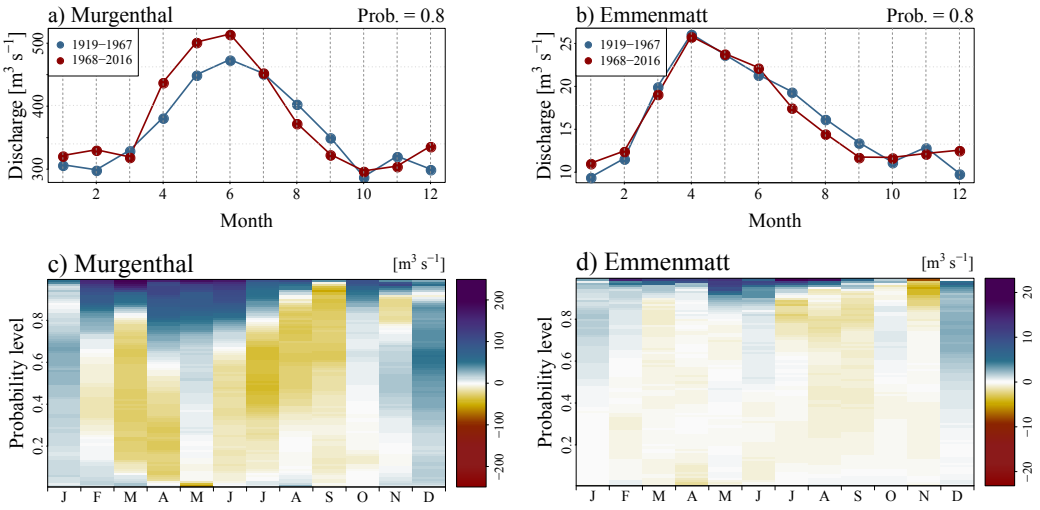


***Figure 2.8:*** *Percentile graph for the gauges Murgenthal (a) and Emmenmatt (b) comparing the time frames 1919-1967 and 1968-2016.*

(Fig. 2.5). We estimate quantiles empirically for the probability level 0.8 (80 % of observed values are below determined threshold) on a monthly level taking all daily values into account. We compare values between the two time frames 1919-1967 and 1968-2016 (Fig. 2.8 a and b). The time frames compared represent the first and second half to the maximum common time period of all river gauges selected (Tab. 2.1). Selecting the visualisation option 'Image plot' within the tool, the differences in quantile values for all probability levels (0.01-0.99) and months are displayed (Fig. 2.8 c and d). At gauge Murgenthal, we detect increasing quantile values for high probability levels for spring and summer (Fig. 2.8 c). At the same time, decreasing values show up for lower probability levels. At Emmenmatt, a similar, but less pronounced signal appears. We suspect changes in precipitation characteristics to contribute to detected changes in runoff quantiles. However, also changes in snowmelt and the impact of anthropogenic modifications of the river network, e.g. the numerous hydropower installations and the Jura water corrections (Wetter et al., 2011; Bodemann and Pfammatter, 2015), need to be considered. In order to pin down the underlying mechanisms causing the detected signals in river runoff, detailed analyses of precipitation and snowmelt are required.

### 2.5.5 Mean graph

Using the analytical tool *Mean graph*, we compare annual cycles for the two time frames 1919-1967 and 1968-2016 and assess the impact of data aggregation prior to the calculation of mean annual cycles. The time frame 1919 to 2016 represents the

maximum time period of all river gauges selected (Tab. 2.1). Gauges investigated, i.e., Plochingen and Stein, are located in the catchment of the Neckar River, one of the main tributaries of the Rhine River (Fig. 2.5). In contrast to the runoff seasonality in Alpine catchments, the Neckar River has a pluvial runoff regime with high runoff during winter and low runoff during summer (Fig. 2.9). Before the calculation of the mean annual cycles, we apply a 0-day, a 30-day or a 90-day moving average filter on the time series. The application of moving average filters has a strong smoothing effect on the annual cycles and affects the time lag between the maximum values of the two time frames. Furthermore, our analyses hint at more runoff in the second, more recent time window (1968-2016), particularly during winter. Studies investigating possible future runoff conditions in similar hydro-climatological settings hint at the possibility of a further increase in runoff, particularly during winter (e.g. Wolf, 2003; Pfister et al., 2004; Menzel et al., 2006; Bosshard et al., 2014).

## 2.6 Conclusion

The Shiny web app *Hydro Explorer* proved to be well suited to investigate large discharge data sets with regard to changes in runoff timing and runoff seasonality in an interactive way. The presented set of analytical tools enables a quick yet comprehensive investigation of daily discharge time series. We find that for the assessment of signal robustness, the ability to easily compare results of different methods, gauges, regions and time frames is crucial. We exemplary investigate a small selection of river gauges in the Rhine River Basin. The global coverage of the underlying GRDC discharge data set enables the exploration of a great diversity of river systems ranging from arid to tropical, from natural to controlled by human activities and from small catchments of only a few square kilometres to the largest basin on the globe.

The implementation of the *Hydro Explorer* as a free and open-source software embedded in an R package provides access to the programme code and enables the re-usage and modification of existing structures. The software architecture facilitates the incorporation of additional data source and keeps working memory at a minimum. The *Hydro Explorer* can serve as powerful tool in- and outside the scientific community to explore, learn, teach and communicate water related issues. An application and re-use of the *Hydro Explorer* in academic teaching at university (e.g. for demonstrating hydrological concepts), environmental research (e.g. for the assessment of changes in riverine habitats) as well as water related industrial sectors (e.g. in hydropower production) is conceivable. Moreover, when maintained at a public server, it also opens up a low-threshold entry point for

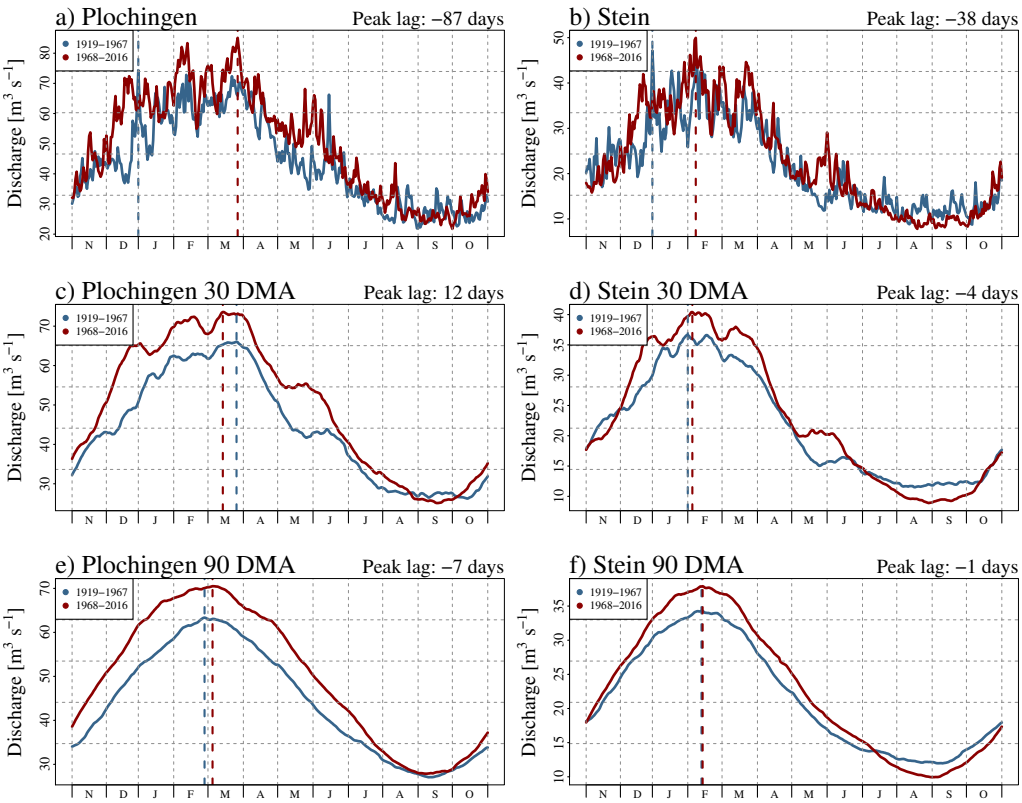


***Figure 2.9:*** *Mean annual cycles of discharge for gauges Plochingen and Stein. Before the calculation of mean annual cycles no (a and b), a 30-day (b and c) or a 90-day (e and f) moving average filter is applied.*

quick insights into properties of runoff regimes to private persons in riparian communities. Climatic changes and human activities can fundamentally alter river runoff. A close investigation and understanding of underlying processes is of great importance. Next steps in the development of the *Hydro Explorer* could be the incorporation of additional analytical tools and the application to other hydro-climatological data sets.

## Software and data availability

An example instance of the web app is available at `http://natriskchange.ad.umwelt.uni-potsdam.de:3838/HydroExplorer/`. Source code and instructions on how to use and modify the web app can be found at `https://github.com/ERottler/meltimr`. Discharge data and watershed boundaries can be requested from the Global Runoff Data Centre, 56068 Koblenz, Germany (GRDC).

## Declaration of interests

The authors declare that they have no known competing financial interests or personal relationships that could have appeared to influence the work reported in this paper.

## Acknowledgements

Discharge data and watershed boundaries were provided by the Global Runoff Data Centre, 56068 Koblenz, Germany (GRDC). The Copernicus Land Monitoring Service, implemented by the European Environmental Agency, provided the European Digital Elevation Model (EU-DEM), version 1.1, used within the maps.

## Funding

This research was supported by the Deutsche Forschungsgemeinschaft (GRK 2043/1-P2) within the NatRiskChange research training group at the University of Potsdam (https://www.uni-potsdam.de/natriskchange/).

# 3 | Long-term changes in central European river discharge for 1869-2016: impact of changing snow covers, reservoir constructions and an intensified hydrological cycle

Published as: Erwin Rottler, Till Francke, Gerd Bürger and Axel Bronstert: Long-term changes in central European river discharge for 1869–2016: impact of changing snow covers, reservoir constructions and an intensified hydrological cycle. *Hydrology and Earth System Sciences*, 24, 1721–1740, https://doi.org/10.5194/hess-24-1721-2020, 2020.

**Keypoints:**

- Set of analytical tools to investigate hydro-climatic time series
- Combination of quantile sampling with moving average trend statistics and empirical mode decomposition
- Long-term changes in river runoff (pluvial, nival and mixed flow regimes)
- Impacts of changes in snow cover and precipitation along with reservoir constructions

## Abstract

Recent climatic changes have the potential to severely alter river runoff, particularly in snow-dominated river basins. Effects of changing snow covers superimpose with changes in precipitation and anthropogenic modifications of the

watershed and river network. In the attempt to identify and disentangle long-term effects of different mechanisms, we employ a set of analytical tools to extract long-term changes in river runoff at high resolution. We combine quantile sampling with moving average trend statistics and empirical mode decomposition and apply these tools to discharge data recorded along rivers with nival, pluvial and mixed flow regimes as well as temperature and precipitation data covering the time frame 1869-2016. With a focus on central Europe, we analyse the long-term impact of snow cover and precipitation changes along with their interaction with reservoir constructions.

Our results show that runoff seasonality of snow-dominated rivers decreases. Runoff increases in winter and spring, while discharge decreases in summer and at the beginning of autumn. We attribute this redistribution of annual flow mainly to reservoir constructions in the Alpine ridge. During the course of the last century, large fractions of the Alpine rivers were dammed to produce hydropower. In recent decades, runoff changes induced by reservoir constructions seem to overlap with changes in snow cover. We suggest that Alpine signals propagate downstream and affect runoff far outside the Alpine area in river segments with mixed flow regimes. Furthermore, our results hint at more (intense) rainfall in recent decades. Detected increases in high discharge can be traced back to corresponding changes in precipitation.

## 3.1 Introduction

In many regions of the world, rivers constitute essential lifelines and form the basis of human livelihood. However, recent climate changes may severely affect the hydrological cycle and jeopardize the functional diversity of river systems. Most severe changes are expected to occur in snow-dominated river basins. In a warmer world, snow cover characteristics and snowmelt contribution to river runoff will change fundamentally. Rising temperatures are expected to cause less winter precipitation to fall as snow and existing snow covers to melt earlier in spring (Barnett et al., 2005; Simpkins, 2018; Kormann et al., 2015; Birsan et al., 2005). Recent studies suggest that rainfall amount and the number of extreme rainfall events increase due to warmer air holding more water along with enhanced evaporation (Lehmann et al., 2015; Coumou and Rahmstorf, 2012; Mueller and Pfister, 2011). Investigating changes in features of snowpack and snowmelt for key mountain regions, Stewart (2009) summarizes "that both temperature and precipitation increases to date have impacted mountain snowpacks" already. For the Rhine River, one of the most important rivers in Europe, Stahl et al. (2016) indicate that "the influence of climate change is visible particularly in the temporal

shifts of seasonal minima and maxima of the hydrological regimes of snow and glacier melt dominated alpine headwater catchments."

In addition to changes in snowpacks and precipitation, anthropogenic modifications of land surface, subsurface properties and the river network alter river runoff. During the 20th century, more than 45 000 large dams were constructed around the world (Word Commision on Dams, 2000). Also in the Rhine River basin, human activities change runoff with regard to amount, its temporal distribution as well as water quality (Wildenhahn and Klaholz, 1996; Belz et al., 2007; Wildi et al., 2004).

The current knowledge of how climatic changes and changing watershed properties impact river runoff comes largely from instrumental records of hydro-climatic variables, particularly temperature, precipitation and runoff. Birsan et al. (2005) state that "as a spatially integrated variable streamflow is more appealing for detecting regional trends than point measurements of precipitation which is highly variable in space and time", but also point out that watershed properties and their changes over time constitute an "obvious complication in interpreting trends in streamflow data." In addition, quality and length of recorded time series often are insufficient to identify and disentangle effects of the various mechanisms. A sufficient length of the time series inter alia is crucial to be able to distinguish between natural climate variability and signals of climate change. Variability of large-scale atmospheric flow on annual to multi-decadal scales, for example, can cause variations in hydro-climatic data, which can either counterbalance or reinforce signals of long-term changes (Hanson et al., 2006; Frei et al., 2000; Kerr, 2000; Scherrer et al., 2016). Studies preparing and investigating long time series of high quality are of great importance and form the basis of our current understanding of features and magnitudes of recent climatic changes (e.g. Vincent et al., 2002; Begert et al., 2005; Schmidli and Frei, 2005; Moberg et al., 2006; Scherrer et al., 2016). Often, simple linear regression approaches are applied to assess characteristics of climatic changes. One frequently used analytical tool in this regard is the robust non-parametric Mann-Kendall trend test (Kendall, 1975; Theil, 1950; Sen, 1968). However, restricting the assessment to linear trends only is hard to justify. The potential of more detailed analyses with regard to seasons, moving time windows (e.g. Kormann et al. (2015)) or quantiles of the target variable have hardly been tapped. To further consolidate and extend findings obtained so far, new sets of analytical tools to extract information stored in this time series need to be developed, tested and applied on climatological and hydrological records.

Our study aims at a better understanding of long-term changes in river runoff and identifying potential underlying driving mechanisms, by analysing daily resolution hydro-climatic time series recorded in central Europe between 1869 and 2016. We assess long-term changes in a highly resolved manner by com-

bining quantile sampling, moving average trend statistics and empirical mode decomposition. The two main research question we want to address are the following:

- What is the long-term impact of changes in snow cover on river runoff?
- How do runoff changes induced by changes in snow cover compare with changes caused by reservoir constructions and changes in precipitation?

## 3.2 Study area and data

We investigate discharge time series from four gauging stations (Fig. 3.1 and Tab. 3.1). The depicted gauges stand out by the exceptional length of their records and represent different types of flow regimes: nival, pluvial and complex. Gauge Wasserburg is located at the Inn River in Upper Bavaria, Germany. The Inn River is a right tributary of the Danube. The river´s source is located in the Swiss Alps and most of its drainage area ($1.20 \cdot 10^4$ km² until gauge Wasserburg) possesses high Alpine character. The other three gauges investigated, namely Basel, Würzburg and Cologne, are located in the Rhine River basin. The Rhine River is one of the largest rivers in Europe. It is a heavily used waterway and livelihood for the region. At gauge Basel, river runoff is dominated by snowmelt and rainfall runoff from the Alps. Gauge Würzburg is located at the Main River in northern Bavaria, Germany. The Main river is a right tributary of the Rhine river. The catchment area until gauge Wuerzburg is $1.40 \cdot 10^4$ km². The city of Cologne is the largest city along the Rhine River and located in the Lower Rhine region after the confluences with all major tributaries. Until Cologne, the Rhine river drains an area of $1.44 \cdot 10^5$ km². For all selected gauges, discharge data at daily resolution have been available since at least 1869. For gauge Basel, statistical tests on daily runoff means conducted by Pfister et al. (2006) show that measured discharge is homogeneous since 1869 (digitally available part of the time series); i.e. the values are free of anthropogenic effects such as change in instrumentation, change in daily recording frequency or lowering of the river bed (Pfister et al., 2006). Other gauging stations investigated are part of the hydrometric observation network of the water authorities in Germany. Recordings are regularly checked to ensure high quality and reliability. Discharge time series were obtained from the Global Runoff Data Centre (GRDC). Data from the GRDC were used as-is without any further treatment. Elevation distributions and monthly Pardé coefficients for investigated river basins are presented in the appendix (Fig. 3.6).

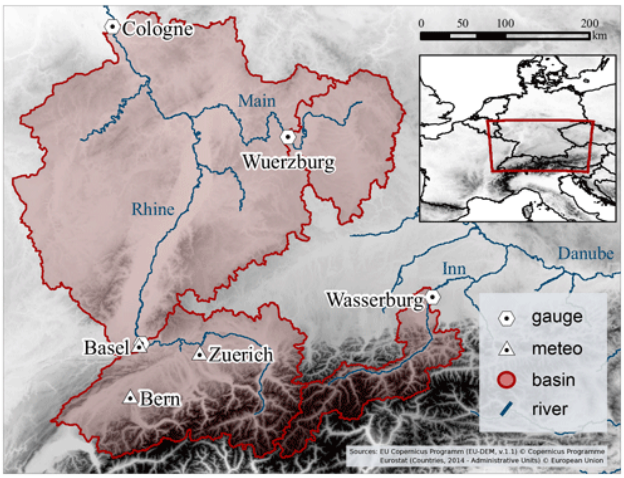


***Figure 3.1:*** *Topographic map of the study area with the locations of river gauges, river basins and meteorological stations.*

***Table 3.1:*** *Database studied: station name, associated river, location (WGS 84), altitude [m], daily resolution time series investigated with temperature (T), precipitation (P) and discharge (D), catchment area, mean runoff (MQ) and data source with the Global Runoff Data Centre (GRDC) and Federal Office of Meteorology and Climatology of Switzerland (MeteoSwiss).*

| Station | River | Lat. | Lon. | Alt. | Vari. | Area [km$^2$] | MQ [m$^3$/s] | Data source |
|---|---|---|---|---|---|---|---|---|
| Basel Binningen | - | 47.5411 | 7.5836 | 316 | T-P | - | - | MeteoSwiss |
| Bern Zollikofen | - | 46.9908 | 7.4639 | 552 | T-P | - | - | MeteoSwiss |
| Zurich Fluntern | - | 47.3781 | 8.5658 | 555 | T-P | - | - | MeteoSwiss |
| Wasserburg | Inn | 48.0593 | 12.2342 | 420 | D | $1.20 \cdot 10^4$ | 355 | GRDC |
| Basel Rheinhalle | Rhine | 47.5594 | 7.6167 | 294 | D | $3.59 \cdot 10^4$ | 1044 | GRDC |
| Cologne | Rhine | 50.9370 | 6.9633 | 35 | D | $1.44 \cdot 10^5$ | 2091 | GRDC |
| Würzburg | Main | 49.796 | 9.926 | 165 | D | $1.40 \cdot 10^4$ | 112 | GRDC |

Furthermore, we analyse daily resolution temperature and precipitation data provided by the Federal Office of Meteorology and Climatology of Switzerland (MeteoSwiss). At MeteoSwiss, a standardized homogenization procedure is applied to a set of monthly temperature and precipitation time series (Begert et al., 2005). During this homogenization procedure attained monthly correction values are also applied on daily resolution data. The homogenization of long climatological time series is necessary to correct for non-climatic factors influencing the data. Currently, homogenized daily temperature/precipitation data are available for 28/73 stations. In the following, we focus on meteorological stations where both temperature and precipitation data have been available since at least 1869 and there is no gap in the data longer than 60 days. In total, nine stations fulfil these criteria. Results of the three most prominent stations are displayed and discussed in the main paper (Fig. 3.1 and Tab. 3.1), information on (Tab. 3.3) and results of (Fig. 3.9) the remaining stations are given in the Appendix. These strict selection criteria with regard to data length and quality strongly limit the number of recordings suitable for analysis. However, even if a smaller database can reduce the significance of attained results, this is a trade-off we need to accept. Only with recordings having sufficient length and quality, can we ensure that the advantages of the proposed analytical tools described in the following chapter can take effect.

## 3.3 Methods

To detect long-term changes in the investigated hydro-climatic data, we combine quantile sampling with moving average trend statistics and empirical mode decomposition (EMD). The selected analytical tools and their combined application to daily time series enable a highly resolved investigation of changes throughout the investigated time frame. The analysis is divided into four steps. Each analysis step complements and extends the information of the previous one, so that step by step, a comprehensive picture of long-term changes takes shape (Fig. 3.3). A list of all abbreviations and acronyms used can be found in the Appendix (Tab. 3.4).

### 3.3.1 Seasonality of river runoff

To investigate the seasonality of river runoff, we estimate quantiles on a daily basis (QDAY). For every day of the year (DOY), we take all available measurements (i.e. 148 daily values for the period 1869-2016) and calculate QDAYs empirically for probabilities ranging from 0.01 to 0.99. In the framework of this study, quantiles are calculated as the $\frac{k-1/3}{n+1/3}$ plotting position, with n as the sample size and k =

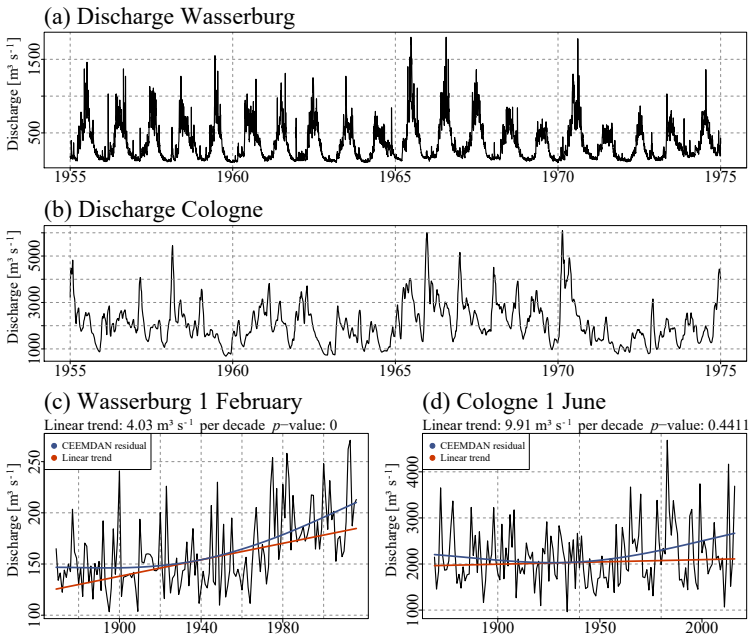


***Figure 3.2:*** *Discharge recordings from gauges Wasserburg (a) and Cologne (b) and measurements from all 1.February / 1.June days for gauge Wasserburg / Cologne after applying a 30-day moving average filter over the entire time series (c, d). The robust Theil-Sen trend estimator and the Mann-Kendall trend test were applied to assess the magnitude and the significance of the linear trends (red line). The CEEMDAN residual is used to extract the non-linear evolution of the trend (blue curve).*

1,....n being the rank (e.g. Hyndman and Fan, 1996). This approach corresponds to type 8 of the 'quantile' function in the R environment (R Core Team, 2019).

### 3.3.2 Changes in seasonality

In order to get a first insight into changes in runoff seasonality, we estimate quantiles from and within a 30 day moving window (QMOV). QMOV operates on discharge data and is independent of previously computed QDAYs. Quantiles are calculated for probabilities between 0.01 and 0.99. The results are continuous quantile time series for each discharge series (Fig. 3.3). To assess the temporal evolution of these values over the observation period, we employ trend analysis. We calculate trend magnitudes of QMOV using the robust Theil-Sen trend estimator (TST) on a daily basis for all quantiles. Since the computation of the trend uses the values of the same DOY of successive years, auto-correlation should not be of any concern. Within the linear regression approach of the TST, trend magnitudes

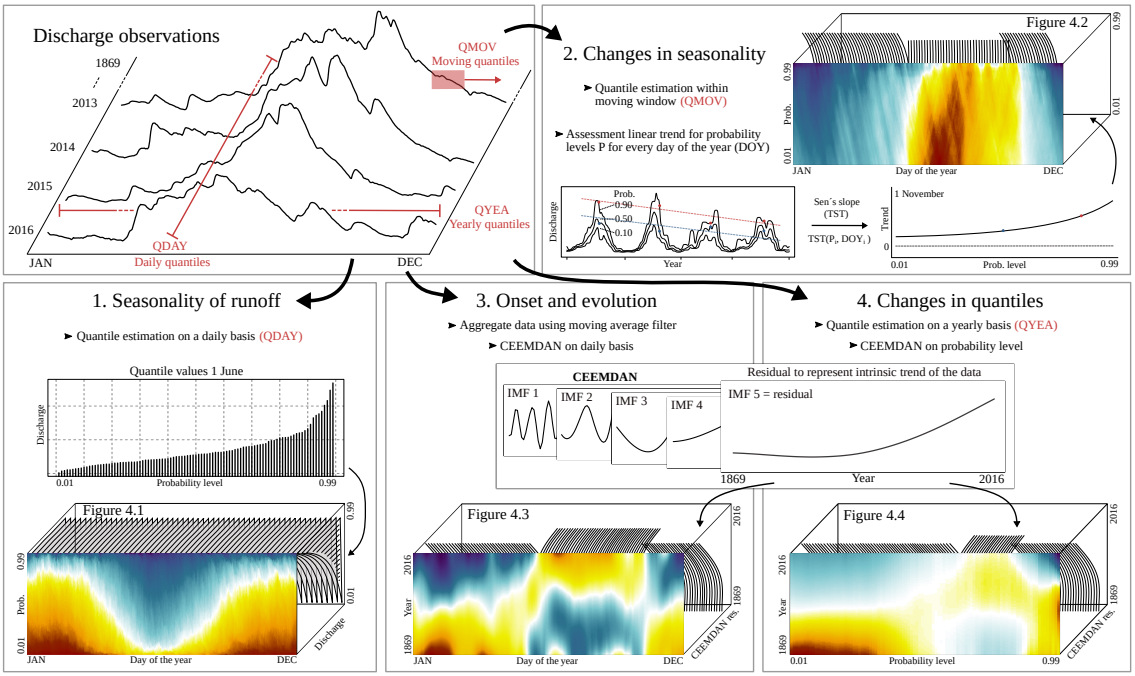


***Figure 3.3:*** *Schematic overview of analytical tools used to detect long-term changes in hydro-climatological time series. The analysis of discharge data is subdivided into four steps, where each step complements and extends the information acquired in the previous step.*

are estimated as the median slope of ranked data values (Theil, 1950; Sen, 1968; Bronaugh and Werner, 2013).

### 3.3.3 Onset and evolution of changes

The use of linear trends to quantify the temporal evolution of hydro-climatic variables often lacks physical justification. The respective signals are likely to be non-linear (Fig. 3.2 c and d). Even when using parametric functions for capturing the non-linear behaviour, e.g. exponential or power-law functions, it is not guaranteed that results will reflect the actual characteristics of underlying processes in the data. An adaptive approach, which does not require a predetermined basis function, is required to get a more flexible characterization of the trend. We employ EMD for this purpose. EMD is an empirical, direct and adaptive method to analyse non-linear trends. It decomposes the signal into oscillatory modes and provides a powerful tool to separate short timescale signals from a general trend (Wu et al., 2007; Huang et al., 1998; Luukko et al., 2016; Huang et al., 1999). To

avoid mode mixing issues, we performed EMD on an ensemble of the initial data signal: ensemble EMD (EEMD) (Wu and Huang, 2009). Each ensemble member is perturbed by low-amplitude white noise and the results are averaged at the end of the computations. To keep the characteristics of a complete decomposition, i.e. all extracted intrinsic mode functions (IMFs) sum up to the original signal, the averaging process is carried out separately for each IMF component (Torres et al., 2011). This extension results in a complete EEMD with additive noise (CEEMDAN). We use an ensemble of 10000 members, a noise strength of 0.5 times the standard deviation of the input signal, and R package 'Rlibeemd' (Luukko et al., 2016) to perform CEEMDAN. The residual of CEEMDAN "can be used to represent the intrinsic trend of the data" (Luukko et al., 2016).

We assess these residuals for discharge, temperature and precipitation on a daily basis after calculating moving average values within a window with a width of 30 days for discharge and temperature and a width of 90 days for precipitation. Testing different window sizes, commonly used monthly (30) and seasonal (90) values proved to be a good compromise between robustness of the signal and preservation of signal variability. To make results of different days comparable, we centre each residual by subtracting its mean. To enable the comparison between CEEMDAN residuals and more commonly used linear approaches, we assess, whether the non-parametric Mann-Kendall trend test (MK) detects statistical significant monotonic trends in the data CEEMDAN was applied to ($\alpha$ = 0.05) (Mann, 1945; Kendall, 1975). Days with significant monotonic changes are marked with points on top of the respective plot panels (third column in Fig. 3.4 and columns one and three in Fig. 3.5).

### 3.3.4 Changes in quantiles

Furthermore, we investigate changes in quantile magnitudes over time. Therefore, quantiles are estimated on an annual level (QYEA) (Fig. 3.3). The temporal evolution of QYEAs over the investigated time frame is assessed by applying CEEMDAN. In the case of precipitation, we only use values from 'rainy days' (i.e. precipitation > 1 mm). The MK test serves to assess the significance of the trends (marked with points on top of the panel (see section 3.3.3)).

## 3.4 Results

### 3.4.1 Seasonality of river runoff

Runoff recorded at gauges Wasserburg and Basel is highly seasonal with high/low runoff during summer/winter (Fig. 3.4 a1, b1). Compared to gauge Wasserburg,

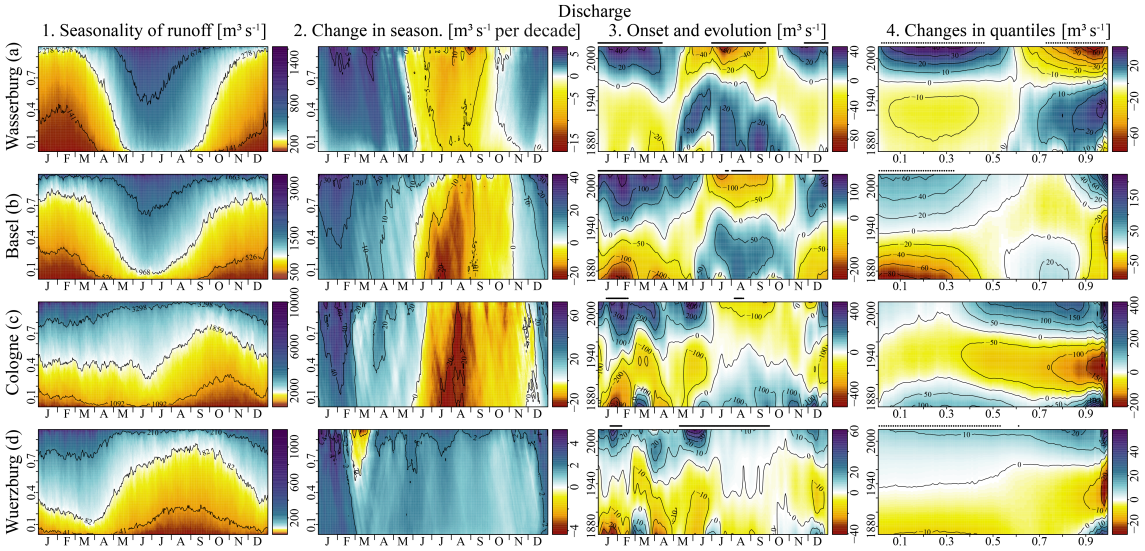


***Figure 3.4:*** *Seasonality of river runoff, change in seasonality, onset and evolution of changes and changes in quantiles for discharge measured at gauges Wasserburg (a), Basel (b), Cologne (c) and Würzburg (d). Isolines in left panels '1. Seasonality of runoff' indicate quantiles for probabilities 0.1, 0.5 and 0.9 determined over the entire time series using all available measurements. Points on top of the panels (two right columns) indicate days/probabilities with significant changes according to the Mann-Kendall trend test. Time frame investigated: 1869-2016.*

more runoff is recorded at Basel during winter, i.e. the contrast between summer and winter is less pronounced. At gauge Wasserburg, very high discharge values are almost solely recorded between the months of May and September. Conversely, at gauge Basel, days with very high runoff show up throughout the year. Downstream from gauge Basel, runoff from rain-dominated tributaries such as the Neckar, Main and Mosel blend with Alpine runoff (see gauge Cologne Fig. 3.4 c1). Rainfall-runoff-dominated basins are characterized by high discharge during winter and the beginning of spring and low discharge in summer, as seen for Würzburg (Fig. 3.4 d1).

### 3.4.2 Changes in seasonality

At gauges Wasserburg and Basel, runoff increases during winter and spring for all quantiles, while it decreases during summer and at the beginning of autumn (Fig. 3.4 a2, b2). This corresponds to a reduction in runoff seasonality. A very similar overall pattern of changes in runoff can be detected at gauge Cologne:

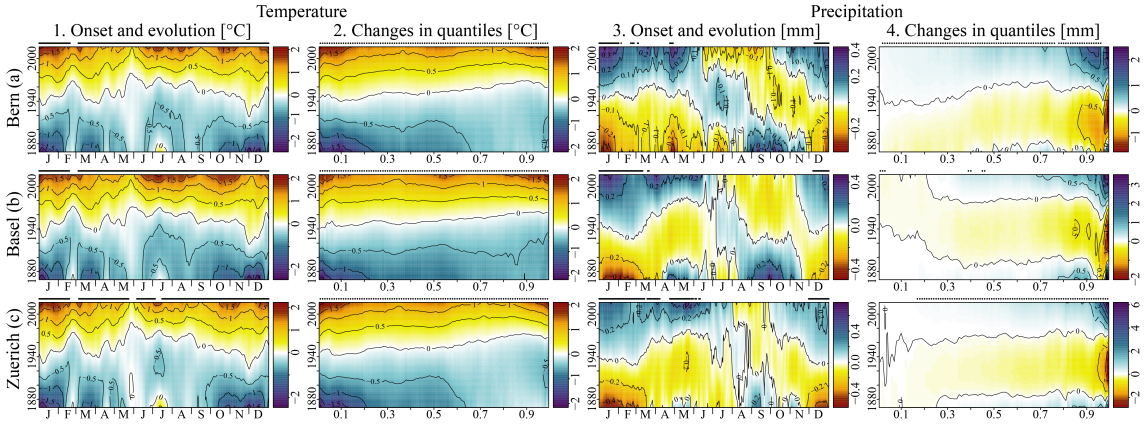


***Figure 3.5:*** *Onset and evolution of changes and changes in quantiles for temperature and precipitation measured at stations Bern (a), Basel (b) and Zurich (c). Points on top of the panels indicate days/probabilities with significant changes according to the Mann-Kendall trend test. Time frame investigated: 1869-2016.*

runoff increases during winter and spring and decreases during summer and autumn (Fig. 3.4 c2). In contrast, at gauge Würzburg, discharge quantiles increase throughout, except for high levels at the end of February and March (Fig. 3.4 d2). Similarly to gauges Basel and Cologne, the strongest increases occur during winter.

### 3.4.3 Onset and evolution of changes

At gauge Wasserburg, pronounced changes in seasonality started in the second half of the 20th century during the 1960s (Fig. 3.4 a3). In contrast, changes at gauge Basel seem to be more gradual and starting earlier in the investigated time period already (Fig. 3.4 b3). At gauge Würzburg, a clear onset of change cannot be detected (Fig. 3.4 d3), however, increases seem to be more uniform and enhanced in recent decades. Patterns of change from snowmelt and rainfall-runoff-dominated tributaries overlap at gauge Cologne (Fig. 3.4 c3).

Looking at the respective evolution of potential drivers, temperatures continuously increased throughout the year (Fig. 3.5 a1, b1, c1). Similar amplitude and interannual patterns are apparent in the three time series. The amount of precipitation increases in recent decades, particularly during winter (Fig. 3.5 a3, b3, c3). The MK trend test detects significant monotonic increases/decrease in runoff during winter/summer for gauges Wasserburg and Basel (Fig. 3.4 a3, b3). For temperature, the MK detects significant increases throughout the year (Fig. 3.5 a1, b1, c1). Precipitation increases significantly during winter (Fig. 3.5 a3, b3,

c3).

### 3.4.4 Changes in quantiles

Since the 1960s, QYEAs have strongly increased/decreased at levels below/above 0.6 at gauge Wasserburg (Fig. 3.4 a4). These changes in QYEAs correspond to the strong decrease in seasonality in recent decades (see section 3.4.2): runoff diminishes in summer and increases in winter. Likewise, at gauge Basel lower QYEAs (levels < 0.6) increase and higher QYEAs (levels 0.6 - 0.8) decrease (Fig. 3.4 b4). However, the onset of changes is earlier and changes are smoother compared to detected signals at gauge Wasserburg. Particularly changes in low QYEAs start to increase at the beginning of the investigated time frame already. In contrast to results from gauge Wasserburg, QYEAs at the highest levels (> 0.8) have been increasing at gauge Basel since the 1960s (Fig. 3.4 b4). QYEAs from gauge Würzburg increase over the entire range investigated (Fig. 3.4 d4). Changes in QYEAs below a level of approximately 0.6 occur earlier and are smoother than for higher levels. There, the increases have been enhanced in recent decades. At gauge Cologne, high QYEAs have increased in recent decades (Fig. 3.4 c4), making it similar to findings from gauges Basel and Würzburg. Also the lower QYEAs have experienced an increase. This increase, however, is not a gradual one over the entire time frame, but is rather a U-shaped process (decline until the 1940s, then increase).

For precipitation, similar pattern seem to show up. Increasing QYEAs hint at more (intense) rainfall in recent decades (Fig. 3.5 a4, b4, c4). Increases in QYEAs in temperature seem to occur earlier and seem to be enhanced at lower temperatures (Fig. 3.5 a2, b2, c2). Changes in quantiles for individual seasons are given in the Appendix (Fig. 3.7 and Fig. 3.8). At gauge Wasserburg, changes in QYEAs are significant according to the MK (Fig. 3.4 a4). The more a trend pattern deviates from a monotonic increase and more U-shaped signals emerge, the more often the MK results in non-significant $p$ values. The main results depicted in Fig. 3.4 are summarized in Tab. 3.2.

## 3.5 Discussions

### 3.5.1 Seasonality of river runoff

Runoff at gauge Wasserburg is dominated by the accumulation and depletion of a seasonal snowpacks. The intra-annual variability of runoff is very high and high flows mainly occur during the snowmelt season and during summer, when higher temperatures enable liquid precipitation in large fractions of the catchment

(Fig. 3.4 a1). There are no bigger lakes that could attenuate flood or low-flow events generated in the basin. In comparison, large lakes constitute an important element of the Rhine River basin until gauge Basel. Furthermore, large parts of the basin are sub-Alpine terrain. As a result, liquid rainfall is an important streamflow component throughout the year and runoff less seasonal compared to gauge Wasserburg (Stahl et al., 2016). A detailed overview of hydrological regimes in Switzerland and their characteristics can inter alia be found in Weingartner and Aschwanden (1992) or Speich et al. (2015). Reconstructing the largest flood events in the High Rhine basin since 1268, Wetter et al. (2011) indicate that about half of all major floods occur during summer. Flood events during summer usually are the result of high baseflow due to a melting Alpine snow cover superimposing with heavy rainfall (Wetter et al., 2011). Extreme flood events during autumn, winter and spring often are caused by long-lasting precipitation events coinciding with strong snowmelt due to rain on snow (RoS) and/or a temporary temperature increase (Wetter et al., 2011; Schmocker-Fackel and Naef, 2010). For higher-elevated river basins, RoS events play an important role in runoff formation (Sui and Koehler, 2001; Merz and Blöschl, 2003). The RoS flood that occurred in the Bernese Alps, Switzerland in October 2011 showed how damaging these kinds of events can be (Rössler et al., 2014). Another example is the RoS events from January 2011, where rainfall released vast amounts of water stored in a temporary snow cover and caused RoS-driven flood events in whole central Europe (Freudiger et al., 2014). However, the importance of different flood-generating mechanisms is changing with recent climatic changes (see e.g. Blöschl et al. (2017, 2019); Berghuijs et al. (2019)).

Even though about one-third of the runoff in the Main River originates from snowmelt (Stahl et al., 2016), there is only little impact of snow accumulation and melt on the seasonal distribution of discharge. It seems that low temperatures rarely prevail long enough to enable the accumulation and preservation of snow over a longer period. Runoff is dominated by large-scale rainfall events occurring in winter and increased evapotranspiration during summer (Fig. 3.4 d1). At gauge Cologne, we have the situation of superimposing nival and pluvial runoff components (Fig. 3.4 c1). This overlap results in a more uniform seasonal distribution of discharge. High QDAYs are higher during winter, whereas low QDAYs are higher during summer (Fig. 3.4 c1). This reversal in the seasonal distribution hints at the importance of different flow components for different flow situations. Runoff due to large-scale rainfall events over the middle and lower parts of the catchment are important for high discharge values, particularly during winter. During summer, snowmelt and glacier melt from the Alpine part of the basin play an important role in the sustenance of runoff in the lower reaches of the Rhine River (Stahl et al., 2016).

### 3.5.2 Changes in seasonality

In the snow-dominated river basins Wasserburg and Basel, the seasonality of river runoff decreases over the investigated time frame. For the increasing runoff values during winter and early spring, several mechanisms have to be taken into account. First of all, changes in the Alpine snow cover have to be considered. In recent decades, rising temperatures have caused less snow accumulation during winter (Laternser and Schneebeli, 2003; Marty, 2008; Scherrer et al., 2004; Wielke et al., 2004; Marty et al., 2017). Thus, a greater fraction of total precipitation is liquid and reaches the river system without being stored in snowpacks. In addition, the frequency of days with temperatures above 0 °C increases, causing parts of any existing snow cover to melt (Scheifinger et al., 2003; Kreyling and Henry, 2011; Zubler et al., 2014; Schädler and Weingartner, 2010). Rising temperatures also result in shorter snow duration, where "shorter snow duration is mainly caused by earlier snow melting in spring than by later first snowfalls in autumn" (Laternser and Schneebeli, 2003). The earlier onset of snow melt in spring represents a much-noticed effect of rising temperatures on Alpine river runoff (e.g. Kormann et al., 2015; Birsan et al., 2005; Stewart, 2009).

Less snow accumulation during the preceding winter results in lower discharges during the following melting period, i.e. late spring and early summer. Furthermore, recent studies suggest that rising temperatures might lead to a reduction in snowmelt rates (Musselman et al., 2017; Wu et al., 2018). "Slower snowmelt in a warmer world may decrease the likelihood that wetness thresholds that permit hydrologic connectivity will be exceeded, leading to spring and summer streamflow declines and lower runoff efficiency" (Musselman et al., 2017).

Changes in the liquid/solid fraction of precipitation overlap with changes in the total amount of rainfall. We observed increased rainfall during winter for all stations investigated. Likewise, numerous other studies point at a recent increase in precipitation, particularly during winter (e.g. Begert et al., 2005; Scherrer et al., 2016; Frei and Schär, 2001). However, increasing catchment evaporation due to increasing radiation, air temperature and vegetation activity might at least partly compensate detected changes in precipitation (Duethmann and Blöschl, 2018; Schädler and Weingartner, 2010; Norris and Wild, 2007; Wild et al., 2007).

At gauge Cologne, we also detect a decrease in discharge during summer and autumn (Fig. 3.4 c2). We hypothesize that this decrease is the result of a downstream propagation of the Alpine signal, possibly overlapping with increasing evaporation rates in the basin. The decrease in summer discharge in the Lower Rhine cannot be attributed to reduced ice melt contributions from the Alpine glaciers. Assessing the snow and glacier melt components of streamflow of the Rhine River for the time frame 1901-2006, Stahl et al. (2016) showed that "despite

the glacier retreat the modelled ice melt component of the streamflow in the Rhine does not show a strong long-term trend over the entire study period, i.e. a systematic decline or increase of this component. The detailed results of the modelling suggests that an increased ice melt due to increased temperature may have been compensated by the reduction in glacier area". Gauge Würzburg, with its discharge increasing throughout the entire year, does not show any detectable changes in seasonality.

### 3.5.3 Onset and evolution of changes

Investigating long-term snow trends of the Swiss Alps, Laternser and Schneebeli (2003) suggest that "mean snow depth, the duration of continuous snow cover and the number of snowfall days in the Swiss Alps all show very similar trends during the observation period 1933-99: a gradual increase until the early 1980s (with significant interruptions during the late 1950s and early 1970s) followed by a statistically significant decrease towards the end of the century".

At gauge Basel, these changes in Alpine snowpacks seem to be insufficient to explain the decrease in runoff seasonality detected. In particular, winter discharge (low QYEAs) increases already from the beginning of the investigated time frame on (Fig. 3.4 b3 and b4). Instead, we suspect anthropogenic alterations of the river network, particularly reservoir constructions, to be an important driver. These might have caused the redistribution of water from summer to winter earlier in the investigated time frame already. Large fractions of the Swiss and Austrian Alpine river systems have been dammed to produce hydropower. The two Alpine countries have the highest specific hydroelectric production per surface area globally (Truffer et al., 2001). The first hydropower station in Switzerland was constructed in 1899 (Verbunt et al., 2005). Dam constructions in the Alpine Rhine and along other Alpine rivers, such as the Aare, Limmat and Reuss, gained momentum in the 1920s and most of the large storage lakes were constructed between 1950 and 1970 (Meile et al., 2011; Wildenhahn and Klaholz, 1996; Wagner et al., 2015; Bosshard et al., 2013) (Fig. 3.10). The total storage volume of large storage lakes (river weirs not included) of the High Rhine/entire Rhine basin is estimated to amount to $1.86/3.12 \cdot 10^9$ m³ (Wildenhahn and Klaholz, 1996). In order to ensure full functional capability of high-head storage hydropower stations, reservoirs need to have sufficient water volume stored at all times. Therefore, reservoirs tend to be filled during summer when discharge is high. Conversely, storages are depleted during low flow in winter (Belz et al., 2007; Meile et al., 2011; Farinotti et al., 2016; Wesemann et al., 2018). A rough estimation supports this notion: assuming the $1.86 \cdot 10^9$ m³ of storage being emptied between December and April (and filled between June and October), mean runoff would increase/decrease

by approximately 10 $m^3/s/dec$ in these months during the investigated time frame, which corresponds to the trend magnitudes depicted in Fig. 3.4 b2. In addition to reservoir constructions, regulations of lake levels and routing of rivers through lakes, e.g. the diversion of the Aare River into Lake Biel in 1887 (part of the First Jura-Waters Corrections), need to be considered (Wetter et al., 2011).

At gauge Wasserburg, pronounced changes in runoff seasonality do not show up until the second half of the 20th century (Fig. 3.4 a3 and a4). In the Inn basin, the constructions of key reservoirs, such as the Gepatsch reservoir (Tyrol, Austria), the Lago di Livigno reservoir (Grisons, Switzerland and Lombardy, Italy) and the Lai da Ova Spin compensation reservoir (Grisons, Switzerland), were not completed until the 1960s. The construction of those big reservoirs coincides with the detected onset of changes in river runoff. We suspect that also in the Inn River basin, the construction and management of reservoirs for hydropower might be an important factor changing seasonality of river runoff. In addition to changes in seasonality, the operation of high-head hydropower stations causes unnatural fluctuation on (sub-)daily timescales (hydropeaking) (Meile et al., 2011; Pérez Ciria et al., 2019) (see also Fig. 3.11). Effects of reservoirs possibly overlap (with) changes induced by changes in snow cover.

Also rainfall-runoff-dominated rivers, such as the Main River at Würzburg, are strongly affected by hydro-engineering installations. One large-scale project inaugurated in 1992 after numerous decades of constructions is the Rhine-Main-Danube waterway. In order to raise low water discharge in the Main River, about $1.55 \cdot 10^8$ $m^3$ ($3.50 \cdot 10^8$ $m^3$) of water is transferred on average per year (in a dry year) from the Danube into the Main River basin via the Main-Danube Canal (Maniak, 2016). The connection from the Rhine River until Würzburg with constructions of weirs to regulate the river´s water level was completed in the 1940s (Wirth, 1995). This onset of water-level regulations in the 1940s coincides with increasing low QYEAs ($< 0.6$) at gauge Würzburg (Fig. 3.4 d4). We suspected that anthropogenic alterations strongly impacted the discharge of the Main River, particularly during low-discharge periods. However, they seem to be insufficient to explain changes in higher QYEAs.

### 3.5.4 Changes in quantiles

We detect increasing high QYEAs at gauges Basel, Cologne and Würzburg (Fig. 3.4 b4, c4 and d4). Possible driving mechanisms might be changes in precipitation: our results hint at more (intense) rainfall in recent decades (Fig. 3.5). In the following, we discuss possible underlying forcing mechanisms of detected signals. These include changes in large-scale circulation patterns, solar dimming/brightening and temperature-moisture feedbacks.

Long-term changes in the occurrence frequencies and/or characteristics of circulation patterns are known to have a strong impact on local climate. More frequent zonal circulation in winter since the 1970s, for example, might be responsible for "more frequent mild and humid winters in Central Europe" (Bárdossy and Caspary, 1990). This increase in zonal circulation follows upon several decades with increased numbers of blocking days during winter (Häkkinen et al., 2011). Blocking in the Atlantic region is anti-correlated with phases of the North Atlantic Oscillation (NAO) (Scherrer et al., 2006; Stein, 2000; Pavan et al., 2000). Negative values of the NAO index "indicate periods of reduced north-south pressure gradient, reduced westerly winds and weaker advection of warm oceanic air onto the cold European landmass" (Parker et al., 2007). Wintertime NAO on the other hand is influenced by the Atlantic Multidecadal Oscillation (AMO): a "positive phase of the AMO results in more frequent negative NAO" (Peings and Magnusdottir, 2014). The AMO depicts multi-decadal (60-70 years) variations in sea surface temperatures in the North Atlantic basin (Peings and Magnusdottir, 2014; Kerr, 2000). After several decades of warm anomalies of sea surface temperatures (positive phase of AMO, which coincided with more frequent blocking days), the North Atlantic started to cool down and to transition into a negative AMO phase in the 1960s (Peings and Magnusdottir, 2014; Häkkinen et al., 2011). This transition into a negative AMO phase and fewer blocking days coincides with more frequent zonal circulation in winter (Bárdossy and Caspary, 1990), more (intense) rainfall (Fig. 3.5 a3, b3, c3, a4, b4, c4) and an increase in discharge, whereas changes seem to overlap with changes induced by anthropogenic alteration of the river network and changes in alpine snow packs (Fig. 3.4 b4, c4, d4).

Generally, detected patterns in temperature time series investigated in the framework of this study are consistent across all stations (Fig. 3.5 and Fig. 3.9). In the case of precipitation, overall patterns are similar, however, stronger variations among stations show up. Precipitation is subject to stronger local and regional variability than temperature. This evidently limits the informative value of precipitation recorded at individual points for discussions on catchment scale. However, variations of local meteorological variables are strongly influenced by large-scale flow and regional-scale weather pattern (Scherrer et al., 2016; Murawski et al., 2018; Weusthoff, 2011). Weather patterns/types represent specific synoptic conditions and lead to certain meteorological conditions in a region. For western Germany, precipitation correlates well on scales of hundreds of kilometres, particularly during winter (Schönwiese and Rapp, 1997). During summer, local convective storms are an important source of rainfall and strong differences in amount and intensity over very short distances are possible (Sodemann and Zubler, 2010; Lavers et al., 2013). However, such convective storms 'are hardly of any relevance for the formation of floods in the large river basins of Central Europe, because the

extent of convective rainstorms is restricted to local occurrence' (Bronstert et al., 2007). Rainfall-runoff processes on larger scales are dominated by advective precipitation. The main moisture source then is the Atlantic Ocean (Sodemann and Zubler, 2010). Following the above-mentioned aspects, we hypothesize that even if superimposed by local variability due to smaller-scale processes and regional variations due to general precipitation gradients, long-term signals in precipitation detected on point scale can provide important information for discussions on catchment scale. However, caution has to be exercised, results of available stations compared and findings not transferred to places outside the region of influence.

Marty (2008) relate detected shifts in snow days in Switzerland to an enhanced temperature increase due to changes in circulation patterns coinciding with "the full magnitude of the greenhouse effect, which is no longer masked by solar dimming". After a multi-decadal decrease from about the 1950s to the 1980s (solar dimming), recent decades saw an increase in regional solar irradiance (solar brightening) due to decreasing amounts of anthropogenic aerosols in the atmosphere (Ruckstuhl et al., 2008; Norris and Wild, 2007; Ruckstuhl and Norris, 2009).

Rapidly rising temperatures have the capacity to affect the entire hydrological cycle. A feedback mechanism of major importance in this respect is the temperature-moisture feedback: rising temperatures result in increasing evaporation and precipitation, which in turn leads to an intensification of the entire hydrological cycle (Huntington, 2006; Held and Soden, 2000). Lehmann et al. (2015) indicate that a "thermally driven moisture increase has significantly contributed to the intensification of extreme rainfalls since the 1980s".

Against the background of recent changes in temperature, precipitation, and frequencies in zonal circulation and following Labat et al. (2004), we suggest that rapid increases in temperatures in recent decades have resulted in an increased sea-land-transport of moisture and increases in precipitation and runoff. Signals possibly overlap with changes in moisture transport due to varying frequencies in zonal circulation and blocking days.

At gauge Wasserburg, in contrast to other gauges investigated, high QYEAs do not increase. We suspect that in this case, high discharges are also controlled by snowmelt processes rather than by liquid rainfall. Furthermore, investigated rain gauges might not depict changes in precipitation in the complex Alpine topography of the catchment. In the High Rhine basin up to gauge Basel, large fractions of the basin are located outside the Alpine ridge and liquid precipitation plays an important role throughout the year. Therefore, impacts of changes in snow cover, reservoir constructions and effects of more (intense) rainfall all seem to be detectable in measured discharge (Fig. 3.4 b4). Changes in snow cover and river regulations, which decrease runoff seasonality, seem to primarily

affect QYEAs below a level of 0.85 and more intense rainfall events increase the magnitude of higher QYEAs.

***Table 3.2:*** *Summary of analysis results presented in Fig.3.4. Table arrangement reflects figure layout.*

| | 1. Seasonality of runoff | 2. Changes in seasonality | 3. Onset and evolution | 4. Changes in quantiles |
|---|---|---|---|---|
| a) Wasserburg | Snow-dominated<br>Nival flow regime | Decrease in seasonality<br>↑ Winter ↓ Summer | 2nd half 20th century | ↑ Low ↓ High |
| b) Basel | Snow-dominated<br>Nival flow regime | Decrease seasonality<br>↑ Winter ↓ Summer | Gradual change<br>Entire time frame | ↑ Low ↓ High<br>↑ Very high |
| c) Cologne | Complex flow<br>Pluvio-nival | ↑ Winter and spring<br>↓ Summer and autumn | No clear onset<br>Nival + pluvial pattern | ↑ All prob. levels<br>U-shape |
| d) Würzburg | Rain-fed<br>Pluvial flow regime | ↑ All seasons | No clear onset | ↑ All prob. levels<br>Gradual + U-shape |

## 3.6 Conclusions

We investigate daily observational data from key river gauges and meteorological stations located in central Europe covering the time frame 1869-2016. Investigated time series stand out by the exceptional length and quality of their continuous recordings. A cascading sequence of analytical tools is used to extract high-resolution signals of long-term changes. In order to acquire a comprehensive picture of long-term changes, we combine quantile sampling with moving average trend statistics and empirical mode decomposition. Given that the recordings have sufficient length and quality, presented tools enable investigations of high resolution and provide detailed insights into underlying trend patterns. A very high quality of the time series is required to prevent non-climatic factors, such as changes in observation practices or site relocation, from affecting the determination of trends (Begert et al., 2005; Scherrer et al., 2016; Begert and Frei, 2018). A sufficient length of the time series is vital to be able to distinguish between natural climate variability and signals of climate change. When adopting strict criteria regarding data length and data quality, the number of stations suitable for analysis strongly decreases. A small database limits the significance of attained results, though. This is a trade-off we need to accept in order to ensure full functionality of presented analytical tools. Consistent results for stations and parameters investigated make us confident that even if the number of stations is limited, we will attain meaningful results that are worth discussing.

The seasonality of the analysed snow-dominated rivers decreases. We suspect river regulations, particularly reservoir constructions, to be the main driver of detected changes. Reservoirs are filled during summer when discharge is high and storages depleted during low flow in winter (e.g. Belz et al., 2007; Meile et al., 2011). In recent decades, runoff changes induced by reservoir constructions seem to overlap with changes in Alpine snowpacks (Laternser and Schneebeli, 2003; Scherrer et al., 2004). Rising temperatures reduce seasonal snow covers and the seasonal redistribution of runoff from winter to summer. An exact separation of effects of reservoirs and changes in snow cover and investigations of possible counterbalancing interactions are still pending and are focus of future research. Furthermore, we suspect that detected decreases in discharge during summer and autumn in the Lower Rhine region at gauge Cologne are the result of a downstream propagation of the Alpine signal, possibly further overlapping with increasing evaporation rates in the basin.

In addition, our results hint at more (intense) rainfall in recent decades, particularly during winter. Detected changes in precipitation seem to intensify high discharges. The detected increase in precipitation (intensity) is not a gradual one over the entire time frame, but rather follows a U-shape (decline until the 1940s,

then increase). Further research is necessary to pin down underlying mechanisms of detected changes in precipitation and runoff. We suspect that detected signals might be due to an increase in sea-land transport of moisture, particularly during winter, being part of a recent intensification of the entire hydrological cycle (Huntington, 2006; Held and Soden, 2000; Lehmann et al., 2015; Labat et al., 2004). Temperature-driven increases in moisture and precipitation possibly overlap with natural multi-decadal variations in sea-land-moisture transport (Parker et al., 2007; Kerr, 2000; Häkkinen et al., 2011; Peings and Magnusdottir, 2014; Bárdossy and Caspary, 1990; Scherrer et al., 2006; Pavan et al., 2000).

Over recent decades, hydrological regimes have been changing at a very fast pace. Some progress has been made in extracting long-term signals of change in hydro-climatic data. However, further studies investigating long-term changes in river runoff focusing on the detection of underlying mechanisms and the disentanglement of their effects are of great urgency and importance.

## Data availability

Climatological data used in this study were obtained from the Federal Office of Meteorology and Climatology of Switzerland, CH-8058 Zurich Airport (MeteoSwiss). Discharge data analysed were provided by the Global Runoff Data Centre, 56068 Koblenz, Germany (GRDC). Data analysis was carried out using the R statistical software (https://www.r-project.org/, last access: 7 April 2020; R Core Team (2019)).

## Author contributions

ER conducted the analysis and wrote the manuscript. TF, GB and AB provided guidance in the process of data analysis and preparation of the manuscript.

## Competing interests

The authors declare that they have no conflict of interest.

## Acknowledgements

The Federal Office of Meteorology and Climatology of Switzerland (MeteoSwiss) and the Global Runoff Data Centre (GRDC) provided climatological and discharge

data, respectively. The Copernicus Land Monitoring Service, implemented by the European Environmental Agency, provided the European Digital Elevation Model (EU-DEM), version 1.1.

## Financial support

This research was supported by the Deutsche Forschungsgemeinschaft (GRK 2043/1-P2) within the NatRiskChange research training group at the University of Potsdam (https://www.uni-potsdam.de/natriskchange/, last access: 7 April 2019).

## Review statement

This paper was edited by Jim Freer and reviewed by Massimiliano Zappa and one anonymous referee.

## Appendix

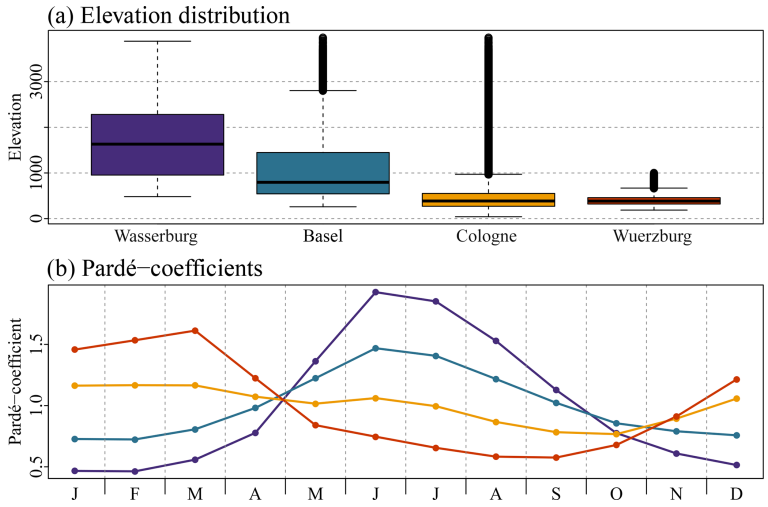


***Figure 3.6:*** *Elevation distribution (raster cells at 500 m resolution calculated based on EU-DEM v.1.1 by the EU Copernicus Programme) and Pardé coefficients (mean monthly discharge divided by the mean annual discharge) (Pardé, 1933; Spreafico and Weingartner, 2005) for investigated river basins Wasserburg, Basel, Cologne and Würzburg.*

***Table 3.3:*** *Additional climate stations investigated: station name, location (WSG 84), altitude [m], daily resolution time series investigated with temperature (T) and precipitation (P) and data source Federal Office of Meteorology and Climatology of Switzerland (MeteoSwiss).*

| Station | Lat. | Lon. | Alt. | Vari. | Data source |
|---|---|---|---|---|---|
| Sion | 46.2186 | 7.3303 | 482 | T-P | MeteoSwiss |
| Samedan | 46.5264 | 9.8789 | 1709 | T-P | MeteoSwiss |
| Neuchatel | 47.0000 | 6.9533 | 485 | T-P | MeteoSwiss |
| Lugano | 46.0042 | 8.9602 | 273 | T-P | MeteoSwiss |
| Geneve / Cointrin | 46.2475 | 6.1278 | 411 | T-P | MeteoSwiss |
| Chaumont | 47.0492 | 6.9789 | 1136 | T-P | MeteoSwiss |

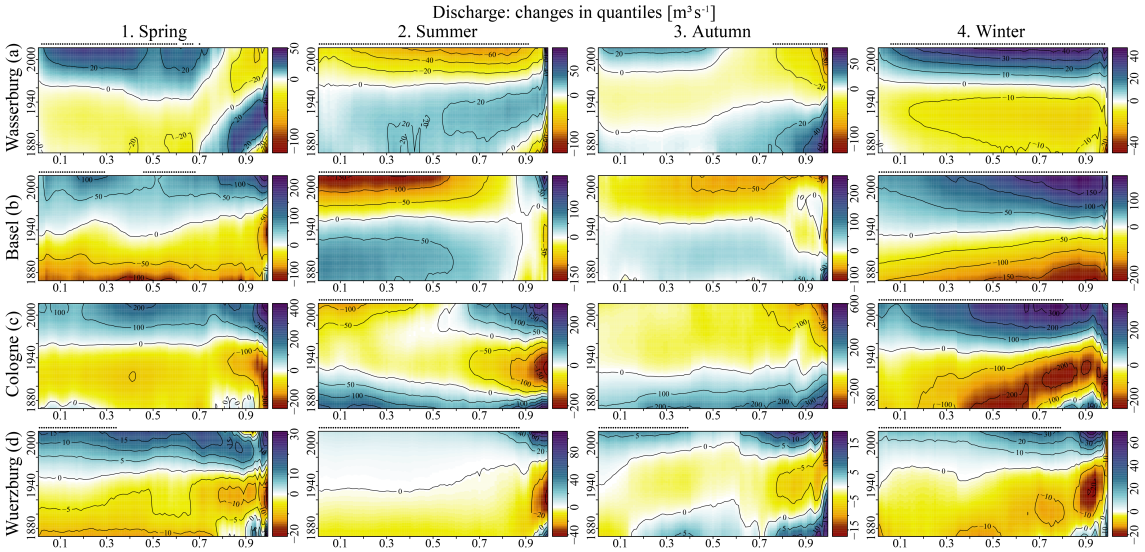


***Figure 3.7:*** *Changes in quantiles for individual seasons (spring: March-May, summer: June-August, autumn: September-November and winter: December-February) for discharge measured at gauges Wasserburg (a), Basel (b), Cologne (c) and Würzburg (d). Points on top of the panels indicate days/probabilities with significant changes according to the Mann-Kendall trend test. Time frame investigated: 1869-2016.*

***Table 3.4:*** *Abbreviations and acronyms in alphabetical order.*

| Abbreviation/Acronym | Description |
|---|---|
| AMO | Atlantic Multidecadal Oscillation |
| CEEMDAN | complete ensemble empirical mode decomposition with additive noise |
| DOY | Day of the year |
| EMD | Empirical mode decomposition |
| EEMD | Ensemble empirical mode decomposition |
| GRDC | Global Runoff Data Centre |
| IMF | Intrinsic mode function |
| MeteoSwiss | Federal Office of Meteorology and Climatology of Switzerland |
| MK | Mann-Kendall trend test |
| NAO | North Atlantic Oscillation |
| QDAY | Quantiles estimated on a daily basis |
| QMOV | Quantiles estimated within moving window |
| QYEA | Quantiles estimated on an annual level |
| RoS | Rain on snow |
| TST | Theil-Sen trend estimator |

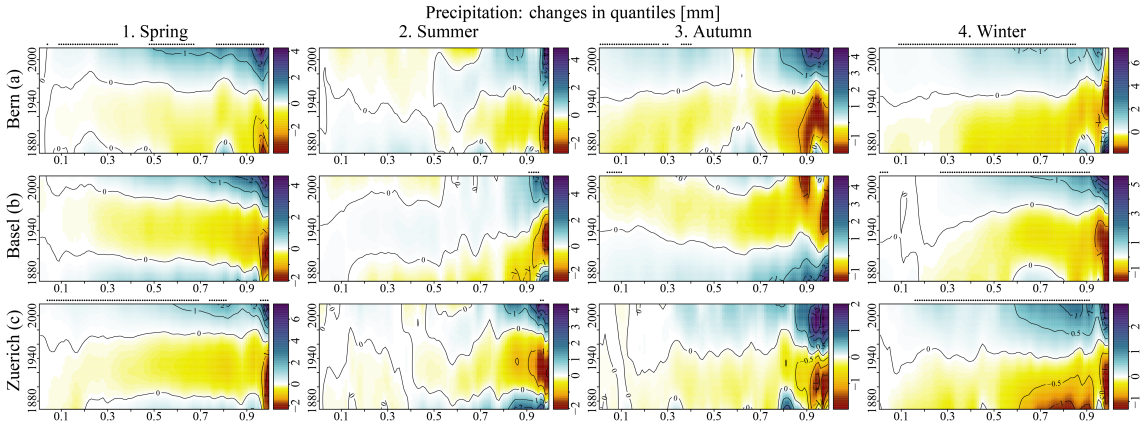


***Figure 3.8:*** *Changes in quantiles for individual seasons (spring: March-May, summer: June-August, autumn: September-November and winter: December-February) for precipitation measured at stations Bern (a), Basel (b) and Zuerich (c). Points on top of panels indicate days/probabilities with significant changes according to the Mann-Kendall trend test. Time frame investigated: 1869-2016.*

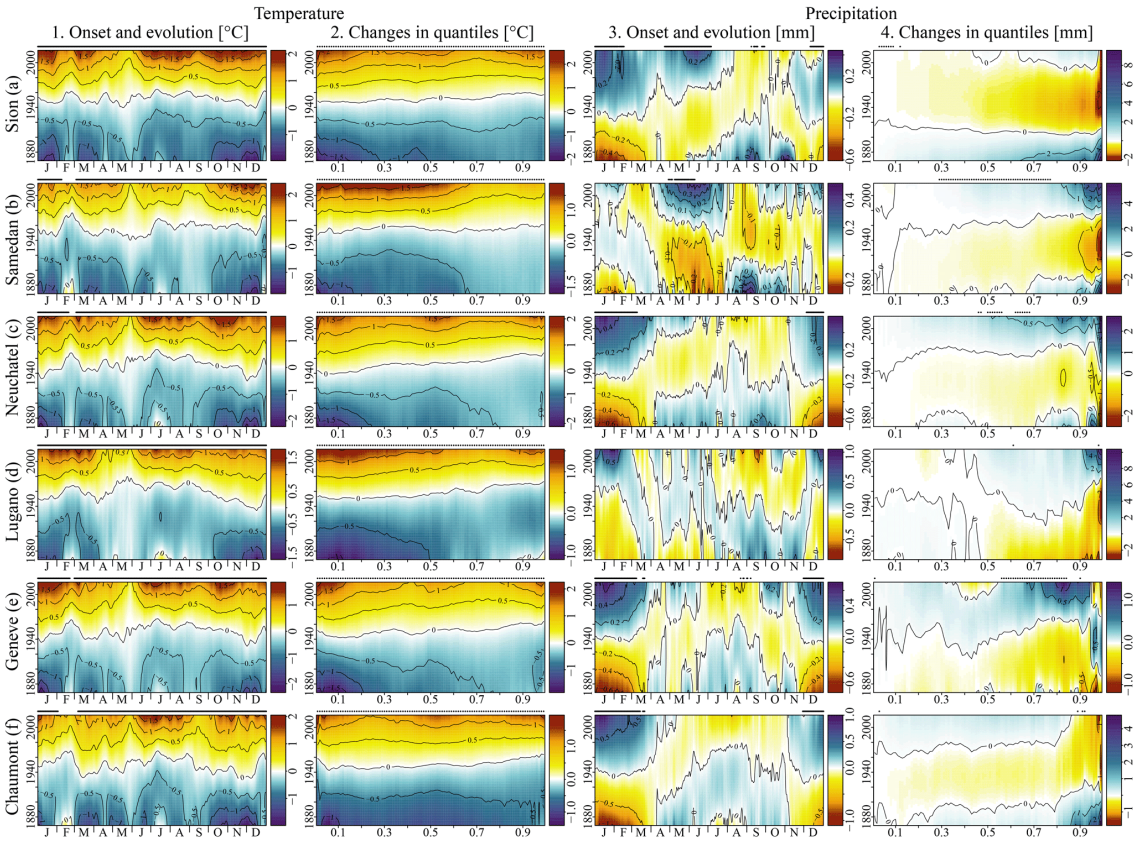


***Figure 3.9:*** *Onset and evolution of changes and changes in quantiles for temperature and precipitation measured at stations Sion (a), Samedan (b), Neuchatel (c), Lugano (d), Geneva (e) and Chamont (f). Points on top of the panels indicate days/probabilities with significant changes according to the Mann-Kendall trend test. Time frame investigated: 1869-2016.*

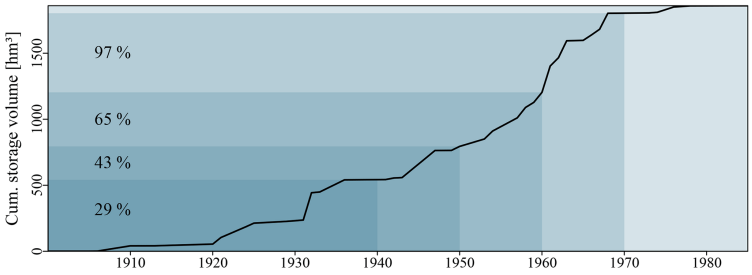


***Figure 3.10:*** *Cumulative storage volume of large storage lakes (active storage volume more than 0.3 hm³) in the High Rhine basin until gauge Basel. The figure is based on information presented in Wildenhahn and Klaholz (1996). Time frame displayed: 1900-1985.*

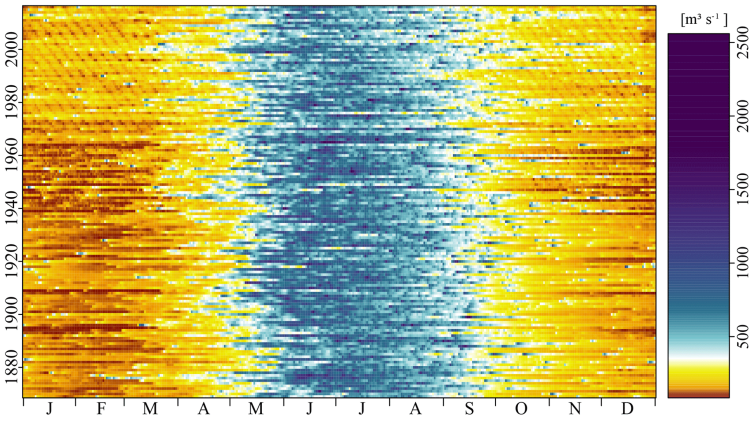


***Figure 3.11:*** *Raster hydrograph for gauge Wasserburg. In recent decades, hydropeaking (weekly pattern) due to the operation of high-head storage hydropower stations imprinted. Time frame displayed: 1869-2016.*

# 4 | Elevation-dependent compensation effects in snowmelt in the Rhine River Basin upstream gauge Basel

Published as: Erwin Rottler, Klaus Vormoor, Till Francke, Michael Warscher, Ulrich Strasser, Axel Bronstert: Elevation-dependent compensation effects in snowmelt in the Rhine River Basin upstream gauge Basel. *Hydrology Research*, nh2021092, https://doi.org/10.2166/nh.2021.092, 2021.

**Keypoints:**

- Impact of rising temperatures on seasonal snowpacks
- Investigations on the point scale for elevation bands and from a catchment perspective
- Threefold effect: snowmelt becomes weaker, occurs earlier and forms at higher elevations
- Meltwater from higher elevations can, at least partly, replace meltwater from elevations below

## Abstract

In snow-dominated river basins, floods often occur during early summer, when snowmelt-induced runoff superimposes with rainfall-induced runoff. An earlier onset of seasonal snowmelt as a consequence of a warming climate is often expected to shift snowmelt contribution to river runoff and potential flooding to an earlier date. Against this background, we assess the impact of rising

temperatures on seasonal snowpacks and quantify changes in timing, magnitude and elevation of snowmelt. We analyse in-situ snow measurements, conduct snow simulations and examine changes in river runoff at key gauging stations.

With regard to snowmelt, we detect a threefold effect of rising temperatures: Snowmelt becomes weaker, occurs earlier and forms at higher elevations. Due to the wide range of elevations in the catchment, snowmelt does not occur simultaneously at all elevations. Results indicate that elevation bands melt together in blocks. We hypothesise that in a warmer world with similar sequences of weather conditions, snowmelt is moved upward to higher elevation. The movement upward the elevation range makes snowmelt in individual elevation bands occur earlier, the timing of the snowmelt-induced runoff, however, stays the same. Meltwater from higher elevations, at least partly, replaces meltwater from elevations below.

## 4.1 Introduction

Alpine landscapes react particularly sensitive towards climatic changes. By the end of the century, glaciers in the European Alps most likely will be gone and seasonal snow packs downsized to a small fraction (Zemp et al., 2006; Horton et al., 2006; Huss, 2011; Fatichi et al., 2014; Gobiet et al., 2014; Beniston et al., 2018b; Hanzer et al., 2018). Cryospheric changes are ongoing and will fundamentally alter river runoff and water availability on regional and global scale (Clow, 2010; Gillan et al., 2010; Stewart, 2009; Viviroli et al., 2011; Laghari et al., 2012; Radić and Hock, 2014).

Snowmelt is an important flood-generating process (Berghuijs et al., 2019; Parajka et al., 2019). In snow-dominated river basins, flooding often occurs during spring and early summer, when high baseflow due to snowmelt overlaps with strong precipitation (Wetter et al., 2011; Vormoor et al., 2015). For Switzerland, changes in mean and extreme regimes in both rainfall- and melt-dominated regions are expected (Addor et al., 2014; Brunner et al., 2019b). Recent studies investigating regional flood discharge trends for Europe indicate that climate change impact on flood timing and frequency is ongoing already (Blöschl et al., 2017, 2019; Bertola et al., 2020).

Studies analysing cryospheric and hydrological climate change impacts often focus on changes in timing and mean annual cycles in relatively small areas, i.e. individual valleys. Seldom, larger catchments covering a wide range of elevations and pre-alpine to high-alpine areas are analysed. So far, only very few studies have resolved changes along the elevation range (e.g. Hunsaker et al., 2012; Kormann et al., 2015). However, in alpine settings, temperature is a function

of both time and elevation. Elevation as additional dimension with regard to changes in snowmelt often receives only little attention.

In this study, we analyse snow observations, conduct snow simulations and analyse discharge records from key gauging stations in the Rhine Basin upstream gauge Basel. We use MODIS snow cover maps to validate our model results. The main goal is to better understand the impact of rising temperatures on alpine snowpacks. We focus on the timing, magnitude and elevation of snowmelt events and assess how changes in snowmelt translate into changes in river runoff.

## 4.2 Study area and data

Study area is the Rhine Basin upstream gauge Basel. The basin covers a total area of $3.59 \cdot 10^4$ km² and an elevation range of almost 4000 m (Fig. 4.1). Gauge Basel is located at 294 m a.s.l. Southern parts of the basin are of high alpine character. Highest mountain peaks reach up to elevations above 4000 m a.s.l. In winter, precipitation often is solid and accumulates in temporary snowpacks. Depending on the elevation, areas are covered by snow for weeks or even months. A considerable fraction of runoff originates from snowmelt (Stahl et al., 2016). In general, elevation is an important factor determining local climatic conditions, vegetation and land use. The basin also encompasses large parts of the Swiss Plateau, hilly to flat areas north of the alpine ridge, which mostly cover elevations between 300 and 1000 m a.s.l. In recent decades, temperatures in the Swiss Alps have been rising at a very fast pace (e.g. Ceppi et al., 2012; Rottler et al., 2019). Studies inter alia hint at changes in forest growth, species distribution and phenology (e.g. Walther et al., 2005; Mietkiewicz et al., 2017; Gehrig-Fasel et al., 2007). Very prominent changes have been observed with regard to glaciers (Zemp et al., 2006; Huss and Farinotti, 2012; Fischer et al., 2014; Beniston et al., 2018b). Strong alteration of runoff due to rising temperatures are expected in glacierized headwater catchments (Huss et al., 2008; Junghans et al., 2011). However, the importance of ice-melt with regard to runoff decreases with the distance to the glacier. At gauge Basel, only 2% of the total annual runoff originate from ice-melt (Stahl et al., 2016). The investigations presented are based on daily records of temperature, rainfall, snow depth and discharge measurements, MODIS snow cover maps, in situ observations of snow water equivalent (SWE), as well as gridded temperature and rainfall data sets.

All station-based meteorological and cryospheric observational data was provided by the Federal Office of Meteorology and Climatology of Switzerland (MeteoSwiss) and the Institute for Snow and Avalanche Research (SLF) from the Swiss Federal Institute for Forest, Snow and Landscape Research (WSL) (Tab. 4.1).

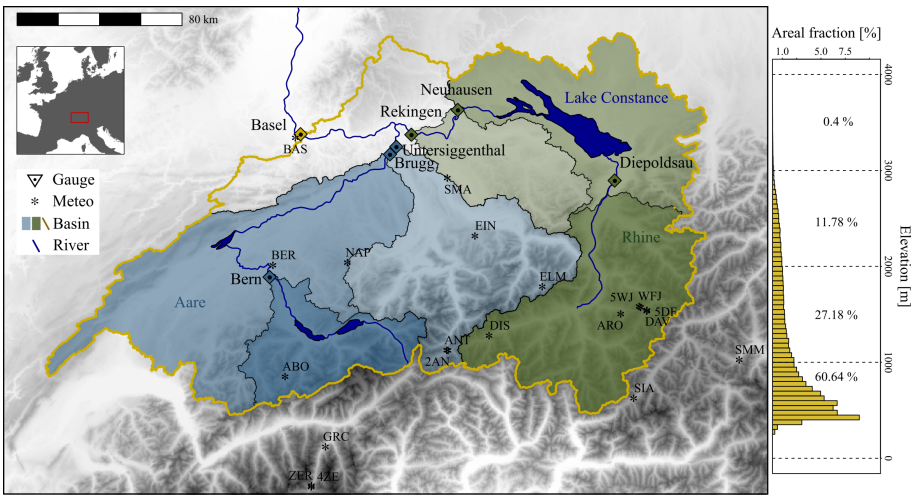


***Figure 4.1:*** *Topographic map of the Rhine Basin upstream gauge Basel (main map) with locations of meteorological stations and nested catchments of the Aare River (Bern-Brugg-Untersiggenthal; blue) and the Rhine River (Diepoldsau-Neuhausen-Rekingen; green) and elevation distribution of the Rhine Basin until gauge Basel (raster cells in 500 m resolution based on EU-DEM v1.1 by the EU Copernicus Programme).*

Discharge times series were obtained from the Global Runoff Data Centre (GRDC). Daily and nearly cloud-free MODIS snow cover maps for the European Alps in a resolution of 250 m and from 2002 onwards were provided by the Institute for Earth Observation, Eurac Research, Bolzano/Bozen, Italy (Matiu et al., 2019, 2020). All data analysis was carried out using the free software R 3.6.1 (R Core Team, 2019).

MeteoSwiss and WSL conduct monitoring and analysis programs for the snowpack in Switzerland at numerous locations. In this study, we focus on a few selected stations. Selected records of snow depth stand out by their length and cover a broad range of elevations, i.e. 555 to 2691 m a.s.l. To examine changes in river runoff, we exert a nested catchment approach in the two main branches of the Rhine River network: the Aare branch (left in Fig. 4.1) and the Rhine branch including Lake Constance (right in Fig. 4.1). The two branches flow together approximately 60 km upstream Basel. The Aare river is the main tributary of the High Rhine. We analyse discharge data from the Aare river recorded at gauges Bern, Brugg and Untersiggenthal. Between gauge Brugg and Untersiggenthal, the two rivers Reuss and Limmat merge with the Aare river increasing the size of the Aare River Basin by about 50 %. The Rhine branch is subdivided into nested basins from gauges Diepoldsau, Neuhausen and Rekingen. The enclosing character of

individual basins enables the backtracking and localisation of changes in runoff. Gridded temperature and precipitation data used to drive snow simulations originate from E-OBS v12 gridded data sets from the European Climate & Dataset (ECA&D) project (Hofstra et al., 2008; Cornes et al., 2018). Within the project "EDgE - End-to-end Demonstrator for improved decision making in the water sector in Europe" by Copernicus, these data were further refined to a 5 km grid using external drift kriging (EDK). EDK addresses altitude effects and provides input data for hydrological modelling at high spatial resolutions (e.g. Zink et al., 2017; Marx et al., 2018; Samaniego et al., 2018a; Thober et al., 2018).

## 4.3 Methods

Our analysis bases on the combination of both observed and modelled data. We analyse changes in snowpacks and snowmelt dynamics and assess the effect of changes in snowpacks on the timing and magnitude of snowmelt-induced runoff. An in-depth analysis of discharge data and governing flood-drivers complements the investigations (Fig. 4.2).

### 4.3.1 Snow observations

In order to get a first insight into observed changes in snowpacks, we display snow observations as raster graphs and determine the mean annual cycle for snow depth and accumulation/melt rates for two time windows: 1958-1987 and 1988-2017. We select the time windows in order to have two 30-year time windows with maximum data availability at individual stations, while keeping a sufficient overlap with the snow simulation period (1951-2014). Enhanced warming since the 1980s strongly affects Swiss snow packs (Laternser and Schneebeli, 2003; Scherrer et al., 2004; Marty, 2008; Philipona et al., 2009; Rottler et al., 2019). By comparing two 30-year windows located before and after the onset of strong changes, we aim to capture signals of change in the snow cover in a robust way. Accumulation/melt rates are calculated as the difference in snow depth between two consecutive days. These mean annual cycles are calculated after applying a 30-day moving average window.

### 4.3.2 Snow simulations: model selection, adaption and verification

We conduct snow simulations in order to extent first insights gained by analysing snow observations. For our study, we need a flexible snow model being able to

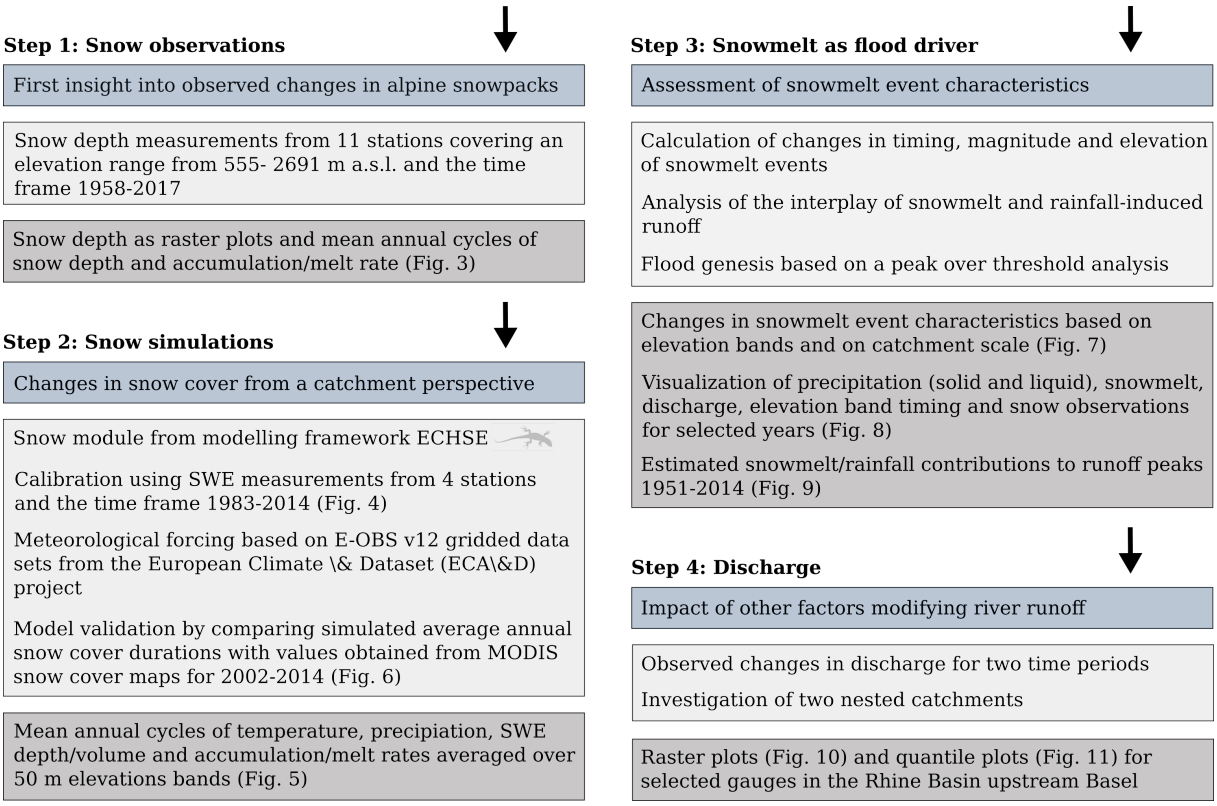


***Figure 4.2:*** *Schematic overview of analytical steps describing main objective, data, methods and visualisation techniques.*

easily operate on spatial scales of several thousand square kilometres and time frames of several decades. Main focus is on the effect of changing temperatures on the timing and magnitude of snowmelt events. As rain-on-snow can be an important driver of high melt rates, the energy input from rainfall needs to be represented. In view of the model requirements, we conduct snow simulations using the energy balance method of the modelling framework ECHSE (Eco-Hydrological Simulation Environment) (Kneis, 2015). In comparison to empirical approaches, physically-based model set-ups allow more detailed investigations of the snow cover processes and offer several possibilities to refine the model set-up if necessary.

ECHSE is an open-source modelling framework developed to facilitate "the rapid development of new, re-usable simulation tools and, more importantly, the safe modification of existing formulations" (Kneis, 2015). The ECHSE environment provides mathematical representations of various hydrological processes, e.g., evapotranspiration, runoff concentration or the dynamics of a snow cover. Recent application of the ECHSE modelling framework include Abon et al. (2016), Kneis

et al. (2017), Pilz et al. (2020). Key feature of ECHSE is its well-documented open source software, which forms the basis for transparent and reproducible studies. In our analysis, we do not build an entire model engine, but focus on the simulation of the Alpine snow cover. The standard ECHSE snow module couples mass and energy balances with snow water equivalent and snow energy content as primary state variables. Snow albedo is considered an auxiliary state variable. The meltwater outflow from the snow pack is computed from available meltwater and the current hydraulic conductivity in the snowpack. A detailed description of the snow module including all equations can be found in Kneis (2014). We use the original functions from the ECHSE online repository written in C++ and conduct simulations in an R environment. In order to avoid instabilities in the melting process, we perform daily snow simulations in 24 intermediate steps, with daily mean temperature input values being disaggregated assuming sinusoidal diurnal temperature variations. Thereby the amplitude was set to 8 °C, and the timing of the maximum value to 14:00 h. Daily precipitation input is equally distributed among all intermediate time steps. An average yearly cycle of global radiation is calculated based on measurements (1981-2017) from the Swiss meteorological station Napf (1404 m a.s.l) and used as radiation input. Values of air pressure, relative humidity, wind speed and cloud coverage currently are assumed constant having values of 1000 hPa, 70 %, 1 m/s and 50 % respectively.

As a first step, we validate the model setup and modifications using measured temperature and precipitation records from meteorological stations and a default parameter set for daily data from two sites in the German low mountain ranges (Kneis, 2014). After ascertaining flawless model operation, we re-calibrate model parameters (see Tab. 4.2) using the particle swarm optimization (PSO) algorithm from the R-package 'ppso' (`https://github.com/TillF/ppso`). This calibration aims to improve model performance by customising parameters to the alpine setting. We employ 5000 model runs and asses model performance using the average root mean square error normalised using the standard deviation of the observations (NRMSE) (Zambrano-Bigiarini, 2017) between simulated and measured snow water equivalent (SWE) for the locations Andermatt, Davos, Zermatt and Weissfluhjoch within the time frame 1983-2014, i.e. maximum overlap of available meteorological input for snow simulations. We use the NRMSE in the attempt to weight stations equally during calibration. We give the NRMSE in percentage. A value of 100% indicates that the RMSE is equal to the standard deviation. In order to facilitate the evaluation of attained values, we also calculate the percentage bias (PBIAS) (Sorooshian et al., 1993) and the Nash-Sutcliffe Efficiency (NSE) (Nash and Sutcliffe, 1970).

Next, we use the resulting parameters and gridded data sets of temperature and precipitation (available for the time frame 1950-2014) to perform snow

simulations for the entire study area upstream gauge Basel. The temperature grid used to drive the simulations was obtained by downscaling from 5 to 1 km resolution using a lapse rate based approach. The lapse rates, i.e, changes of temperature with elevation, were determined for every day individually based on the temperature grid and information on elevation from the EU-DEM v.1.1 by the EU Copernicus Programme (resampled to a resolution of 1 km). Based on the information on temperature and elevation, we calculate lapse rates as linear trends using the Theil-Sen trend estimator (Theil, 1950; Sen, 1968; Bronaugh and Werner, 2013). To downscale temperature to the 1-km-grid, the temperate lapse rates are multiplied by the elevation differences calculated as the difference between the elevation of the 1 km resolution grid cells to the elevation of the respective cell in the 5-km-grid.

In the following, we aggregate results into 50 m elevation bands and calculate annual cycles of mean average and trends in SWE, SWE area volume totals and accumulation/melt rates. Accumulation/melt rates are calculated as difference in SWE volume between two consecutive days. In addition, we asses mean annual cycles and trends for temperature and precipitation. Trends are determined using the Theil-Sen trend estimator (Theil, 1950; Sen, 1968; Bronaugh and Werner, 2013) after applying a 30-day moving average filter. Grid points showing a continuous accumulation of snow over the simulation period were classified as 'glacier points' and not included into this analysis (2.75 % of the data points). In order to validate our modelling approach, we calculate annual average snow cover durations and compare with satellite-based snow cover maps. With regard to snow simulations, areas are considered covered by snow when SWE is equal or exceeds 2 mm. All points classified as 'water body' in more than 90 % of the MODIS maps, where treated as lake surfaces and not included into the analysis.

### 4.3.3 Snowmelt as flood driver

Interested in snowmelt as flood-generating process, we calculate the total snowmelt within a 14-day moving window for all 50 m elevation bands from modelling results, i.e. snowmelt rates, determine the annual maximum ($max14$) thereof and assess the two characteristics timing ($T - max14$) and magnitude ($M - max14$). In addition, we determine the mean elevation of defined $max14$ within a 30-day moving window ($E - max14$). In order to assess changes over time, we compare $max14$ characteristics between the two 30-year time frames 1954-1983 and 1984-2013. We also calculate timing and magnitude of $max14$ on catchment-scale ($T - max14 - C$ and $M - max14 - C$) for the total snow volume in the basin. We assess trend magnitude and significance of these variables using the Theil-Sen trend estimator and the Mann-Kendall trend test (Mann, 1945; Kendall, 1975).

In order to improve our understanding of the interplay between snowmelt-induced runoff and rainfall-induced runoff with regard to the annual maximum runoff events, we take a closer look at the 3-day sums of precipitation and 14-day sums of modelled snow accumulation/melt and visualise these variables along with observed discharge measured at gauge Basel. We differentiate between solid and liquid precipitation following the temperature threshold obtained during model calibration (see Tab. 4.2). In addition, we add information on the timing $T - max14$ for all elevation bands to identify elevations contributing most to the snowmelt. Measurements of snow depth from five selected stations are added to enable an additional visual comparison of snowmelt timing in different elevations. We visualise these variables for selected years. We select years with the aim to give an insight into the different possible interactions between liquid/solid precipitation and the build-up and melt of the seasonal snow cover.

For characterising floods according to their genesis, we use a peak-over-threshold approach: we determine runoff peaks above the 95-percent-quantile observed at gauge Basel for the time window 1951-2014 (i.e. time frame of snow simulations). In order to ensure the independence of detected peaks, two runoff peaks need to be apart at least 14 days. Similar to the approach presented in Vormoor et al. (2016), we distinguish rainfall and snowmelt-driven events by estimating their snowmelt and rainfall contributions based on gridded data. We use the ratio of snowmelt of the preceding 14 days to snowmelt of the preceding 14 days plus liquid precipitation of the preceding 3 days and compare the two time windows 1951-1982 and 1983-2014 for all seasons and for events observed between February and June.

### 4.3.4 Discharge

In addition to changes in snow cover, many other factors can cause changes in runoff in snow-dominated river basins (e.g., the modification of the river network, the construction and operation of reservoirs of high-head hydropower plants or changes in precipitation characteristics). The last step of our analysis aims at setting changes in snow cover in relation to other factors. Therefore, we analyse discharge observations for the simulation period 1951-2014 and an extended time frame 1919-2016. At all gauging stations, continuous daily data is available at least since 1919. The extension of the study period enables the assessment of more robust signals of change less influenced by climate variability. With the aim of getting an overview of runoff seasonality and intra/inter-annual runoff variability, we display discharge measured as raster graphs (Keim, 2000; Koehler, 2004). A horizontal line in the figure represents one year of measured discharge. Furthermore, we calculate quantile discharge values on a monthly level based on

all daily values of a month for the time windows 1951-1982, 1983-2014, 1919-1967 and 1968-2016. These time windows have been chosen to locate two time windows with maximum length in the two time periods investigated, respectively. In the time window 1968-2016, quantiles for the month of January, for example, are based on 49 times 31 daily values. Probability levels investigated range from 0.01 to 0.99. Changes in quantile values between the two investigated time frames are determined by subtracting the value of the older time window from the recent one.

## 4.4 Results

### 4.4.1 Snow observations

Seasonal snowpack characteristics are subject to strong inter-annual variability (Fig. 4.3 a). In recent decades (1988-2018), seasonal snowpacks are diminished at all stations compared to 1958-1988 (Fig. 4.3 b). Our results indicate that accumulation is reduced. Maximum snow depth is often reached earlier in the year already. For stations above 1000 m, a pattern of increased melt rates at the beginning of the snowmelt period and a reduction in maximum melt rates shows up (Fig. 4.3 c). Snowpacks have thawed completely earlier in the year already. Changes in measured snow depth only are an indication for changes in water stored in the snow cover. During compaction of a snowpack, for example, snow depth can decrease, while water content stays the same.

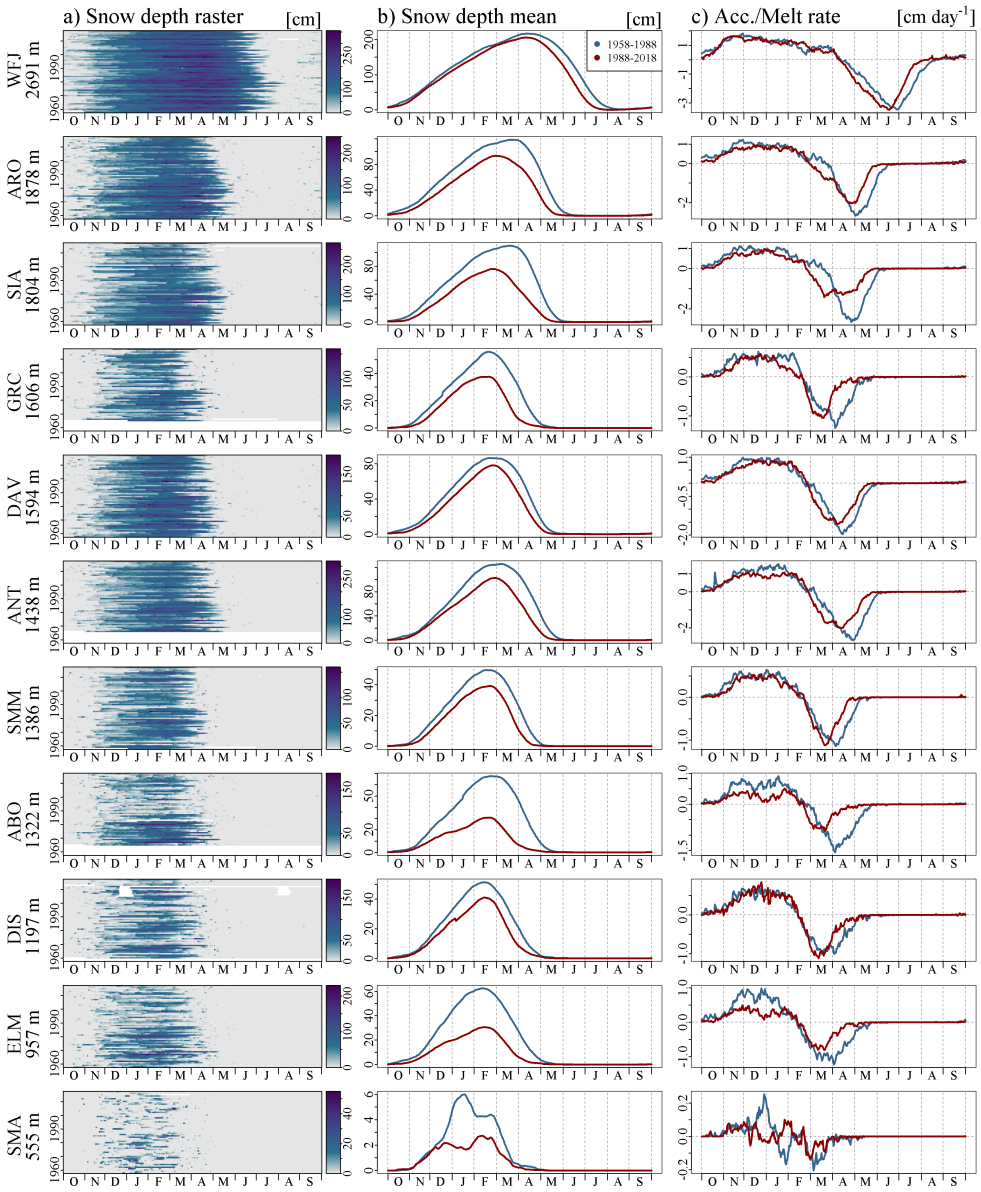


***Figure 4.3:*** *Snow observation from selected stations for the time frame 1958-2018: a) snow depth, b) comparison of mean average annual cycles of snow depth and c) accumulation/melt rates calculated as difference in snow depth between two consecutive days for the two 30-year time windows 10/1958-09/1988 (blue) and 10/1988-09/2018 (red). Mean annual cycles and accumulation/melt rates are computed after applying a 30-day moving average filter. See Table 4.1 for station codes.*

### 4.4.2 Snow simulations: calibration, validation and application of snowpack model

The snow simulations at the point scale indicate that the calibrated snow model captures the dynamic of high alpine snow packs well (Fig. 4.4). The average NRMSE of the four stations is 46 %, the average PBIAS -5.8 % and the NSE 0.78. Both timing of accumulation and melt are in good agreement with observed values. The attained NRMSE indicates that the RMSE is on average less than half a standard deviation of measured values. Furthermore, results indicate that highest SWE values observed at the peak of the snow season tend to be underestimated (e.g. Fig.4.4 c and d). A factor possibly contributing to this uncertainty is a bias in the driving data caused by undercatch of snowfall (Savina et al., 2012) and consequently, reduced precipitation input to the snow simulations.

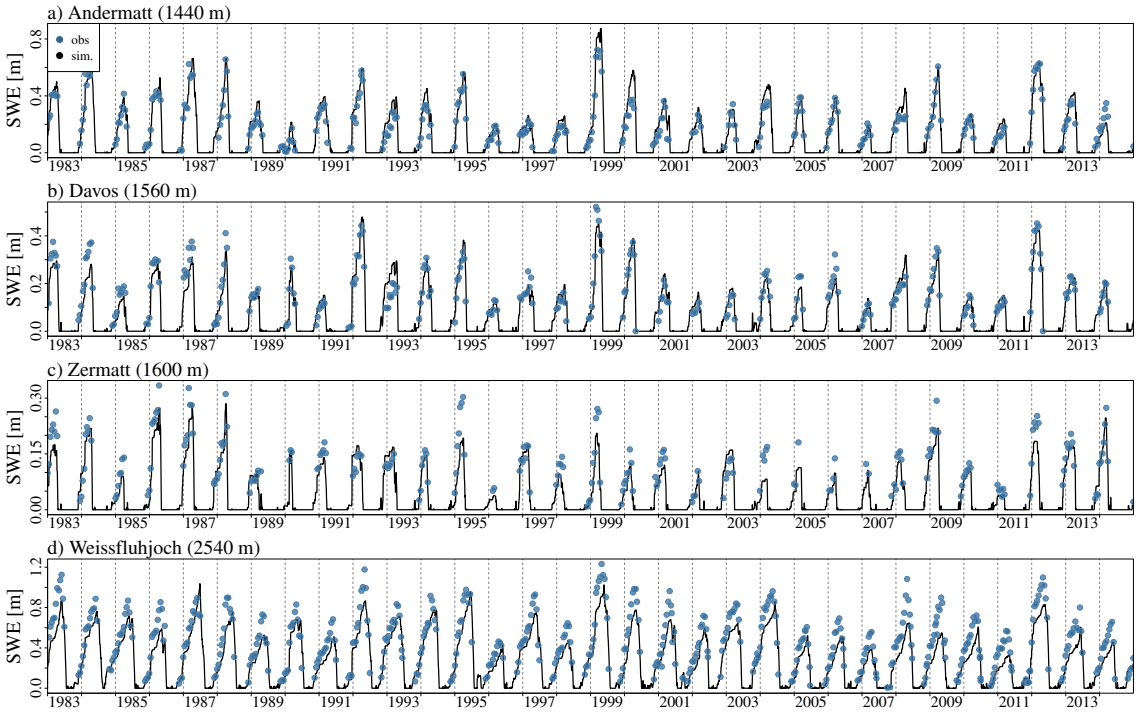


***Figure 4.4:*** *Simulations and measurements of snow water equivalent (SWE) for stations a) Andermatt, b) Davos, c) Zermatt and d) Weissfluhjoch. Time frame investigated: 1983-2014.*

At the catchment scale, SWE depth and snow cover duration increase with elevation (Fig. 4.5 a). Total SWE volume is distributed more uniformly along the elevation range, as the areal fraction an elevation band covers decreases with elevation (Fig. 4.5 c and Fig. 4.1). Similar to results from snow observations, the

simulations indicate that SWE depth and volume is reduced in recent decades, particularly before and during the melt season (Fig. 4.5 b and d). We detect a decline also in snow accumulation for elevation bands below approximately 2000 m. Annual averages and trends in snow melt/accumulation rates, i.e. snow volume changes between two consecutive days, are depicted in Fig. 4.5 e and f. The time window where snow is accumulating widens with elevation (Fig. 4.5 e). At the highest elevation bands investigated, snow is accumulating from October until April. The snowmelt season lasts approximately from February at the lowest elevations to July at the highest elevation. Negative values in Fig. 4.5 f indicate either decreases in accumulation or increases in snowmelt (initial negative values further decrease). Positive values in Fig. 4.5 f, on the other hand, indicate either increases in accumulation or decreases in snowmelt. Simulation results hint at an increase in snowmelt at the beginning of the snowmelt period and at an earlier disappearance of the snow at the end of the melting season. For most part of the year, decreases in snowmelt rates at the end of the snowmelt season (blue diagonal feature in Fig. 4.5 f) coincides with increases from higher elevations. In May, for example, snowmelt rates between approximately 1500 and 2000 m seem to decrease, while snowmelt rates above 2000 m increase. Mean annual cycles of average temperatures point at strong differences in temperature depending on elevation and time of the years (Fig. 4.5 g). Trends in temperature are positive and subject in inter-annual variability (Fig. 4.5 h). With regard to precipitation, increases and decreases in precipitation show up (Fig. 4.5 h).

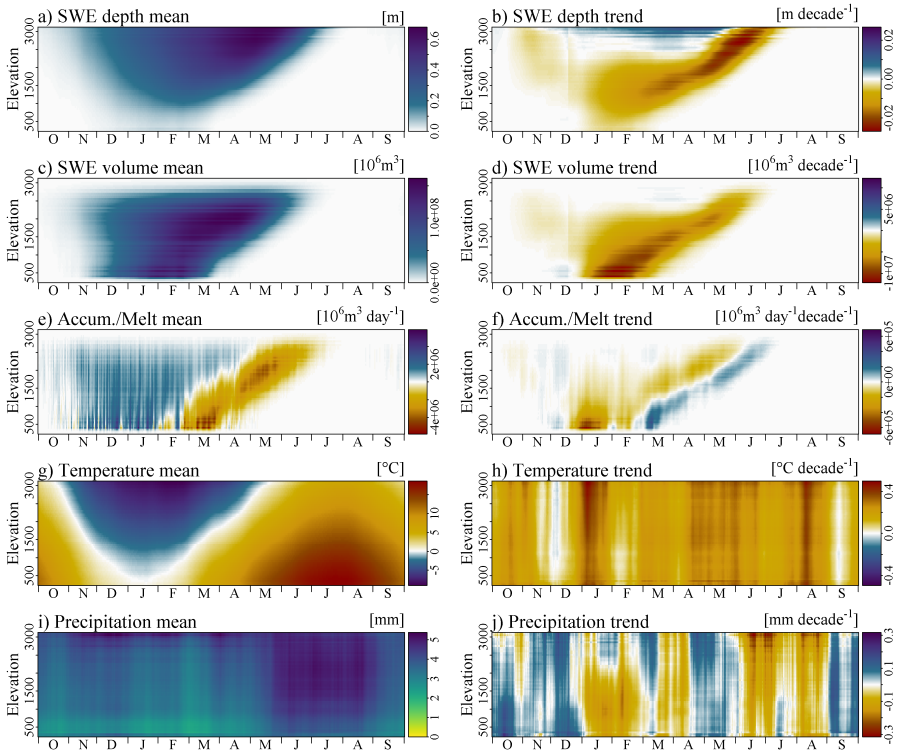


***Figure 4.5:*** *Snow simulation results for the Rhine Basin upstream gauge Basel for the time frame 01/10/1951 - 30/09/2014 aggregated into 50 m elevation bands: a) Mean depth snow water equivalent (SWE), c) mean SWE volume, e) mean SWE volume change, i.e. accumulation/melt calculated as difference in SWE volume between two consecutive days, g) mean temperature, i) mean precipitation, b) trends in SWE depth, d) trends in mean SWE volume, f) trends in average daily SWE volume change, h) trends in temperature and j) trends in precipitation.*

In general, patterns of average annual snow cover duration are similar for simulations and MODIS snow cover maps (Fig. 4.6). The features of the terrain reflect in the duration of the seasonal snow cover. On the Swiss Plateau and on the valley bottoms, there are only few days with snow cover. On the other hand, the high alpine parts are characterised by a short snow-free period. However, differences show up, particularly for two types of areas: 1) In very high elevations, particularly in glaciated areas, satellite-based maps show more days with snow cover, and 2) in the valleys of the Alpine Rhine in the South-East; the satellite-based maps show less days with snow cover as compared to the simulation results.

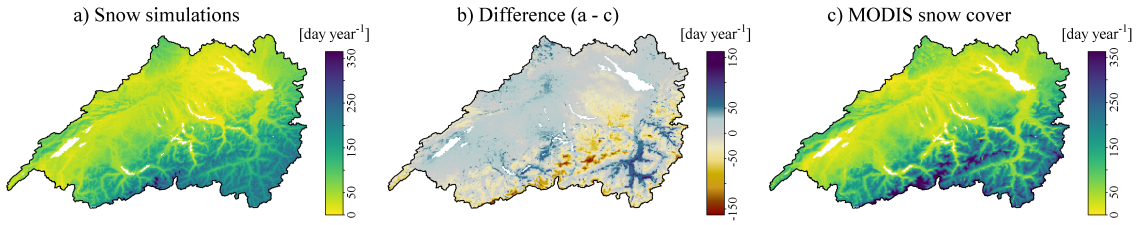


***Figure 4.6:*** *Average annual snow cover duration a) simulated and c) based on daily MODIS snow cover maps (Matiu et al., 2020). The difference between (a) and (c) is depicted in (b). Time frame investigated: 01/08/2002 - 31/07/2014.*

### 4.4.3 Snowmelt as flood driver

In recent decades, $max14$ events occur earlier in the year and are weaker in magnitude (Fig. 4.7 c). Comparing $E - max14$ for the two 30-year time frames 1954-1983 and 1984-2013, our results suggest a shift upward the elevation range by about 170 m. On the basin scale, our analysis shows a wide temporal spread of $max14$ ranging from February to June (Fig. 4.7 c). No significant change in timing ($T - max14 - C$) nor magnitude ($M - max14 - C$) can be detected.

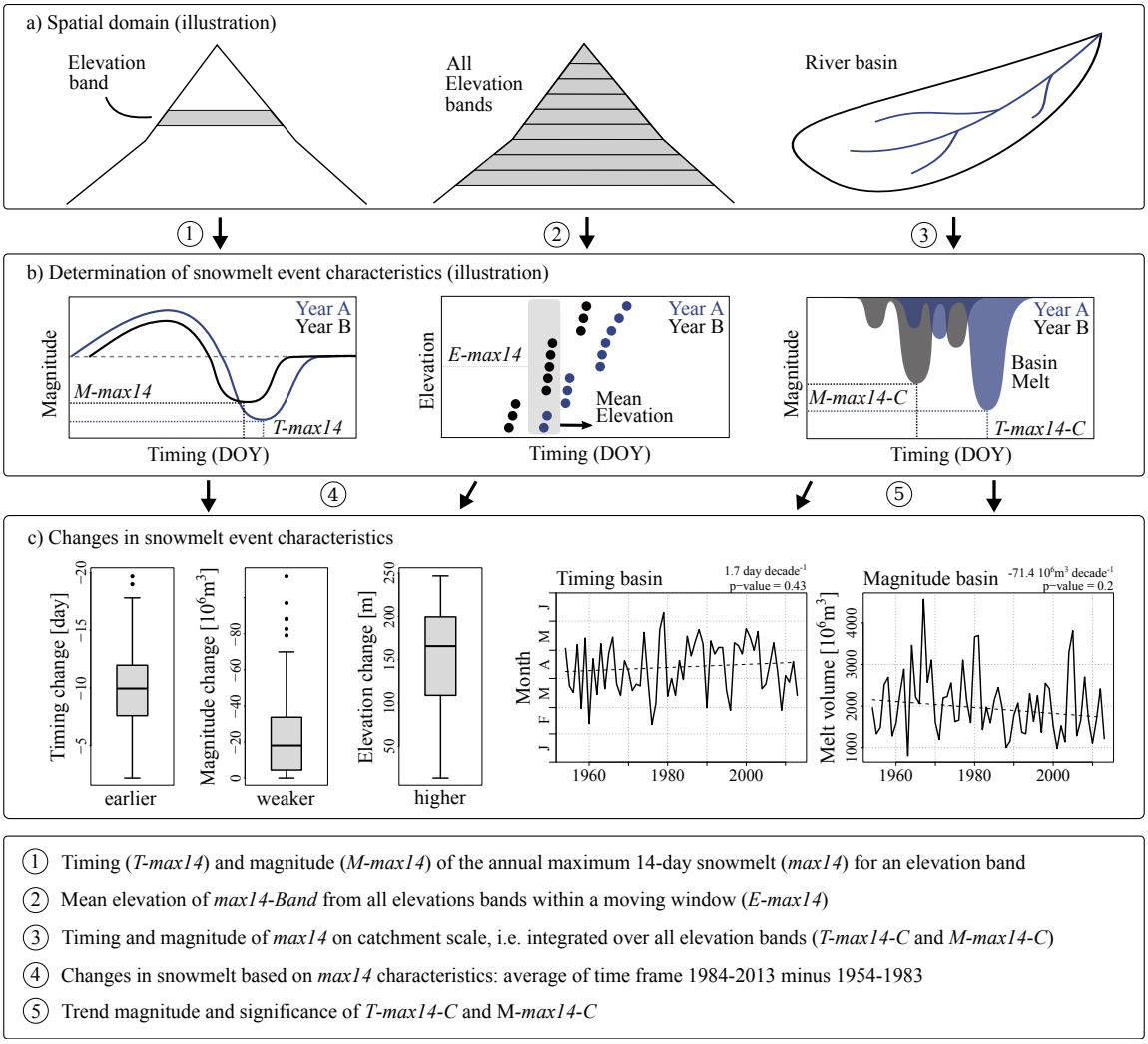


***Figure 4.7:*** *Determination of snowmelt event characteristics for elevation bands and on catchment scale: a) Spatial domains, b) Illustrations of the determination of snowmelt event characteristics and c) changes in snowmelt event characteristics based on model simulations. Numbers 1 to 5 describe analytical steps taken.*

Fig. 4.8 describes the interplay of precipitation and snowmelt with regard to the annual runoff maximum for four selected hydrological years. In the year 1969/1970, the highest discharge value is observed at the end of February after strong, mainly liquid, precipitation in the basin (Fig. 4.8 a). According to the model results, a part of the precipitation input is solid and stored in temporary snow packs ( 23 %). Our results indicate that the runoff event is exclusively rain-fed, no snowmelt is contributing. In the year 1978/1979, the annual runoff maximum is recorded in June. Rainfall-induced runoff overlaps with high baseflow

due to snowmelt from high elevations (Fig. 4.8 b). In the two years 1980/1981 and 1987/1988, the annual runoff maximum is recorded in March (Fig. 4.8 c and d). In March 1981, strong snowmelt from low elevations overlaps with a moderate rainfall event. In March 1988, heavy precipitation is the main driver of the runoff peak observed. A part of the rainfall is stored in high elevation snowpacks. The temporarily stored water is released in the following months. Snowmelt from low elevations (below 1000 m a.s.l.), on the other hand, seems to contribute to the observed runoff peak.

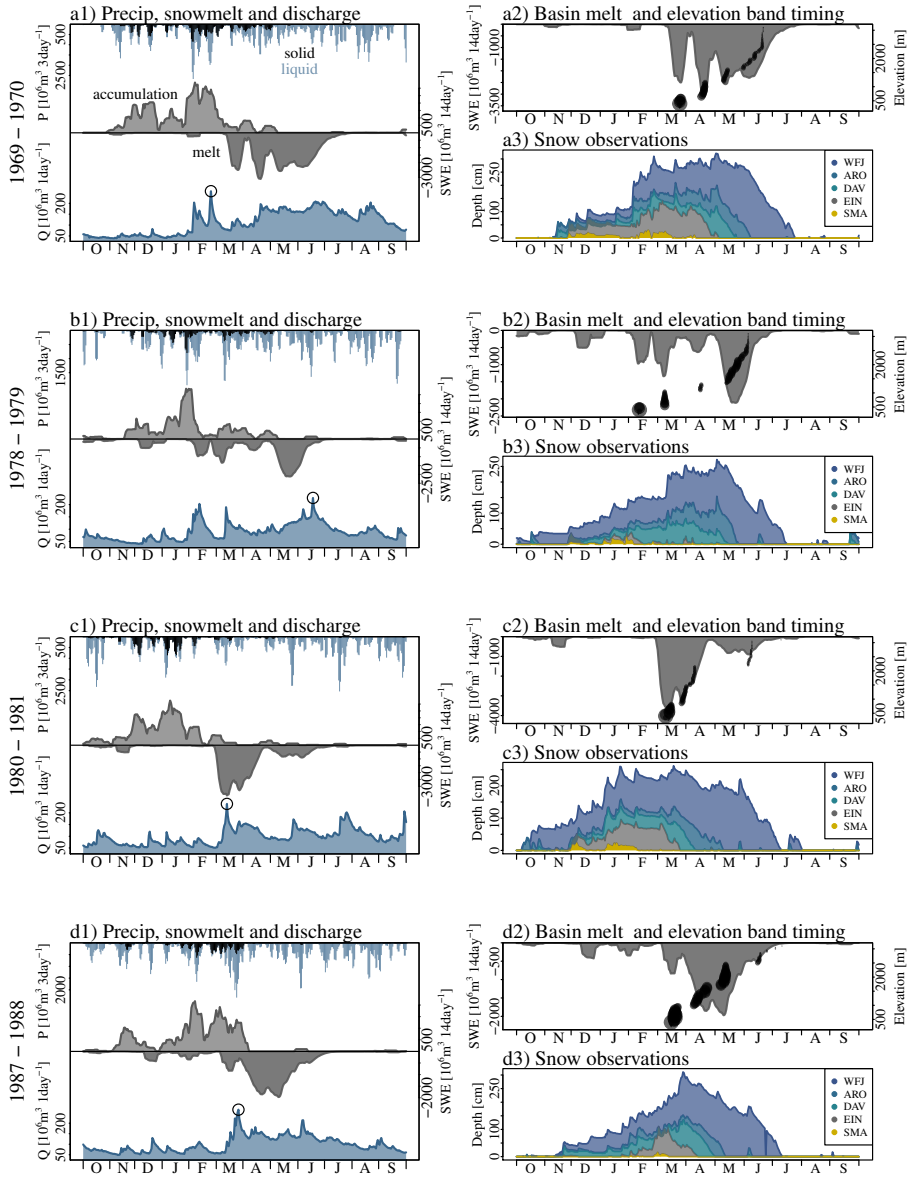


***Figure 4.8:*** *Simulated snowmelt dynamics and corresponding measured discharge for four selected years in the Rhine Basin until gauge Basel: 1) 3-day moving window sum of precipitation (black/blue indicating solid/liquid precipitation), 14-day moving window sum of snow accumulation/melt (grey) and daily discharge measured at gauge Basel with circles indicating annual runoff maxima, 2) total 14-day moving window sum of snowmelt (grey) with black dots indicating the timing of max*14 *(point size in proportion to magnitude of melt event) and 3) snow depth measurements from stations Weissfluhjoch (WFJ - 2691 m), Arosa (ARO - 1878 m), Davos (DAV - 1594 m), Einsiedeln (EIN - 957 m) and Zuerich (SMA - 555 m) (areas between two successive stations coloured according to higher elevated station). Years displayed: a) 1969/1970, b) 1978/1979, c) 1980/1981 and d) 1987/1988.*

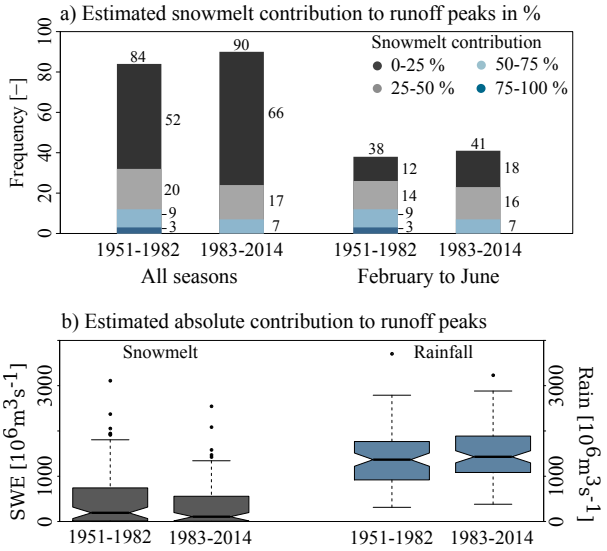


***Figure 4.9:*** *Frequency of discharge peaks above the 95-percent-quantile observed at gauge Basel for the time frame 1951-2014 (two peaks at least fourteen days apart): a) Events classified according to the ratio of snowmelt of the preceding 14 days and snowmelt of the preceding 14 days plus precipitation the preceding 3 days and b) magnitudes of total 14-day snowmelt and 3-day liquid precipitation preceding the detected runoff peaks. Time windows compared: 1951-1982 and 1983-2014.*

In total, we detect 174 independent discharge peaks above the 95th percent quantile at gauge Basel for the time frame 1951-2014 (Fig. 4.9). With regard to the events of all seasons, precipitation is the dominant flood-generating process. Between the months February to June, snowmelt-induced runoff is more important compared the whole year. Our results indicate that for the time window February and June, 49 out of the 79 detected events for the time frame 1951-2014 potentially have snowmelt contributions of more than 25%. The total number of events and the number of precipitation-dominated events increases in the more recent time frame (1983-2014) with regard to both 'All seasons' and 'February to June'. This overall increase goes along with a decrease in snowmelt contribution to detected events. The number of discharge peaks with potential snowmelt contributions of >50% decreases from 12 to 7. Absolute contributions of snowmelt/rainfall tend to decrease/increase (Fig. 4.9 b).

### 4.4.4 Discharge

Seasonal snowpacks are an important factor redistributing runoff from winter to summer at all gauges investigated (Fig. 4.10). Runoff seasonality is most pronounced in the alpine part of the catchment (Fig. 4.10 f and g). A strong weekly pattern of reservoir operations for hydropower production with higher runoff during weekdays than on the weekend is imprinted at gauge Diepoldsau since the 1960s ('dashed pattern' in Fig. 4.10 g).

In the Rhine branch including Lake Constance, our results hint at a decrease in runoff during summer (Fig. 4.11 a5, a6, a7, b5, b6 and b7). At the same time, runoff increases during winter and spring. In the Aare branch including gauges Bern, Brugg and Untersiggenthal, decreases in runoff during summer seem to be less pronounced (Fig. 4.11 a1, a2, a3, b1, b2 and b3). The most prominent signal in the Aare branch arises at gauge Brugg: High runoff values increase from the beginning of spring until the beginning of summer (Fig. 4.11 a3 and b3). At gauge Basel, signals from the two branches overlap and a general redistribution of runoff from summer to winter superimposes with increases in high runoff values from spring until the beginning of the summer (Fig. 4.11 a1 and b1). With increasing length of the time windows, patterns showing up get more stable and differences between neighbouring quantiles and months are less abrupt.

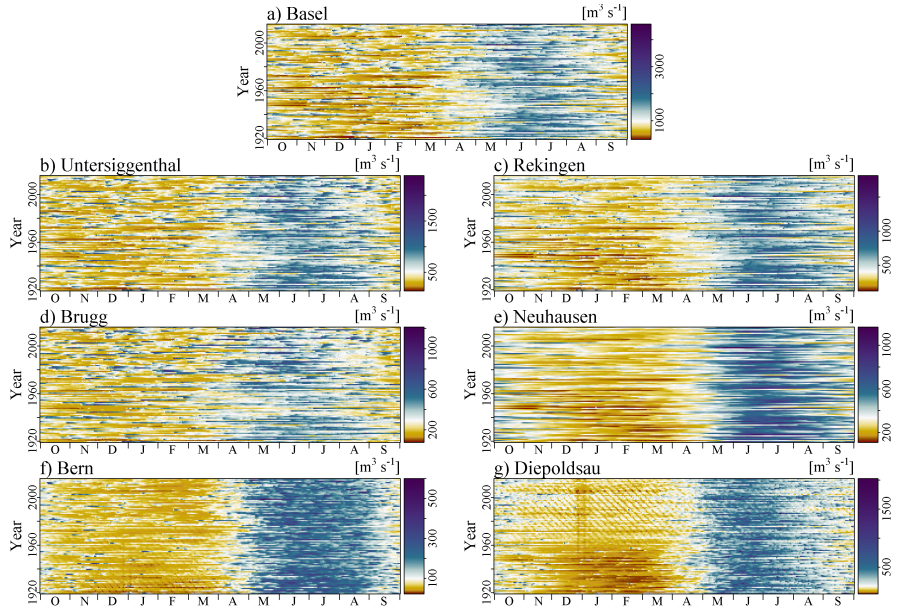


***Figure 4.10:*** *Raster plots for discharge for the time frame 1919-2016 for river gauges a) Basel, b) Untersiggenthal, c) Rekingen, d) Brugg, e) Neuhausen, f) Bern and g) Diepoldsau. Left (b, d and f) and right (c, e and g) column, respectively, represent nested catchments of the Aare and Rhine River, which merge upstream gauge Basel.*

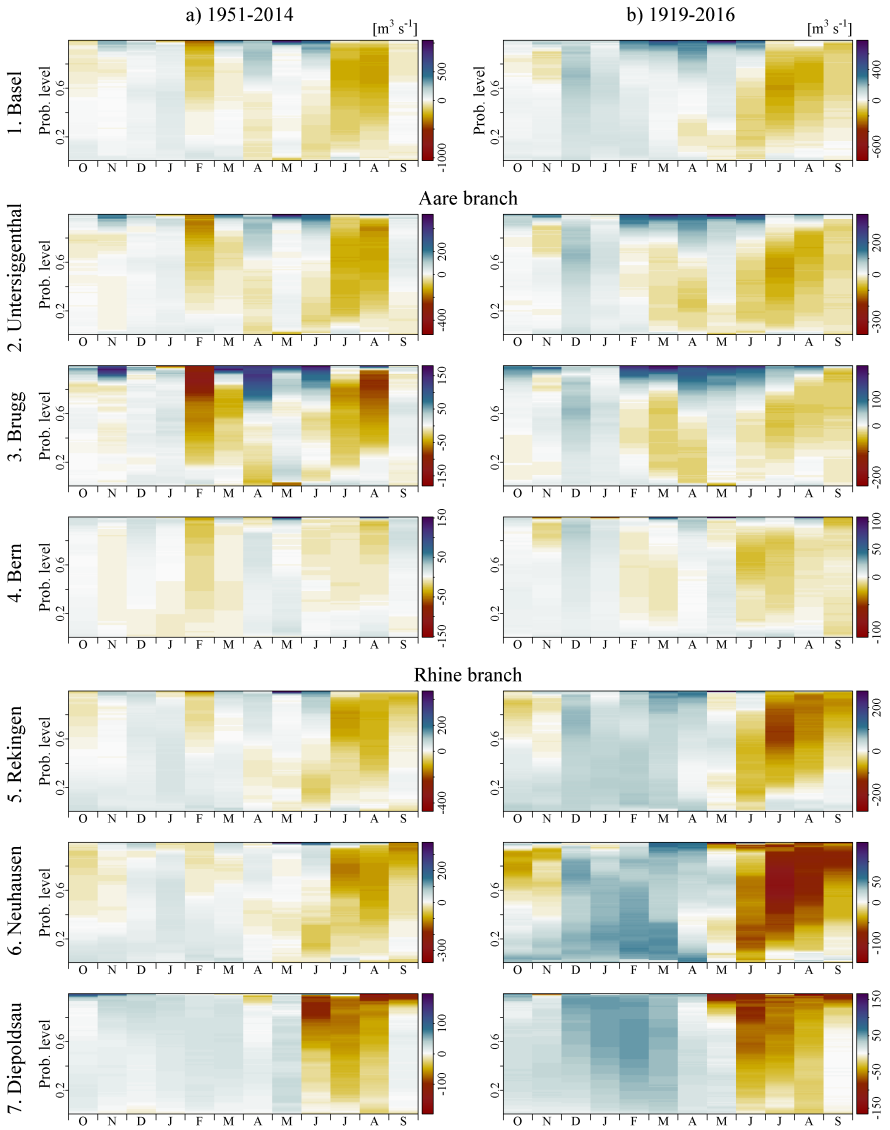


***Figure 4.11:*** *Changes in runoff quantiles from the time window a) 1951-1982 to 1983-2014 and b) 1919-1967 to 1968-2016 for probability levels 0.01 to 0.99 determined with all daily runoff values of a month (quantile value of the earlier time window subtracted from the recent time window). Stations investigated: 1. Basel, 2. Untersiggenthal, 3. Brugg, 4. Bern, 5. Rekingen, 6. Neuhausen and 7. Diepoldsau. Stations 2, 3 and 4 and stations 5, 6 and 7, respectively, represent nested catchments of the Aare and Rhine River, which merge upstream gauge Basel.*

## 4.5 Discussion

### 4.5.1 Snowmelt events characteristics

Rising temperatures reduce seasonal snow packs (Fig. 4.3 and 4.5) (Laternser and Schneebeli, 2003; Scherrer et al., 2004; Marty, 2008; Marty and Blanchet, 2012; Klein et al., 2016). The effects seem most pronounced at elevations below 2000 m. In those elevations, our simulation results hint at strong decreases during both snow accumulation and snowmelt (Fig. 4.5 b and d). In addition, we detect indications of potential elevation-dependent compensation effects for parts of the year (approximately March to June) (Fig. 4.5 f).Increases/decreases in meltwater outflow seem to be partly compensated by changes in meltwater from the snow cover from elevations below/above. The reduction in seasonal snowpacks goes along with decreases in maximum melt rates (Fig. 4.7 c). Detected changes go along with results from Musselman et al. (2017), who indicate that a "shallower snowpack melts earlier, and at lower rates, than deeper, later-lying snow-cover" and "that the fraction of meltwater volume produced at high snowmelt rates is greatly reduced in a warmer climate".

According to our analysis, rising temperatures do not just decrease the maximum melt rates, we identify a threefold effect: Snowmelt becomes weaker, occurs earlier and originates from higher elevations (Fig. 4.7 c). If we refer to a fixed location (e.g., at an observational site) we can detect the shift forward in time. Conversely, if looking at a fixed time of year, the location of the melt event (i.e. contributing elevation bands) moves upward the elevation range (Fig. 4.12 a).

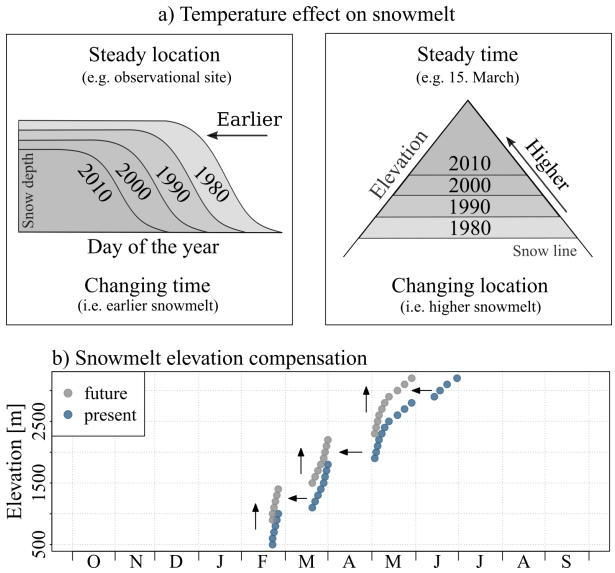


***Figure 4.12:*** *Idealised effects of rising temperatures on snow cover: a) earlier and higher snowmelt and b) idealised change in elevation-dependent contribution to snowmelt with points indication elevation bands mostly contributing to snowmelt. Arrows indicate shifts forward in time and upward the elevation range, respectively.*

### 4.5.2 Snowmelt as flood driver

In the Rhine Basin upstream gauge Basel both snowmelt and precipitation seem to be important flood-drivers. Even moderate precipitation events can cause the annual runoff maximum, when superimposing with snowmelt-induced runoff (e.g., Fig. 4.8 c). Investigations of snow observations and snow simulations demonstrate that snowmelt-induced runoff originates from a wide range of elevations. However, due to this wide elevation range, snowmelt does not occur simultaneously at all elevations. Our results indicate that elevation bands commonly melt together in blocks (Fig. 4.8 a2, b2, c2 and d2). The beginning and end of a snowmelt event occurring in the basin, seems to be determined by the passage of warm air masses, the respective elevation range affected by accompanying temperatures and snow availability. We hypothesise that in a warmer climate with similar sequences of weather conditions, snowmelt is moved up to higher elevation, i.e. the block of elevations bands contributing most to the snowmelt-induced runoff is located at higher elevations (Fig. 4.12 b). The movement upward the elevation range makes snowmelt in individual elevation bands (e.g., $T - max14$ within an elevation band) occur earlier, the timing of the snowmelt-induced runoff, however,

stays the same. Snowmelt from higher elevation might, at least partly, replaces meltwater from lower elevations. Investigating five peak discharge events in the mountain river basin of the Merced River in California, US, Biggs and Whitaker (2012) were able to show that for each discharge peak, between 60% to 80% of the snowmelt originated from elevations that only covered between 22% and 38% of total basin relief. They refer to the elevations contributing most to a runoff event as the 'critical zone'.

### 4.5.3 Role of precipitation

The analysis of the annual runoff maximum of the hydrological year 1969-1970 indicates in an exemplary way, how precipitation alone can cause high runoff values (Fig. 4.8 a). According to our analysis, no snowmelt is contributing to the runoff peak. On the contrary, part of the precipitation is solid and stored in temporary snowpacks. The accumulation of snow reduces the effective precipitation, i.e. precipitation translating into river runoff. In the following, we will refer to this effect of partial storage of precipitation in snowpacks as protective effect of snow accumulation. Strong precipitation events do not have an immediate effect, when their water is stored in snowpacks. However, with rising temperatures, the snowline moves upward and larger fractions of the basin potentially receive liquid precipitation (Barnett et al., 2005; Scherrer and Appenzeller, 2006; Allamano et al., 2009a,b; Kormann et al., 2015; Beniston et al., 2018b). Hence, in a warmer climate, the protective effect of snow accumulation is reduced. Effective precipitation might increase. A simple calculation supports this notion: Without the protective effect (all precipitation liquid), the cold season (October until March) annual maxima 3-day rainfall events would have been stronger by 11.4 % on average in our simulations. Recent studies point at the increasing importance of rainfall-induced runoff with regard to flooding in catchments influenced by a seasonal snow cover (e.g. Middelkoop et al., 2001; Addor et al., 2014; Vormoor et al., 2016; Brunner et al., 2019b; Rottler et al., 2020). Our analysis of runoff peaks observed at gauge Basel further supports these investigations (Fig. 4.9). The number of runoff peaks with mostly precipitation as flood-driver tends to increase, while at the same time, events with a majority of snowmelt-induced runoff decreases.

With the analysis of observed discharge, we complete our analysis by assessing changes induced by other factors. The extension of the time frame back to 1919, beyond the simulation period, helps to reduce the impact of inter-annual to decadal climate variability, e.g., due to varying frequencies of weather types (Rottler et al., 2019). We attribute detected increases in high runoff values during spring and early summer (Fig. 4.11) to variations in rainfall characteristics. The nested catchment approach indicates, that increases in high runoff values

during spring and early summer are most prominent at gauge Brugg, whose catchment covers large parts of the Swiss Plateau and whose discharge is strongest influenced by rainfall-induced runoff compared to the other gauges investigated. Another factor having strong impact on the runoff in Rhine River basin upstream gauge Basel, are the numerous large reservoirs that have been constructed for hydropower production during the course of the 20th century (e.g. Wildenhahn and Klaholz, 1996; Bosshard et al., 2013). In the Alpine Rhine Basin until gauge Diepoldsau, for example, the total storage volume is about 10% of the total annual runoff (Bosshard et al., 2013). The redistribution of water from summer to winter and a weekly pattern with high/low discharge on weekdays/weekends, are well known effects of reservoir operations (Fig. 4.10 g) (Verbunt et al., 2005; Belz et al., 2007; Meile et al., 2011; Pérez Ciria et al., 2019; Rottler et al., 2020).

### 4.5.4 Model performance and limitations

We are confident that our modelling approach enables investigations of snow cover changes. Temporal dynamics and absolute values have been reproduced for the stations, patterns realistically generated on the catchment scale. Elevation-dependent differences in snowpack characteristics are represented well. However, our modelling approach includes several assumptions and simplifications that require caution and limit the explanatory value of our simulations. In the framework of our snow model, we do not address changes in incoming solar radiation. Instead, the simple mean annual cycle we use as input inter alia does not supply information on recent regional brightening effects (Norris and Wild, 2007; Ruckstuhl et al., 2008; Ruckstuhl and Norris, 2009; Duethmann and Blöschl, 2018). Thus, our modelling set-up is solely driven by variations and changes in temperature and precipitation. However, the energy-based concept enables us to address energy input during rain-on-snow events, which is a phenomenon poorly reflected by empirical approaches. Rain-on-snow is an important flood-generating process in upland basins (e.g. Freudiger et al., 2014; Rössler et al., 2014; Sui and Koehler, 2001). The current modelling set-up does not include redistribution of snow by wind or avalanches (e.g. Freudiger et al., 2017; Warscher et al., 2013; Kerr et al., 2013; Musselman et al., 2015). Missing redistribution processes increase the uncertainty with regard to snow volume distribution along the elevation range. Furthermore, aspect and slope can be important parameters controlling snow accumulation and snowmelt.

With regard to the detected differences between simulated annual snow cover durations and MODIS snow cover maps, we identify several possible factors contributing to these differences: First, the current model setup does not resolve very high elevations. The resolution of 1 km in combination with the simple

lapse rate-based approach to downscale temperature does not capture the highest elevations in the basin. Likewise, it introduces a smoothing effect to the very low-lying cells, resulting in an overestimation of snow cover there. In addition, we suspect the precipitation input is not capturing the full altitudinal gradient. It seems that climatic conditions, particularly in the valley bottoms in the South-East are not well captured in the meteorological input used to drive the snow simulations. Precipitation patterns seem too coarse to capture the strong differences over short distances in this complex terrain (Freudiger et al., 2016). In addition, the parameters fitted for the observations at the four snow gauges possibly do not capture the entire range of conditions in the basin. Particularly the snow simulated in the comparatively dry valleys in the South-East and in the highest altitudes might need an adapted set of parameters to describe its properties more accurately.

## 4.6 Conclusions

We analyse snow and discharge observations and simulate the Alpine snow cover in order to get a better understanding of how changes in snowmelt timing translate into changes in river runoff. Focus of the study is the Rhine River Basin upstream gauge Basel. We are confident that the physically-based snow model set-up used represents the snow cover dynamics in the basin well. However, several assumptions and simplification advice caution, most importantly the lapse-rate based approaches applied to downscale gridded temperature input, simple seasonal cycle used as radiation input and the neglect of snow redistribution processes.

Our results point at strong decreases in seasonal snow packs in recent decades. With regard to snowmelt events, we detect a threefold effect of rising temperatures: Snowmelt becomes weaker, occurs earlier and forms at higher elevations (Fig. 4.7 c). Investigations on the catchment scale indicate that snowmelt-induced runoff can originate from a wide range of elevations. Due to the wide range of elevations covered in the basin, snowmelt does not occur simultaneously at all elevations. Elevations bands rather melt together in blocks (Fig. 4.8). The beginning and end of the release of meltwater seems to be determined by the passage of warm air masses, the respective elevation range affected by accompanying temperatures and snow availability. We hypothesise that in a warmer world with similar sequences of weather conditions, snowmelt is moved upward to higher elevations, i.e. the block of elevation bands providing most water to the snowmelt-induced runoff is located at higher elevations (Fig. 4.12 b). The movement upward the elevation range makes snowmelt in individual elevations bands occur earlier, the timing of

the snowmelt-induced runoff, however, stays the same. Meltwater from higher elevations, at least partly, replaces meltwater from elevations below.

Furthermore, our analysis points at the protective effect of snow accumulation with regard to flooding. Precipitation in form of snow in part of the catchment reduces the effective precipitation, i.e. precipitation directly translating into river runoff. With rising temperatures, the snowline moves upwards and an increased fraction of the precipitation possibly is liquid instead of solid (Scherrer and Appenzeller, 2006; Allamano et al., 2009b; Vormoor et al., 2015). The analysis of discharge time series enabled the assessment of other factors modifying river runoff, i.e. more intense rainfall increasing high runoff quantiles in spring and early summer and the construction of reservoirs for hydropower production redistributing runoff from summer to winter (Meile et al., 2011; Bosshard et al., 2013; Pérez Ciria et al., 2019; Rottler et al., 2020).

This study represents a further step towards understanding how changes in alpine snowpacks translate into changes in river runoff. Future studies need to further investigate the proposed hypotheses describing elevation-dependent compensation effects. Investigations using meso-scale hydrological modelling frameworks in combination with satellite-data derived snow cover maps seem predestined for such a task.

## Acknowledgements

We thank the Federal Office of Meteorology and Climatology of Switzerland (MeteoSwiss), the Institute for Snow and Avalanche Research (SLF) from the Swiss Federal Institute for Forest, Snow and Landscape Research (WSL), the Institute for Earth Observation, Eurac Research and the Global Runoff Data Centre, 56068, Koblenz, Germany (GRDC) for providing meteorological, snow cover and hydrological data, respectively. We acknowledge the datasets generated in the EDgE proof-of-concept project performed under a contract for the Copernicus Climate Change Service (http://edge.climate.copernicus.eu, last access: 27 October 2020). ECMWF implements this service and the Copernicus Atmosphere Monitoring Service on behalf of the European Commission.

## Funding

This research was supported by the Deutsche Forschungsgemeinschaft (GRK 2043/1-P2) within the NatRiskChange research training group at the University

of Potsdam.

## Data availability statement

Data cannot be made publicly available readers should contact the corresponding author for details.

# Appendix

***Table 4.1:*** *Data base studied: Station ID, station name, location (WGS 84), altitude [m], daily resolution time series investigated with snow depth (SD), snow water equivalent (SWE), discharge (D), temperature (T), precipitation (P) and radiation (R) and data source with Federal Office of Meteorology and Climatology of Switzerland (MeteoSwiss), Institute for snow and avalanche research (SLF) from the Swiss Federal Institute for Forest, Snow and Landscape Research and Global Runoff Data Centre (GRDC).*

| ID | Station | Lat. | Lon. | Alt. | Vari. | Data source |
|---|---|---|---|---|---|---|
| WFJ | Weissfluhjoch | 46.8333 | 9.8000 | 2691 | SD-T-P | MeteoSwiss |
| ARO | Arosa | 46.8000 | 9.6833 | 1878 | SD | MeteoSwiss |
| SIA | Segl-Maria | 46.4333 | 9.7666 | 1804 | SD | MeteoSwiss |
| ZER | Zermatt | 46.0292 | 7.7531 | 1638 | T-P | MeteoSwiss |
| GRC | Graechen | 46.2000 | 7.8333 | 1606 | SD | MeteoSwiss |
| DAV | Davos | 46.8166 | 9.8500 | 1594 | SD-T-P | MeteoSwiss |
| ANT | Andermatt | 46.6333 | 8.5833 | 1438 | SD-T-P | MeteoSwiss |
| SMM | Sta. Maria, Val Muestair | 46.6000 | 10.4333 | 1386 | SD | MeteoSwiss |
| ABO | Adelboden | 46.5000 | 7.5666 | 1322 | SD | MeteoSwiss |
| DIS | Disentis | 46.7000 | 8.8500 | 1197 | SD | MeteoSwiss |
| ELM | Elm | 46.9166 | 9.1833 | 957 | SD | MeteoSwiss |
| EIN | Einsiedeln | 47.1331 | 8.7567 | 910 | SD | MeteoSwiss |
| SMA | Zuerich/Fluntern | 47.3833 | 8.5666 | 555 | SD-P | MeteoSwiss |
| BER | Bern / Zollikofen | 46.9908 | 7.4639 | 552 | P | MeteoSwiss |
| BAS | Basel / Binningen | 47.5411 | 7.5836 | 316 | P | MeteoSwiss |
| NAP | Napf | 47.0047 | 7.9400 | 1404 | R | MeteoSwiss |
| 5WJ | Weissfluhjoch | 46.8294 | 9.8093 | 2540 | SWE | SLF |
| 4ZE | Zermatt | 46.0234 | 7.7512 | 1600 | SWE | SLF |
| 5DF | Davos Flueelastr. | 46.8125 | 9.8482 | 1560 | SWE | SLF |
| 2AN | Andermatt | 46.6329 | 8.5919 | 1440 | SWE | SLF |
| - | Basel, Rheinhalle | 47.5594 | 7.6167 | 294 | D | GRDC |
| - | Untersiggenthal | 47.5166 | 8.2348 | 373 | D | GRDC |
| - | Brugg | 47.4825 | 8.1949 | 380 | D | GRDC |
| - | Bern | 46.9331 | 7.4480 | 552 | D | GRDC |
| - | Rekingen | 47.5704 | 8.3300 | 370 | D | GRDC |
| - | Neuhausen | 47.6823 | 8.6259 | 430 | D | GRDC |
| - | Diepoldsau | 47.3831 | 9.6409 | 456 | D | GRDC |

***Table 4.2:*** *Calibrated model parameters of the energy balance method: symbol, description and value obtained during calibration.*

| Symbol | Description | Value | Unit |
|---|---|---|---|
| $k_{satSnow}$ | Saturated hydraulic conductivity of snow | $5.11 \cdot 10^{-4}$ | m/s |
| specCapRet | Capillary retention volume as fraction of solid SWE | $1.03 \cdot 10^{-2}$ | - |
| $T_{crit}$ | Threshold temperature for rain/snow fall | -1.00 | °C |
| $\mu$ | Weighting parameter: Snow surface temperature weighted average between air temperature and depth average temperature | 0.76 | - |
| densDrySnow | Snow dry density | 571.60 | $kg/m^3$ |
| emissivitySnowMin | Minimum emissivity old snow | 0.90 | - |
| emissivitySnowMax | Maximum emissivity of fresh snow | 0.96 | - |
| albedoMin | Minimum snow albedo after a long time without snowfall | 0.67 | - |
| albedoMax | Maximum snow albedo right after snowfall | 0.91 | - |
| agingRate_tAirNeg | Rate to describe snow aging process at negative temperatures | $1.00 \cdot 10^{-8}$ | -/s |
| agingRate_tAirPos | Rate to describe snow aging process at positive temperatures | $4.73 \cdot 10^{-5}$ | -/s |

# 5 | Projected changes in Rhine River flood seasonality under global warming

Under review: Erwin Rottler, Axel Bronstert, Gerd Bürger and Oldrich Rakovec: Projected changes in Rhine River flood seasonality under global warming. *Hydrology and Earth System Sciences*, 2021.

**Key points:**

- The mesoscale Hydrologic Model (mHM) forced with climate projections
- Future characteristics of nival, pluvial and mixed hydrological regimes
- Changes scrutinized for 1.5, 2.0 and 3.0 °C global warming levels
- Impact of changes in snowmelt, precipitation and evapotranspiration

## Abstract

Climatic change alters the frequency and intensity of natural hazards. In order to assess potential future changes in flood seasonality in the Rhine River Basin, we analyse changes in streamflow, snowmelt, precipitation, and evapotranspiration at 1.5, 2.0 and 3.0 °C global warming levels. The mesoscale Hydrological Model (mHM) forced with an ensemble of climate projection scenarios (five general circulation models under three representative concentration pathways) is used to simulate the present and future climate conditions of both, pluvial and nival hydrological regimes.

Our results indicate that future changes in flood characteristics in the Rhine River Basin are controlled by increases in antecedent precipitation and diminishing snow packs. In the pluvial-type sub-basin of the Moselle River, an increasing

flood potential due to increased antecedent precipitation encounters declining snowpacks during winter. The decrease in snowmelt seems to counterbalance increasing precipitation resulting in only small and transient changes in streamflow maxima. For the Rhine Basin at Basel, rising temperatures evoke changes from solid to liquid precipitation, which enhance the overall increase in precipitation sums, particularly in the cold season. At gauge Basel, the strongest increases in streamflow maxima show up during winter, when strong increases in liquid precipitation encounter almost unchanged snowmelt-driven runoff. The analysis of snowmelt events for gauge Basel suggests that at no point in time during the snowmelt season, a warming climate results in an increase in the risk of snowmelt-driven flooding. Snow packs are increasingly depleted with the course of the snowmelt season. We do not find indications of a transient merging of pluvial and nival floods due to climate warming.

## 5.1 Introduction

Current climatic changes entail changes in the frequency and intensity of natural hazards. Among other things, rising temperatures reinforce heat waves (Meehl and Tebaldi, 2004; Della-Marta et al., 2007; Fischer and Schär, 2010) and dry spells (Blenkinsop and Fowler, 2007; Samaniego et al., 2018a; Grillakis, 2019) and more intense precipitation increases the risk posed by floods and land slides (Dankers and Feyen, 2008; Rojas et al., 2012; Alfieri et al., 2015; Crozier, 2010; Huggel et al., 2012). Fundamental changes are expected in snow-dominated regions (Hock et al., 2019); alpine climatic changes go along with declining seasonal snow packs (Steger et al., 2013; Beniston et al., 2018a; Hanzer et al., 2018), thawing permafrost (Serreze et al., 2000; Schuur et al., 2015; Elberling et al., 2013; Beniston et al., 2018a) and retreating glaciers (Zemp et al., 2006; Huss, 2011; Radić and Hock, 2014; Hanzer et al., 2018). Those cryospheric changes, in turn, impact water availability in and outside mountain areas (Barnett et al., 2005; Stewart, 2009; Junghans et al., 2011; Viviroli et al., 2011). The European Alps, for example, are the source region of numerous large rivers that form the basis of the economic and cultural development in various cities and communities (Beniston, 2012).

Recent studies suggest that rapid climatic changes have already altered flood characteristics in river systems across Europe. For example, Blöschl et al. (2019) indicate that during 1950–2010, increasing rainfall and soil moisture led to higher river flood discharges in northwestern Europe, while decreasing rainfall together with higher evapotranspiration rates decreased flood discharge in southern parts of the continent. Detected trends in flood magnitudes seem to align with trends in the spatial extent of the floods (Kemter et al., 2020). A further distinction of floods

depending on return period and catchment area enables a detailed investigation of processes generating floods (Bertola et al., 2020). Most important mechanisms driving flooding in Europe are extreme precipitation, snowmelt and soil moisture excess (Berghuijs et al., 2019).

In large and diverse river basins, such as the the Rhine River Basin, all relevant mechanisms generating riverine floods can be detected. The southern part of the basin is influenced by snowmelt from the Alps and therefore commonly classified as nival (Belz et al., 2007; Speich et al., 2015). The runoff of a nival hydrological regime is primarily controlled by the accumulation and melt of a seasonal snow cover. Hence, runoff is low during winter and high during summer. The main tributaries of the Rhine River are rainfall-dominated. Runoff is high during winter and low during summer. Flooding in the rainfall-dominated tributaries usually occurs in winter and is driven by large-scale advective precipitation (Pfister et al., 2004; Bronstert et al., 2007).

Investigating changes in runoff seasonality and flood-generating mechanisms is important to assess challenges in future water resources management. Previous investigations conducted in Switzerland (e.g., Horton et al., 2006; Addor et al., 2014; Brunner et al., 2019a), Austria (e.g., Kormann et al., 2015, 2016; Hanzer et al., 2018), Norway (e.g., Vormoor et al., 2015, 2016) or the United States (e.g. Brunner et al., 2020b,a) point at changes in snowmelt- and rainfall-generated runoff. For the Rhine River, studies have indicated that changes in both nival and pluvial flow alter hydrological regimes and their high/low flow characteristics (e.g., Middelkoop et al., 2001; Belz et al., 2007; Hurkmans et al., 2010; Huang et al., 2013; Alfieri et al., 2015; Stahl et al., 2016; Thober et al., 2018; Marx et al., 2018; Huang et al., 2018). Projections of discharge attained using hydrological models proved key in the attempt to assess the impact of climatic changes.

The aim of the present study is to investigate future changes in rainfall- and snowmelt-induced flooding in the Rhine River. We use the mesoscale Hydrologic Model (mHM; Samaniego et al., 2010; Kumar et al., 2013) forced with an ensemble of climate projection scenarios (five general circulation models under three representative concentration pathways) to assess projected changes in streamflow, snowmelt, rainfall and evapotranspiration characteristics under 1.5, 2.0, and 3.0 °C global warming. Special focus is on the hypothesis of a transient merging of nival and pluvial flow regimes by climate change, which suggests that in a warmer world, earlier snowmelt-induced floods originating from the Alps might superimpose with more intense rainfall-induced runoff from pluvial-type tributaries, creating a new flood type with potentially disastrous consequences (Fig. 5.1).

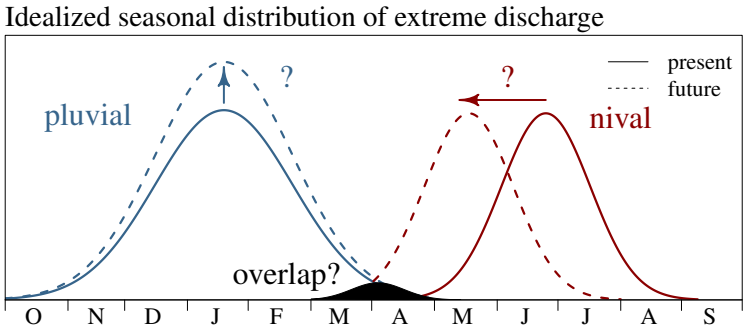


***Figure 5.1:*** *Idealised seasonal distribution of nival and pluvial flood frequencies and potential overlap due to climate change.*

## 5.2 Data and Methods

### 5.2.1 Model set-up

The mesoscale hydrologic model (mHM) v.5.10 (Samaniego et al., 2010; Kumar et al., 2013; Samaniego et al., 2018b) is used to detect and assess projected changes in Rhine River floods under future climate conditions (Fig. 5.2 and 5.3). mHM is a spatially distributed hydrologic model based on grid cells. Key feature of mHM is the Multiscale Parameter Regionalization (MPR) technique, which allows to account for subgrid variability and provides simulations in seamless manner over multiple resolutions (e.g., Kumar et al., 2013; Rakovec et al., 2016; Samaniego et al., 2017). During MPR, high resolution physiographic land surface descriptors are translated into model parameters in the two phases of MPR, i.e., regionalization and upscaling. In the framework of this study, the high resolution physiographical datasets describing the main features of the terrain, e.g., digital elevation model, aspect, slope, soil texture, geological formation type, land cover and leave area index (LAI), are in 500 m resolution (Samaniego et al., 2019). The mHM model set-up distinguishes six soil layers up to a depth of 2 m based on Hengl et al. (2017). For each soil horizon the soil types are defined based on clay content, sand content and bulk density. We distinguish eight hydrogeological units. The baseflow recession parameters characterising each unit are determined during model calibration. Long-term climatologic monthly LAI maps are based on Mao and Yan (2019). Using a modified IGBP MODIS Noah classification scheme, 23 LAI classes are distinguished, whereby classes representing croplands, grassland, coniferous forest, mixed forest and mosaics of cropland and natural vegetation being the most common classes in the basin. More information on physiographical datasets, the mapping on a common 500 m $\times$ 500 m spatial resolution and underlying data sources is presented in Samaniego et al. (2019).

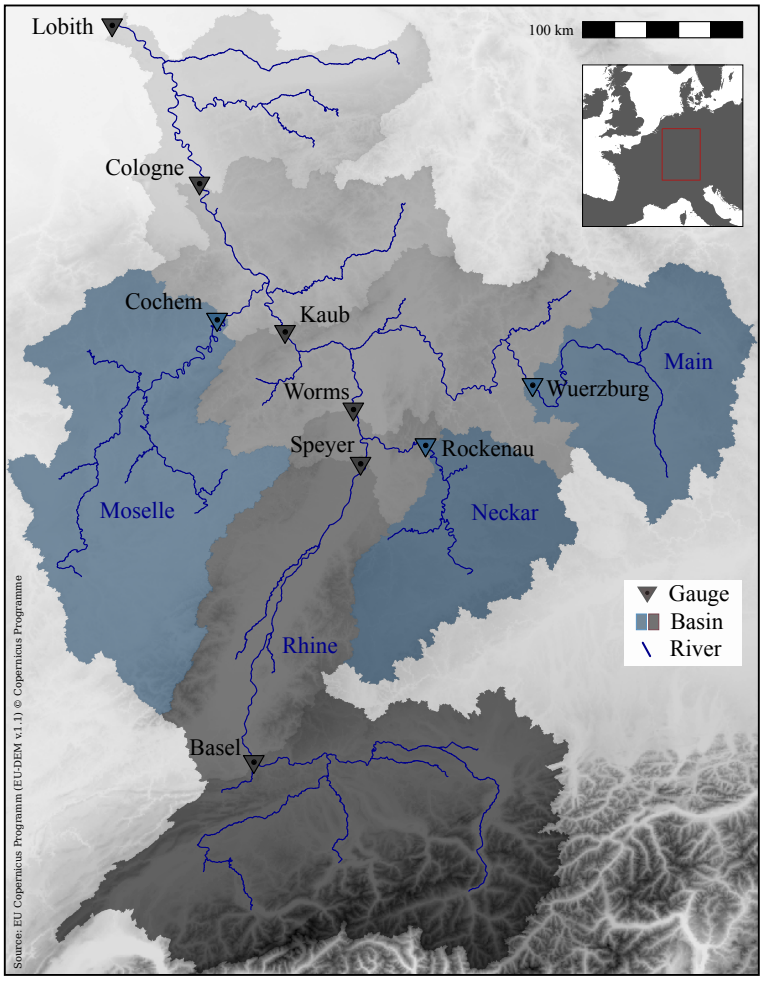


***Figure 5.2:*** *Topographic map of the Rhine River Basin at gauge Lobith with locations of all gauges and sub-basins investigated.*

All dominant hydrological processes are modelled at 5 km spatial resolution.

Meteorological forcing data of the model consists of daily average, maximum and minimum temperature and precipitation. Observational data sets are based on the E-OBS v12 gridded data sets (Haylock et al., 2008). Climate model data originates from the Inter-Sectoral Impact Model Intercomparison Project (ISI-MIP) (Hempel et al., 2013a,b; Warszawski et al., 2014). ISI-MIP bases on Global Climate Model (GCM) runs performed during the fifth phase of the Coupled Model Intercomparison Project (CMIP5; Taylor et al., 2012). Within ISI-MIP, daily data from five Global Climate Models (GCMs), i.e., GFDL-ESM2M, HadGEM2-ES, IPSL-CMSA-LR, MIROC-ESM-CHEM, NorESM1-M, were bias corrected and bi-linearly interpolated to a $0.5^\circ \times 0.5^\circ$ grid. Bias correction of climate model data represents an indispensable step in climate change impact modelling applications. Systematic

deviation, e.g., due to imperfect model representations of atmospheric processes or errors in the parameterisation chain, need to be corrected (Ehret et al., 2012). A detailed description of the trend-preserving statistical bias correction method developed and applied within ISI-MIP, which includes an additive correction approach for temperature and a multiplicative correction for precipitation, is presented in Hempel et al. (2013b). GCM data used cover the period 1950–2099 and include three representative concentration pathways (RCPs) 2.6, 6.0 and 8.5. In the framework of the project "EDgE - End-to-end Demonstrator for improved decision making in the water sector in Europe" by order of the Copernicus Climate Service (`edge.climate.copernicus.eu`), meteorological data sets were interpolated to a 5 km grid using external drift kriging (Samaniego et al., 2019).

mHM forced with E-OBS meteorological data is calibrated for the Rhine Basin at gauge Lobith against observed streamflow at the three gauges Lobith, Basel and Cochem during 1951–1975 using the Dynamically Dimensioned Search algorithm (DDS; Tolson and Shoemaker, 2007) and the Nash-Sutcliffe efficiency (NSE; Nash and Sutcliffe, 1970). In the framework of this multi-basin calibration, we simultaneously optimise NSE values for the three gauges and attain one set of global parameters, which we apply to the entire basin. We use a multi-basin approach to ensure that rainfall and snowmelt triggered runoff from both nival and pluvial dominated sub-basins as well as streamflow in the main channel of the Rhine River are considered during calibration. MPR enables the sampling in a lower-dimensional space, in turn, speeding up the convergence of the optimization algorithm (Samaniego et al., 2010). In total, we calibrate 47 global parameters using 1000 model iterations. A detailed overview of global parameters and their linkage with basin predictors in the regionalization transfer functions are presented in Samaniego et al. (2010) and Kumar et al. (2013). In order to evaluate the model performance in all important sub-regions of the entire Rhine River, the mHM performance is evaluated at additional six independent gauges (Fig. 5.2) and during an independent evaluation period (1976–2000) using the NSE and the Kling-Gupta-Efficiency (KGE; Gupta et al., 2009) (Table 5.1). Analyses evaluating streamflow simulations for the historic time frame 1951–2000 are given in the Appendix (Fig. 5.10, 5.11 and 5.12). Similar to investigations presented in the supplementary material of Thober et al. (2018), we assess streamflow maxima and the 90 % streamflow quantile of the hydrological year. In addition, we evaluate the timing of annual streamflow maxima and 90 % streamflow quantiles on a monthly basis. All observational discharge times series are obtained from the Global Runoff Data Centre (GRDC).

***Table 5.1:*** *River gauges investigated: Location (WGS 84), GRDC identification number, catchment area, Nash-Sutcliffe efficiency (NSE) and Kling-Gupta efficiency (KGE) between observed and modelled runoff (NSE / KGE). The model has been calibrated against observation from the three gauges (Lobith, Basel and Cochem) with the NSE as objective function during 1951–1975.*

| Name | GRDC-ID | Lat. | Lon. | Area ($km^2$) | 1951–1975 | 1976–2000 | 1951–2000 |
|---|---|---|---|---|---|---|---|
| Lobith | 6435060 | 51.840 | 6.110 | $1.61 \cdot 10^5$ | 0.91 / 0.93 | 0.90 / 0.89 | 0.91 / 0.91 |
| Cologne | 6335060 | 50.937 | 6.963 | $1.44 \cdot 10^5$ | 0.92 / 0.96 | 0.92 / 0.94 | 0.92 / 0.95 |
| Cochem | 6336050 | 50.143 | 7.168 | $2.71 \cdot 10^4$ | 0.84 / 0.75 | 0.87 / 0.77 | 0.85 / 0.77 |
| Kaub | 6335100 | 50.085 | 7.765 | $1.03 \cdot 10^5$ | 0.90 / 0.90 | 0.92 / 0.92 | 0.91 / 0.91 |
| Wuerzburg | 6335500 | 49.796 | 9.926 | $1.40 \cdot 10^4$ | 0.73 / 0.81 | 0.79 / 0.84 | 0.76 / 0.83 |
| Worms | 6335180 | 49.641 | 8.376 | $6.89 \cdot 10^4$ | 0.85 / 0.87 | 0.88 / 0.90 | 0.87 / 0.88 |
| Rockenau | 6335600 | 49.438 | 9.005 | $1.27 \cdot 10^4$ | 0.75 / 0.74 | 0.74 / 0.71 | 0.74 / 0.73 |
| Speyer | 6335170 | 49.324 | 8.449 | $5.31 \cdot 10^4$ | 0.82 / 0.88 | 0.86 / 0.90 | 0.84 / 0.89 |
| Basel | 6935051 | 47.559 | 7.617 | $3.59 \cdot 10^4$ | 0.71 / 0.83 | 0.75 / 0.85 | 0.73 / 0.84 |

The multiscale Routing Model (mRM; Thober et al., 2019) is used for routing river runoff using the adaptive time step scheme (aTS). The kinematic wave equation (Lighthill and Whitham, 1955), a simplification of the Saint-Venant equation (de Saint-Venant, 1871), is solved using a finite difference scheme. The kinematic wave equation only needs little information on the river topography and assesses the advection and the attenuation of flood waves. The time step selected within aTS only depends on the spatial resolution and is independent of the temporal resolution of the meteorological forcing. In our model set-up, water is routed through the river network at a temporal resolution of 30 min. The high-resolution river network is based on a 500 x 500 m digital elevation map and is upscaled to operate on a 5 km routing resolution. Within the upscaling process, the flow direction in the lower resolution (routing resolution) is equal to the flow direction in the underlying high-resolution grid cell with the highest flow accumulation (Samaniego et al., 2010). The stream celerity is determined as a function of terrain slope (Thober et al., 2019).

All dominant hydrological processes are modelled at 5 km spatial resolution. We estimate reference crop evapotranspiration following the Hagreaves-Samani equation, an empirical approach using minimum climatological data (Hargreaves and Samani, 1985; Samani, 2000). The empirical coefficient of the equation is determined during calibration. The usage of this simple approach enables a consistent set-up across historical and future model space. The actual evapotranspiration is estimated based on the fraction of roots in the soil horizons and a stress factor for reducing potential values calculated based on the actual soil moisture. The stress factor is determined using the Feddes equation (Feddes et al., 1976). If the soil moisture is below the permanent wilting point, evapotranspiration is reduced to zero. In case the soil moisture is above field capacity, the evapotranspiration equals the fraction of roots. If the soil moisture is in between the permanent wilting point and field capacity, evapotranspiration is reduced by the fraction of roots times the stress factor. The mHM set-up distinguishes six soil layers up to a total depth of 2 m. Organic matter is possible until 0.3 m. In total, more than 2000 soil types with different clay content, sand content and bulk density are defined. Land surface with impervious cover are treated as free-water surfaces and actual evapotranspiration is estimated with an additional evaporation coefficient. More details of the soil parameterization in mHM can be found in Livneh et al. (2015).

The canopy interception is modelled with a maximum interception approach. The maximum interception capacity is estimated based on the given LAI values. Water can leave the interception storage as throughfall, which is estimated as a function of the current and maximum canopy water content and the incoming precipitation. Evaporation from the canopy storage depends on the current and maximum canopy water content and the potential values of evapotranspiration.

We simulated snow using an empirical degree-day approach, whereas degree-day-factors differ depending on the dominant land use class. In order to account for snowmelt following the energy input from liquid rainfall, degree-day factors are increased depending on the amount of liquid precipitation. Degree-day factors only can increase to a certain threshold value. Due to the spatial resolution of 5 km, our model set-up does not capture the highest elevations in the basin. To also capture the snow dynamics at mountain peaks, meteorological input data would need to be at higher spatial resolution and more advanced snow/ice processes would need to be considered. Surface runoff from impervious areas is calculated based on a linear reservoir exceedance approach. Interflow from the unsaturated zone is determined using a nonlinear reservoir with saturation excess. Groundwater is assumed as a linear reservoir. mHM does not included glacier and lake modules yet.

The changes in mHM-based flood seasonality are further differentiated and scrutinised for three different warming levels: 1.5, 2.0 and 3.0 °C. Within each future model run, the 30-year time windows when the warming levels (compared to the historic time window 1971–2000) are reached, are determined. The period 1971–2000 is assumed to be warmer by 0.46 °C compared to pre-industrial levels already (Vautard et al., 2014). For example, when comparing 30-year running temperature means from the IPSL-CM5A-LR model run under RCP 6.0, temperatures reach 1.5 °C warming compared to pre-industrial levels in the 30-year time window 2009–2038, 2.0 °C warming during 2028–2057 and a 3.0 °C warming in the period 2066–2095. 14 GCM-RCP realisations reach 1.5 °C, 13 reach 2.0 °C, and 8 reach 3.0 °C global warming. A detailed description of the determination of warming levels including a table with 1.5, 2.0 and 3.0 °C time periods of GCM-RCP realisation (Table S1) is given in the supplementary material of Thober et al. (2018).

### 5.2.2 Changes in streamflow characteristics

In order to assess the changes in flood characteristics, we determine the timing and magnitude of annual and monthly maxima of streamflow, precipitation (total and liquid), snowmelt and actual evapotranspiration for the hydrological year starting on the 1st of October (Tab. 5.2). In case of precipitation, we investigate maxima of 5-day sums ($P_{max5}$). Investigating thousands of annual streamflow maxima for different Swiss catchments with regard to flood-triggering precipitation, Froidevaux et al. (2015) conclude that precipitation 2 to 3 days before an event is an important determinant of flood magnitude. To account for larger catchment sizes and hence longer travel times in our study catchments, we chose a five 5-day window. For snowmelt and evapotranspiration, we extend this time window to 10

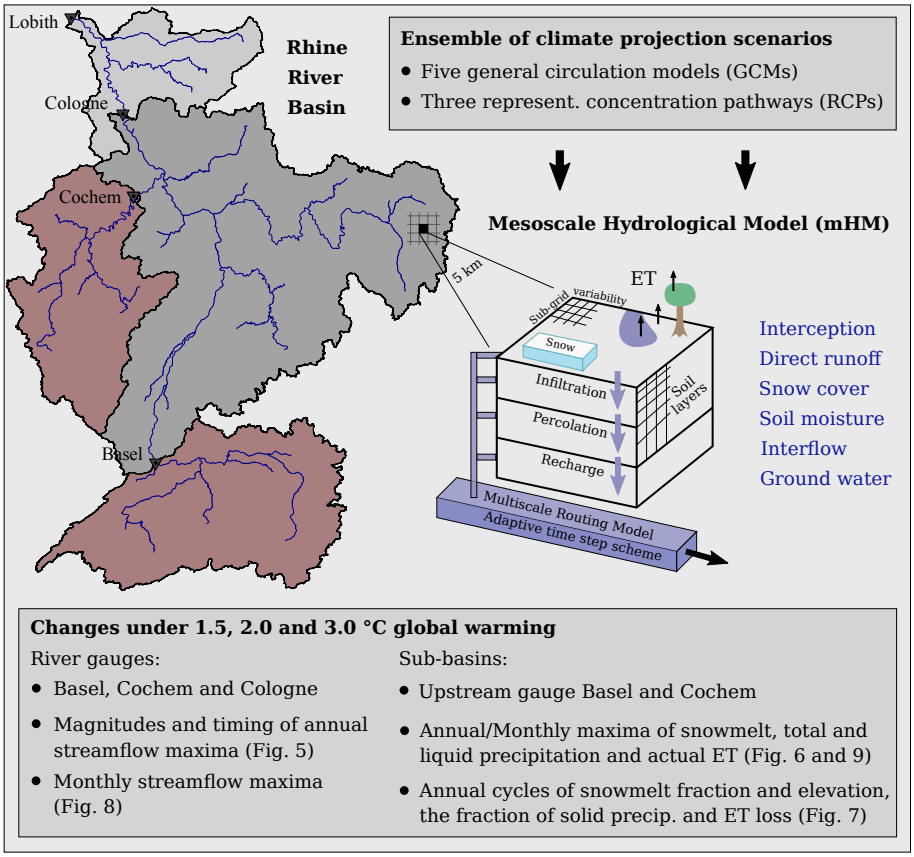


***Figure 5.3:*** *Scheme of the analytical set-up depicting gauges (Basel, Cochem and Cologne) and sub-basins (at gauges Basel and Cochem) investigated in detail.*

days and assess the magnitude and timing of 10-day sums ($S_{max10}$ and $ET_{max10}$). We assume that in order to have substantial impact on streamflow, meteorological conditions favouring snowmelt or evapotranspiration need to prevail longer than only a few days. According to our experience, a 10-day window width provides a good estimate to assess potential impacts on streamflow.

In the case of annual maxima, we display the timing and magnitude as boxplots and histograms. The length of the boxplot whiskers is 1.5 times the interquartile range (IQR). However, if no data point exceeds this distance, the whiskers only reach until the minimum/maximum value. The notches extent to $+/- 1.58 \cdot \frac{IQR}{\sqrt{n}}$ with n being the length of the data vector (McGill et al., 1978; R Core Team, 2019). The notches roughly represent 95% confidence intervals for the difference in two medians. For visualisation purposes, we do not display whiskers and outliers of boxplots displaying monthly maxima values. Histograms always depict the probability density and have a total area of one. To estimate the snowmelt contribution

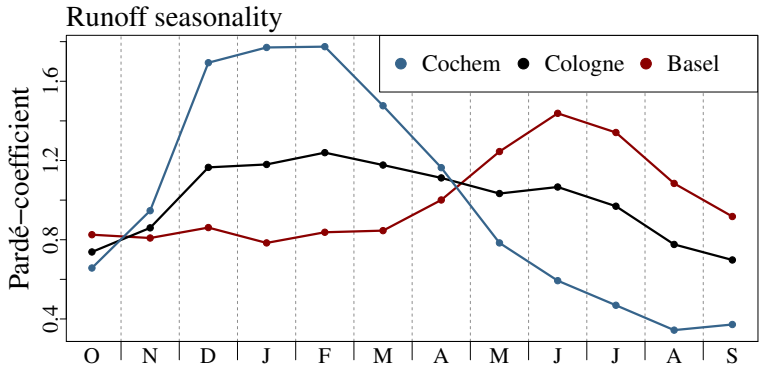


***Figure 5.4:*** *Pardé-coefficients (ratio of average monthly discharge and the mean annual discharge) (Pardé, 1933; Spreafico and Weingartner, 2005) for gauges Cochem, Basel and Cologne calculated based on measured discharge from the time frame 1971 to 2000.*

with regard to annual streamflow peaks, we calculate the ratio between snowmelt the preceding 10 days and snowmelt the preceding 10 days plus precipitation the preceding 5 days ($S_{frac}$). Furthermore, we estimate evapotranspiration loss as the ration between actual evapotranspiration the preceding 10 days and snowmelt the preceding 10 days plus precipitation the preceding 5 days ($ET_{loss}$). In addition, we determine mean average annual cycles of $S_{frac}$, the average elevation of the snowmelt ($S_{elev}$) and the solid fraction of precipitation ($P_{solid}$) and the median average annual cycle of $ET_{loss}$.

In the framework of the analysis, we focus on the three gauges: Basel, Cochem and Cologne (Fig. 5.3). Selected gauges and sub-basins enable a detailed insight into changes in pluvial and nival processes and changes in the main channel of the Rhine River. Gauge Basel is located at the transition from High to Upper Rhine. The basin upstream gauge Basel encompasses large areas of high alpine character. Snowmelt during spring and early summer is an important runoff/flood-generating process (Wetter et al., 2011; Stahl et al., 2016). Runoff at gauge Cochem (Moselle River) is characterised by a pluvial flow regime with high runoff during winter and low runoff during summer (Fig. 5.4). Flooding typically occurs in winter and early spring due to large-scale advective precipitation (Pfister et al., 2004; Bronstert et al., 2007). The gauge Cologne is located in the Lower Rhine region after the confluences of the main tributaries Moselle, Neckar and Main (Fig. 5.2). Streamflow at gauge Cologne is characterised by a complex flow regime containing both nival and pluvial characteristics.

***Table 5.2:*** *Names/Abbreviations, descriptions and units of variables investigated on sub-basin level.*

| Variable | Description | Unit |
|---|---|---|
| $P_{max5}$ | 5-day precipitation maxima (total or liquid) | mm |
| $S_{max10}$ | 10-day snowmelt maxima | mm |
| $ET_{max10}$ | 10-day actual evapotranspiration maxima | mm |
| $S_{frac}$ | Contribution of snowmelt to streamflow estimated as the ratio between snowmelt the preceding 10-days and snowmelt the preceding 10 days plus liquid precipitation the preceding 5 days | % |
| $ET_{loss}$ | Evapotranspiration loss estimated as the ratio between actual evapotranspiration the preceding 10-days and snowmelt the preceding 10 days plus liquid precipitation the preceding 5 days | % |
| $S_{elev}$ | Average elevation of snowmelt | m |
| $P_{solid}$ | Solid fraction of precipitation (snowfall) | % |

## 5.3 Results

### 5.3.1 Annual maxima

The magnitudes of annual streamflow maxima at gauge Basel increase with rising temperatures (Fig. 5.5 a). However, this increase is not linear with the magnitude of the warming. The most prominent increase shows up between the historic time frame (1971–2000) and the 1.5 °C warming level. According to the model simulations, the median of annual streamflow maxima increases from 2557 $m^3$ $s^{-1}$ in the historic period to 2827 $m^3$ $s^{-1}$ supposing a warming of 1.5 °C. Among the different warming levels we distinguish marginal differences (Fig. 5.5 a). At gauge Basel, annual streamflow maxima occur throughout the year (Fig. 5.5 d). In the historical period, runoff peaks cluster during spring and early summer (snowmelt season). In a warming climate, this cluster is more and more dispersed and annual maxima are increasingly recorded during winter, in particular for the 3 °C warming level. At gauge Cochem, no clear signals of change are detected, neither for the magnitudes nor the timing of annual streamflow maxima (Fig. 5.5 b and e). At gauge Cologne, streamflow maxima tend to be stronger at the selected warming levels compared to the historic time frame (Fig. 5.5 c and f). Again, differences among warming levels are small.

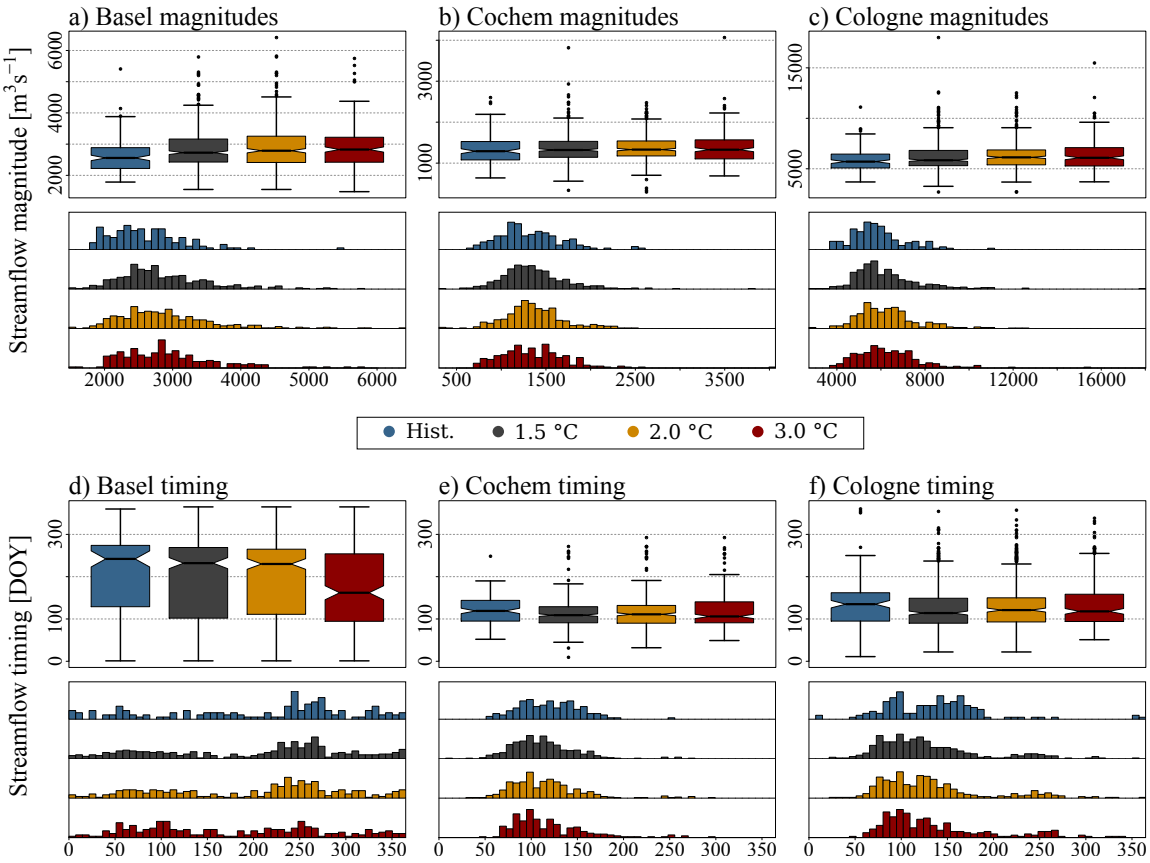


***Figure 5.5:*** *Magnitudes and timing (hydrological year starting 1. October) of annual streamflow maxima simulated for gauges Basel, Cochem and Cologne under selected warming levels (14 GCM-RCP realisations reach 1.5 °C, 13 reach 2 °C and 8 reach 3 °C warming) and displayed as boxplots and histograms. Histograms depict probability density and have a total area of one.*

For both gauges Basel and Cochem, the estimated contribution of snowmelt to annual streamflow maxima ($S_{frac}$) strongly decreases with rising temperatures (Fig. 5.6 a and b). At gauge Basel (Cochem), the median of $S_{frac}$ decreases from 15.7% (23.0%) during the historical time frame to 6.7% (0.2%) at a 3 °C warming. At a 3 °C warming, only 27.2% (16.8%) of the annual streamflow maxima have an estimated snowmelt contribution of more than 15% at gauge Basel (Cochem). For both gauges Basel and Cochem, magnitudes of $S_{max10}$ diminish (Fig. 5.6 c and d). The median of annual $S_{max10}$ for gauge Basel (Cochem) is around 32.6 mm (23.9 mm) in the historic time frame and is reduced to 20.6 mm (8.5 mm) at a 3 °C warming. At gauge Basel, $S_{max10}$ do not only get weaker, they also tend to be recorded earlier in the hydrological year (Fig. 5.6 e). At gauge Cochem, the timing

of annual 10-day snowmelt maxima ($S_{max10}$) remains unchanged (Fig. 5.6 f). In both sub-basin, liquid and total annual $P_{max5}$ increase with rising temperatures (Fig. 5.6 g, h, i, and j). At gauge Basel (Cochem), the median of liquid annual $P_{max5}$ increases from 63.4 mm (43.9 mm) in the historic time frame to 74.4 mm (50.5 mm) at a 3 °C rise in temperature. The median of the estimated evaporation loss during the genesis of annual streamflow maxima ($ET_{loss}$) is 21.8% (9.2%) at gauge Basel (Cochem) during the historic time period (Fig. 5.6 k an l). At gauge Basel, $ET_{loss}$ remain fairly stable for moderate warming levels (1.5 and 2 °C) and strongly decreases to 15.4 mm at a 3.0 °C warming, as streamflow peaks more frequently are recorded during winter. At gauge Cochem, the median of $ET_{loss}$ remains almost unchanged and has a value of 9.4% at a 3 °C warming. Magnitudes of annual $ET_{max10}$ increase with rising temperatures (Fig. 5.6 m and n). At a 3 °C warming, the median of $ET_{max10}$ magnitudes increases by 11.7% (6.2%) for gauge Basel (Cochem) compared to the historic simulations.

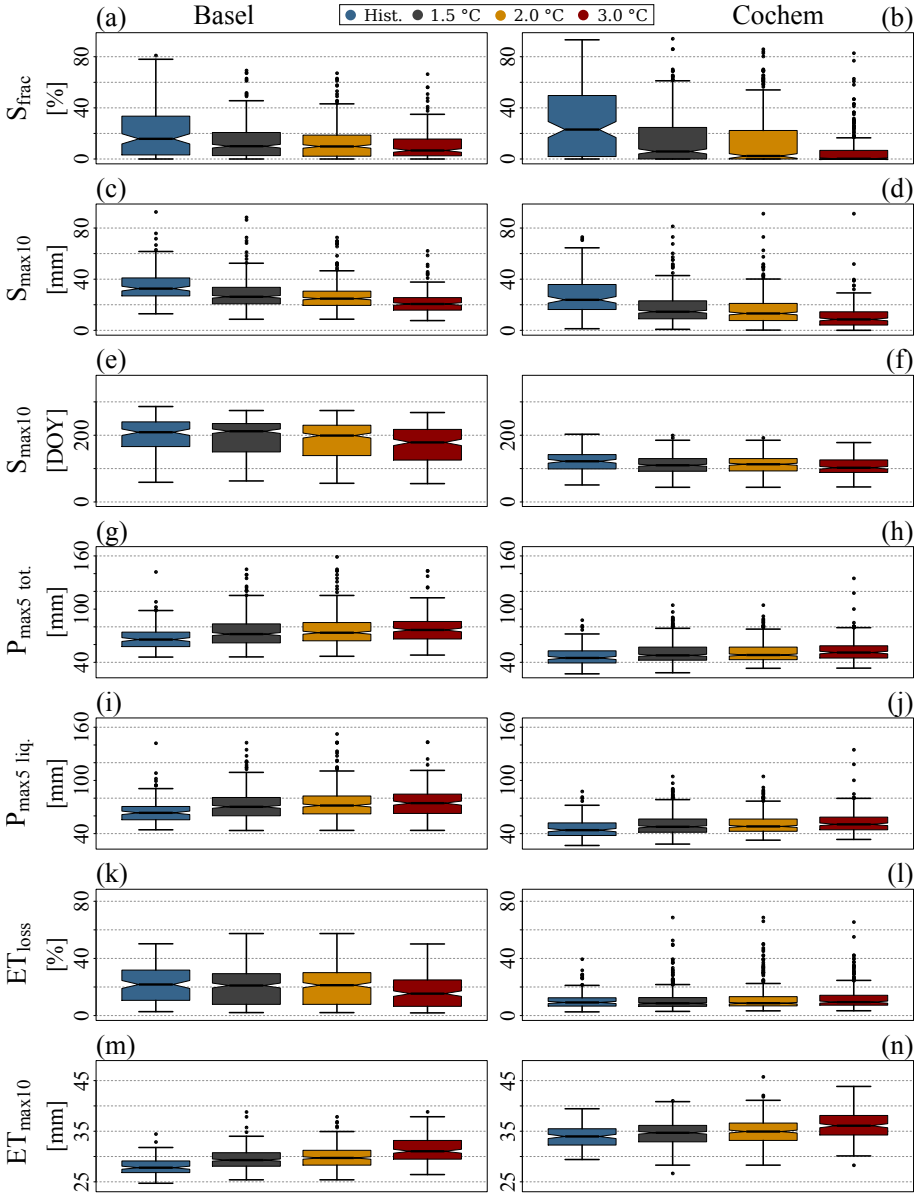


***Figure 5.6:*** *Estimated contribution of snowmelt to the annual streamflow maxima ($S_{frac}$; a and b), magnitudes (c and d) and timing (e and f) of annual 10-day snowmelt maxima ($S_{max10}$), magnitudes of annual total (g and h) and liquid (i and j) 5-day precipitation maxima ($P_{max5}$), estimated evapotranspiration loss during the genesis of annual streamflow maxima ($ET_{loss}$; k and l) and magnitudes of annual 10-day actual evapotranspiration maxima ($ET_{max10}$; k and l) for sub-basins at Basel (left column) and Cochem (right column) under selected warming levels (14 GCM-RCP realisations reach 1.5 °C, 13 reach 2 °C and 8 reach 3 °C warming).*

### 5.3.2 Annual cycles

At gauge Basel (Cochem), the solid fraction of precipitation ($P_{solid}$) reaches values of 69.9 % (43.9 %) during winter in the historic time frame (Fig.5.7 a and b). Our results indicate that at a 3 °C warming, on average, the fraction of solid precipitation will be reduced to less than 40 % (17 %) at gauge Basel (Cochem) in winter. At gauge Basel, the estimated average contribution of snowmelt to streamflow ($S_{frac}$) reaches values values up to 40 % during winter, spring and early summer (Fig. 5.7 c). Strongest decreases in $S_{frac}$ show up in summer (Fig. 5.7 c). In the Moselle catchment at gauge Cochem, $S_{frac}$ values strongly decrease during the cold season (Fig. 5.7 d). Upstream of Basel, the average melt elevation ($S_{elev}$) is moving upward the elevation range throughout the year (Fig. 5.7 e). On average, $S_{elev}$ is 359 m higher at 3 °C warming compared to the historic time period. At gauge Cochem, $S_{elev}$ is restricted to elevations below 1100 m (Fig. 5.7 f). Simulation results hint at higher $S_{elev}$, particularly at the beginning and end of the snow season. However, changes are less prominent compared changes detected at gauge Basel. At gauge Basel, the estimated average evapotranspiration loss ($ET_{loss}$) is below 100 % almost throughout the year (Fig. 5.7 g). Only during summer months and more frequently with stronger warming, $ET_{loss}$ reach values above 100 %. At gauge Cochem, $ET_{loss}$ are below 100 % between October and March (Fig. 5.7 h). During the course of the summer, average $ET_{loss}$ can reach values up to almost 400 %.

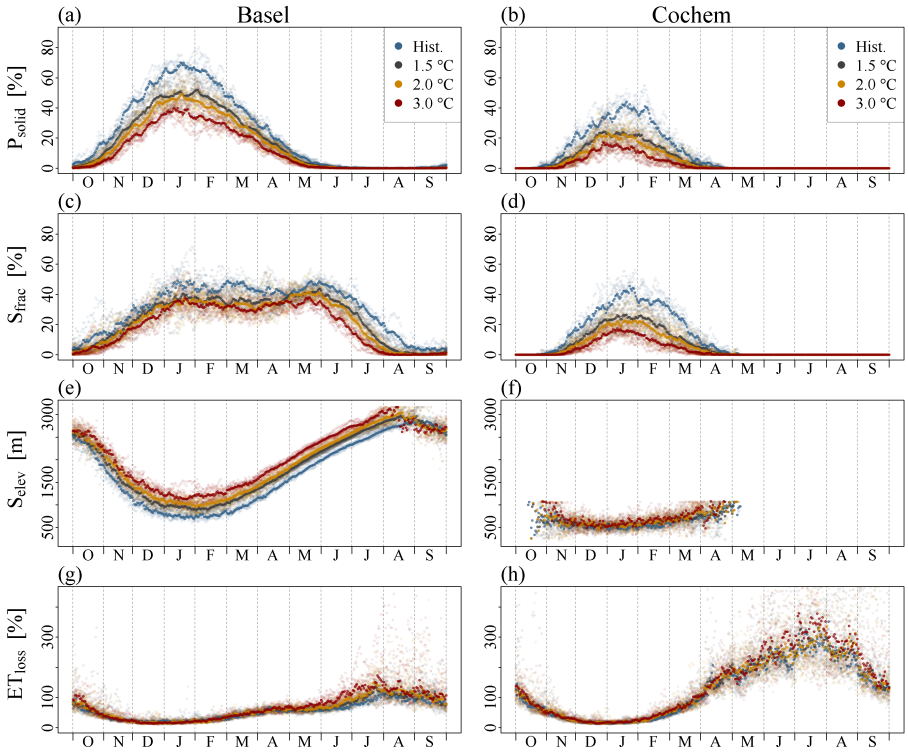


***Figure 5.7:*** *Mean annual cycles of the fraction of solid precipitation ($P_{solid}$; a and b), estimated contribution of snowmelt to streamflow ($S_{frac}$; c and d), average elevation of snowmelt ($S_{elev}$; e and f) and estimated evapotranspiration loss ($ET_{loss}$; g and h) for sub-basins at Basel and Cochem under selected warming levels (14 GCM-RCP realisations reach 1.5 °C, 13 reach 2 °C and 8 reach 3 °C warming).*

### 5.3.3 Monthly maxima

At gauge Basel, monthly streamflow maxima generally increase during winter and decrease in late summer (Fig. 5.8 a). Streamflow maxima in May and June seem to increase in magnitude at the more moderate warming levels (up to a warming of 2 °C) and decrease as warming progresses. A similar pattern of initial increases in monthly maxima and a subsequent stabilisation or even a decrease at higher warming levels shows up in December and January at gauge Cochem (Fig. 5.8 b) and in all winter months at gauge Cologne (Fig. 5.8 c). In general, patterns of change in monthly streamflow maxima at gauge Cologne seem to reflect an overlap of features visible at gauges Basel and Cochem.

At gauge Basel, magnitudes of $S_{max10}$ remain fairly stable during winter (Fig. 5.9 a). Strong decreases in $S_{max10}$ show up in spring and are most pronounced

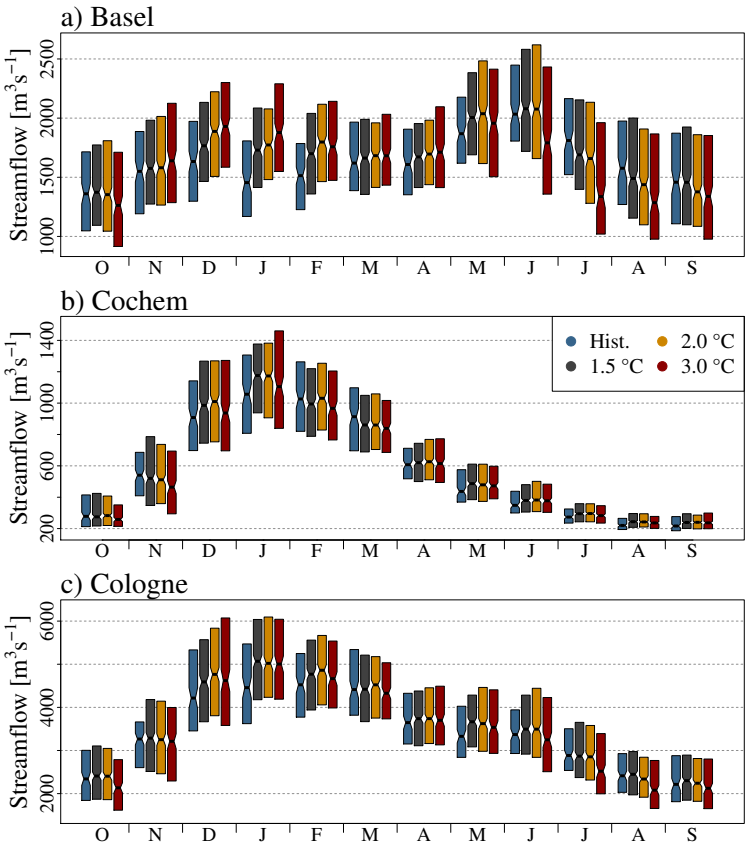


***Figure 5.8:*** *Magnitudes of monthly streamflow maxima simulated for gauges a) Basel, b) Cochem and c) Cologne under selected warming levels (14 GCM-RCP realisations reach 1.5 °C, 13 reach 2 °C and 8 reach 3 °C warming). Whiskers and outliers of the boxplots are not displayed.*

from May to July. In the Moselle catchment at gauge Cochem, $S_{max10}$ strongly decrease throughout the cold season (Fig. 5.9 b). $P_{max5}$ tend to increase throughout the year (Fig. 5.9 c, d, e and f). In the Moselle catchment, no big differences between changes in liquid and total $P_{max5}$ are detected. In the Rhine Basin upstream gauge Basel, rising temperatures seem to evoke changes from solid to liquid precipitation, which enhance the overall increase in 5-day precipitation sums, particularly in the cold season (Fig. 5.9 c and e). Our model simulation suggest that evapotranspiration only plays a minor role in the Rhine Basin during winter (Fig. 5.9 g and h). We detect highest values of $ET_{max10}$ reaching up to 35 mm for the sub-basin at Cochem during summer. Values of $ET_{max10}$ increase with rising temperatures.

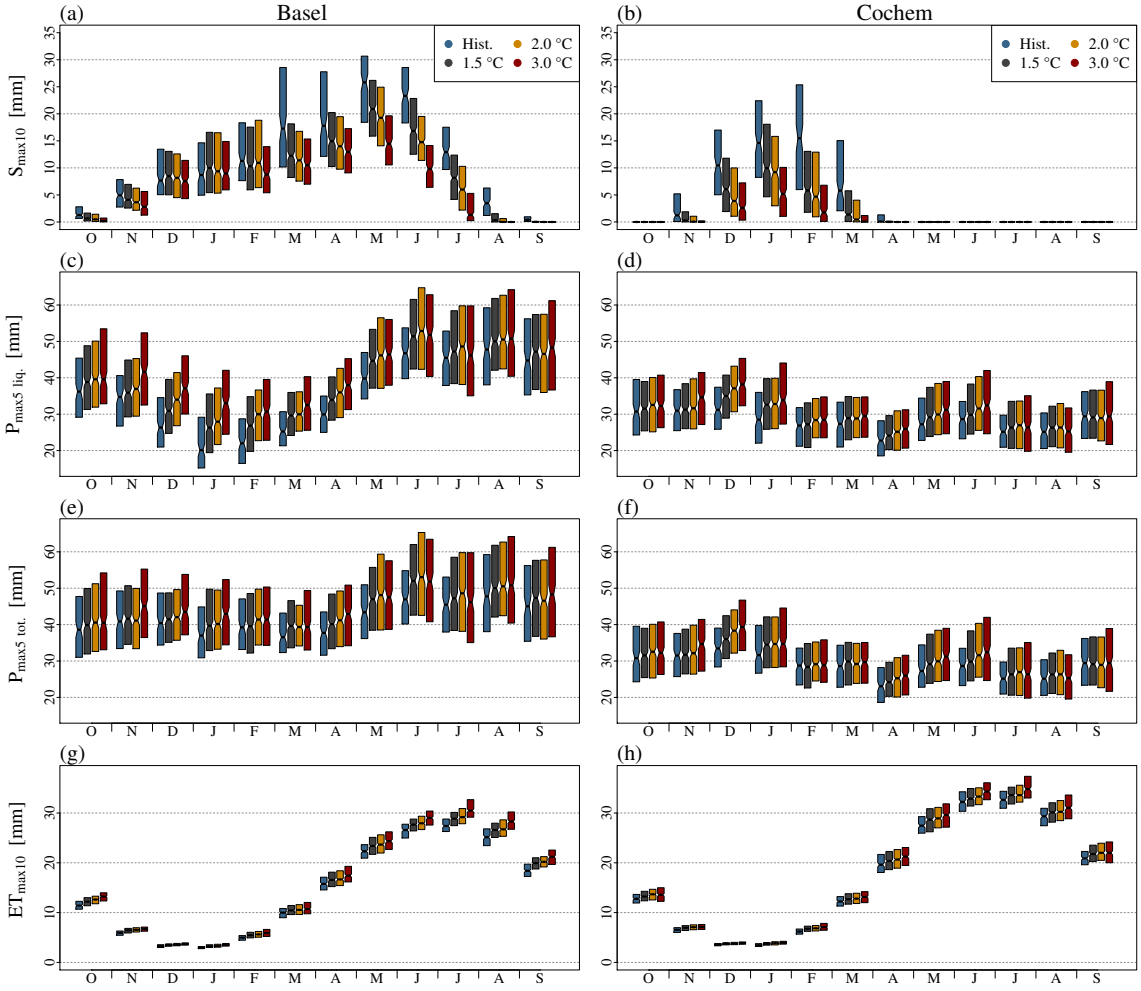


***Figure 5.9:*** *Magnitudes of 10-day snowmelt maxima ($S_{max10}$; a and b), liquid (c and d) and total (e and f) 5-day precipitation ($P_{max5}$) and 10-day actual evapotranspiration maxima ($ET_{max10}$; g and h) for sub-basins at Basel and Cochem under selected warming levels (14 GCM-RCP realisations reach 1.5 °C, 13 reach 2 °C and 8 reach 3 °C warming). Whiskers and outliers of the boxplots are not displayed.*

## 5.4 Discussion

Rising temperatures diminish seasonal snow covers (see also Bavay et al., 2009; Rousselot et al., 2012; Schmucki et al., 2015; Beniston et al., 2018a). As a result, the importance of snowmelt as a flood-generating process decreases (Fig. 5.6 a, b, c and d). In the Rhine Basin at Basel, 10-day snowmelt maxima ($S_{max10}$)

decrease for all months of spring and summer (Fig. 5.8 a). At no point in time during the snowmelt season, a warming climate results in an increase in risk of snowmelt-driven flooding. Our results indicate that the detected earlier timing of the annual snowmelt maxima (Fig. 5.6 e) is not due to an increase in snowmelt magnitudes earlier in the year. It rather seems that events early in the snowmelt season, even if weakened by rising temperatures, more often are the strongest of the year already, as snow packs are increasingly depleted within the course of the snowmelt season. For the basin at Basel, we can not find indications that an earlier snowmelt due to rising temperatures shifts the risk of snowmelt-driven flooding forward in time. Despite the temporal shift forward of annual snowmelt maxima, flood hazard seems to decrease, as the temporal shift concurs with a strong decrease in snowmelt magnitudes (Fig. 5.6 c). Our findings go along with results from Musselman et al. (2017), who suggest that a "shallower snowpack melts earlier, and at lower rates, than deeper, later-lying snow-cover". However, the disappearance of snow packs and glaciers is likely to favour low-flow conditions along the Rhine River (Junghans et al., 2011; Stahl et al., 2016). Another factor having the potential to initiate or reinforce low-flow situation are increasing values of evapotranspiration, particularly during summer (Fig. 5.9 g and h).

Our results indicate that at Basel during winter, the lack of snowmelt from lower elevations, at least partly, is compensated by snowmelt from areas located at higher elevations (Rottler et al., 2021) (Fig. 5.7 c and e and Fig. 5.9 a). This compensation effect seems to be increasingly insufficient as the snowmelt season progresses and the snowline moves upward. We suggest that in winter, the almost unchanged potential of snowmelt-induced runoff at Basel encounters increased antecedent precipitation (Fig. 5.9 c), in turn, resulting in a strong increase in streamflow maxima (Fig. 5.8 a). Our results confirm previous studies suggesting that rising temperatures might lead to stronger precipitation events (e.g., Lehmann et al., 2015; Alfieri et al., 2015; King and Karoly, 2017; Bürger et al., 2019; Rottler et al., 2020) (Fig. 5.6 g-j and Fig. 5.9 c-f) and a shift from solid to liquid rainfall (e.g., Allamano et al., 2009b; Addor et al., 2014; Davenport et al., 2020) (Fig. 5.7 a and b). In catchments having mixed hydrological regimes with rainfall and snowmelt, rising temperatures seem to lead to a shift from snowmelt to rainfall as most important flood generating process (Vormoor et al., 2015, 2016). Reconstructing the largest floods in the High Rhine since 1268, Wetter et al. (2011) indicate that about half of all large events occurred during summer due heavy precipitation combined with high baseflow from snow- and ice-melt. Our results indicate that with rising temperatures, most flood events will occur in winter (Fig. 5.5 d).

In March and April, the increase in rainfall amounts in the basin at Basel compares to increases in winter, the magnitudes of streamflow maxima, however, hardly change (Fig. 5.8 a). We suggest that the increasing potential of rainfall-

induced flooding is counterbalanced by decreasing snowmelt (Fig. 5.9 a and c). Furthermore, our results hint at a transient increase in flood magnitudes during May and June (Fig. 5.8 a). It seems that during those two months, snowmelt is still strong enough to support an increase in streamflow peaks due to increased antecedent precipitation at moderate warming levels (1.5 °C and 2.0 °C). With further rising temperatures, however, the magnitudes of streamflow maxima reduce along with declining snowmelt (Fig. 5.8 a). The mHM model set-up that we use to simulate the Rhine River does not include a lake module. The simulation results attained for the Rhine Basin, particularly for gauge Basel, can be further refined by the representation of the large lakes located in Switzerland and Southern Germany (Imhoff et al., 2020). The large storage volume and the possibility to regulate lake levels dampen streamflow peaks.

For gauge Cochem and the associated sub-basin of the Moselle River, we detect similar counterbalancing effects between snowmelt and rainfall: an increasing flood potential due to increased precipitation amounts encounters declining snow packs. Again, decreases in snowmelt magnitudes seem to counterbalance increased precipitation resulting in comparatively small and transient increases in streamflow maxima (Fig. 5.8 b and Fig. 5.9 b and d). As highest mountains in the sub-basin only reach up to around 1300 m a.s.l., snowmelt compensation effects, i.e., snowmelt from higher elevations, at least partly, replaces the lack of snowmelt from lower elevation, only plays a marginal role. Analysing changes in frequencies of rain-on-snow (RoS) events with flood-generating potential for large parts of Europe for the historic time frame 1950–2011, Freudiger et al. (2014) hint at similar processes changing flood hazard. Their analyses suggest an increase in flood hazard from RoS events in medium-elevation mountain ranges in the Rhine River Basin in winter due to increased rainfall and a decrease in RoS events in spring due to decreases in snow cover. Although important Rhine tributaries, such as the Moselle River, often are characterised as pluvial-type rivers, the importance of snowmelt as runoff component must not be underestimated. Simulating the Rhine River for the time frame 1901–2006, Stahl et al. (2016) suggest that at gauge Cochem, 26 % of the annual streamflow originates from snowmelt. During winter, this fraction increases up to almost 40 % (see also Fig. 5.7 b). However, the inter-annual variability of annual streamflow and the relative fractions of streamflow components is high, particularly in pluvial-type tributaries of the Rhine River (Stahl et al., 2016).

In Cologne, which is located at the main stream after the confluence of all major tributaries, signals emerging from the different sub-basin superimpose. Accordingly, we detect increases in runoff peaks during winter (Fig. 5.8 c). Detected increases seem to level off as temperatures continue to rise beyond the 2 °C warming level. We do not find indications supporting the hypothesis

describing the creation of a new flood type in the Rhine River Basin due to a transient merging of nival and pluvial flood types. We detect counterbalancing effects between changes in snowmelt and precipitation within the sub-basins. Rising temperatures strongly reduce snowfall, snow accumulation and the snow volume available for melt. The reduction in snowmelt-driven runoff during flood genesis seems to impede the increase in streamflow peaks due to increases in antecedent precipitation. Caution has to be exercised labelling basins such as the Moselle catchment as pluvial-type or the Rhine Basin at Basel as nival-type. In both sub-basins, snowmelt and precipitation are important factors for flood generation. In the framework of this study, we mostly focus on changes in streamflow seasonality and analyse average changes in streamflow generating mechanisms. A detailed analysis of isolated extremes simulated is still pending.

## 5.5 Conclusions

We investigate changes in flood seasonality in the Rhine River Basin under 1.5, 2.0 and 3.0 °C warming using the spatially distributed hydrologic model mHM. In order to improve our understanding of changes in rainfall- and snowmelt-driven runoff, we carried out a detailed inspection of the Rhine River Basin at Basel and the Moselle River Basin at Cochem. We detect significant changes in both rainfall- and snowmelt-driven runoff peaks. Rising temperatures deplete seasonal snowpacks. As a consequence, the importance of snowmelt as flood-generating process diminishes. At no time during the year, a warming climate results in an increase in the risk of snowmelt-driven flooding. Furthermore, solid precipitation (snowfall) strongly decreases during winter. The shift from solid to liquid precipitation further enhances the overall increase in antecedent precipitation.

Our results indicate, that in order to understand changes in annual and monthly streamflow maxima, the examination of counterbalancing effects between changes in snowmelt- and rainfall-driven runoff is crucial. We suggest that future changes in flood characteristics in the Rhine River Basin are controlled by increased precipitation amounts on the one hand, and reduced snowmelt on the other hand. The nature of their interaction defines the type of change in runoff peaks. In the case of the Moselle River, increased rainfall amounts during winter, at least partly, are counterbalanced by reduced snowmelt contribution to the streamflow peaks, resulting in only small or transient changes. In the Rhine Basin at Basel, strong increases in antecedent liquid precipitation encounter almost unchanged snowmelt-driven runoff during winter. Hence, streamflow maxima increase strongly. During May and June, our results hint at a transient

increase in streamflow magnitudes at gauge Basel (Fig. 5.8 a). It seems that snowmelt is still strong enough to support an increase in streamflow peaks due to increased antecedent precipitation at moderate warming levels (1.5 °C and 2.0 °C). With further rising temperatures, however, the magnitudes of streamflow maxima reduce along with declining snowmelt (Fig. 5.8 a). In addition to a strong decline in snow packs in the Alps, we detect an upward movement of the snowmelt elevation. It seems that during winter, snowmelt from higher elevation, at least partly, can replace snowmelt for elevations below (Rottler et al., 2021). Our findings confirm previous investigations suggesting a shift from snowmelt to precipitation as most important flood generating mechanism (Vormoor et al., 2015, 2016). We can not find indications of a transient merging of pluvial and nival flood types in the Rhine Basin.

The understanding of future changes in flood characteristics along the Rhine River and its tributaries is of great importance for water resources and flood management. Within this study, some progress has been made in assessing the importance of rainfall and snowmelt as flood-generating processes under different warming levels. However, only further studies pursuing the improvement of meteorological input data and hydrological modelling can ensure a comprehensive understanding of future flood characteristics in the Rhine River. Next steps could be the implementation and validation of a physically-based snow routine and a glacier module in mHM in order to substantiate our current results regarding the relevance of snowmelt magnitude and timing for the generation of Rhine floods. The usage of satellite-based snow cover maps during model calibration and/or validation might further improve the simulation of the snow cover dynamics. A streamflow component model enabling the tracing of river flow originating processes (e.g., Stahl et al., 2016) might ameliorate the understanding of snowmelt and rainfall as flood-generating processes at different Rhine gauges. Furthermore, the representation of lakes (e.g., Imhoff et al., 2020) and reservoirs and their management might improve streamflow simulations, particularly during low-flow conditions.

# Code and data availability

Source code of the hydrologic model mHM v.5.10 can be accessed at `https://git.ufz.de/mhm/mhm` (last access: 8 October 2020). R-scripts used to analyse simulation results are available at `https://github.com/ERottler/mhm_rhine` (last access: 9 November 2020). Discharge data can be requested from the Global Runoff Data Centre, 56068, Koblenz, Germany (GRDC). Further data sets used can be made available upon request

## Author contributions

ER conducted the analysis and wrote the manuscript. AB, GB and OR provided support and guidance in the process of model set up, data analysis and preparation of the manuscript.

## Competing interests

The authors declare that they have no conflict of interest.

## Acknowledgements

This research was supported by the Deutsche Forschungsgemeinschaft (GRK 2043/1-P2) within the NatRiskChange research training group at the University of Potsdam (https://www.uni-potsdam.de/natriskchange/, last access: 2 October 2020). We acknowledge the datasets generated in the EDgE proof-of-concept project performed under a contract for the Copernicus Climate Change Service (http://edge.climate.copernicus.eu, last access: 8 October 2020). ECMWF implements this service and the Copernicus Atmosphere Monitoring Service on behalf of the European Commission. We acknowledge EDgE colleagues Rohini Kumar and Stephan Thober for establishing the mHM model setup and performing the downscaling of the CMIP5 data sets, respectively. We acknowledge the E-OBS dataset from the EU FP6 project ENSEMBLES (http://ensembles-eu.metoffice.com) and the data providers in the ECA&D project (http://www.ecad.eu). We acknowledge the ISI-MIP project for providing the bias corrected CMIP5 climate model data. The Copernicus Land Monitoring Service, implemented by the European Environmental Agency, provided the European Digital Elevation Model (EU-DEM), version 1.1. We also acknowledge the HOKLIM project (https://www.ufz.de/hoklim) by the German Ministry for Education and Research (grant number 01LS1611A). We also thank various other organisations and projects for providing data used in this study, including JRC, ESA, NASA, USGS, GRDC, BGR, UNESCO, ISRIC, and EEA.

## Appendix

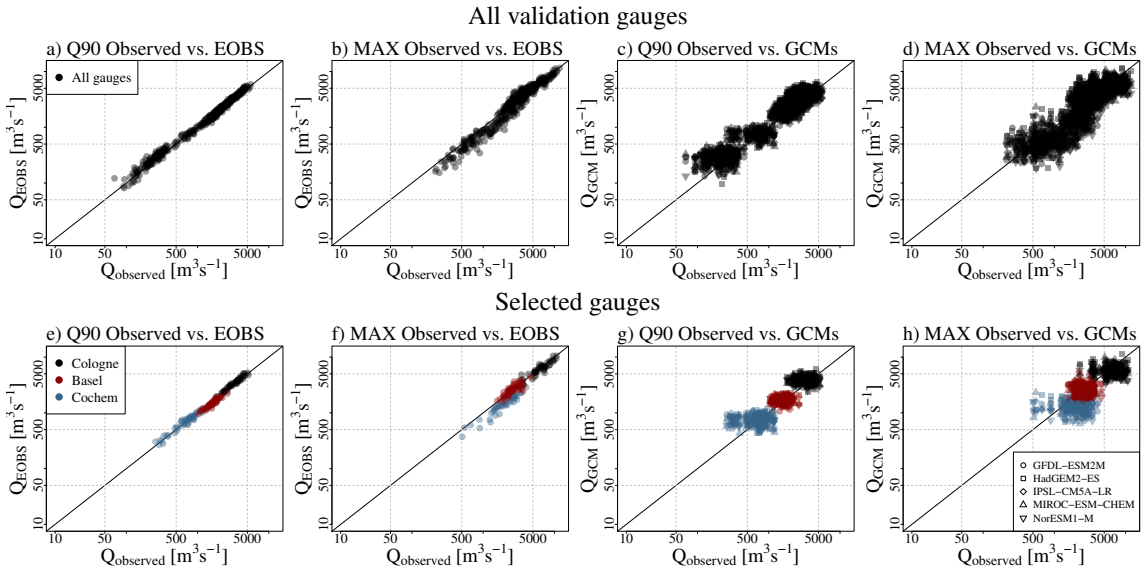


***Figure 5.10:*** *Scatter plot of observed and simulated annual streamflow maxima (MAX) and the 90 % streamflow quantile (Q90) of the hydrological year starting 1 October for all validation gauges (a-d; Fig. 5.2) and for selected gauges (e-h). Panels a, b, e and f depict observed discharge and simulated discharge using E-OBS-based meteorological forcing. Panels c, d, g and h depict observed discharge and simulated discharge using climate model data from the ISI-MIP project. Time frame investigated: 1951–2000.*

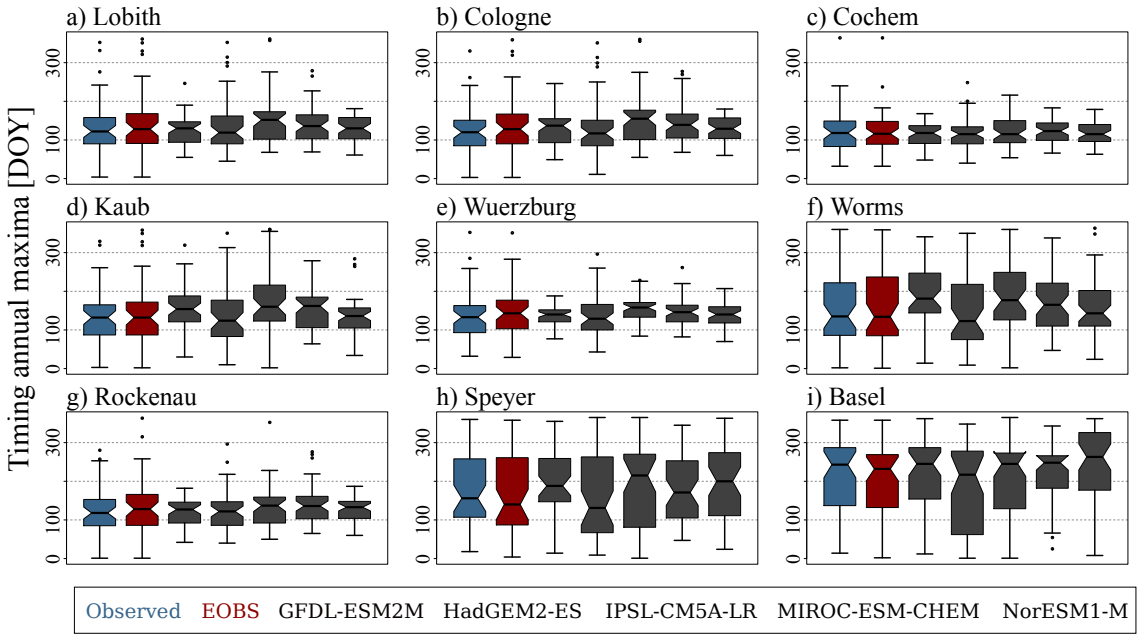


***Figure 5.11:*** *Timing of annual streamflow maxima observed and simulated using E-OBS-based meteorological forcing and climate model data from the ISI-MIP project for all validation gauges (Fig. 5.2). Time frame investigated: 1951–2000.*

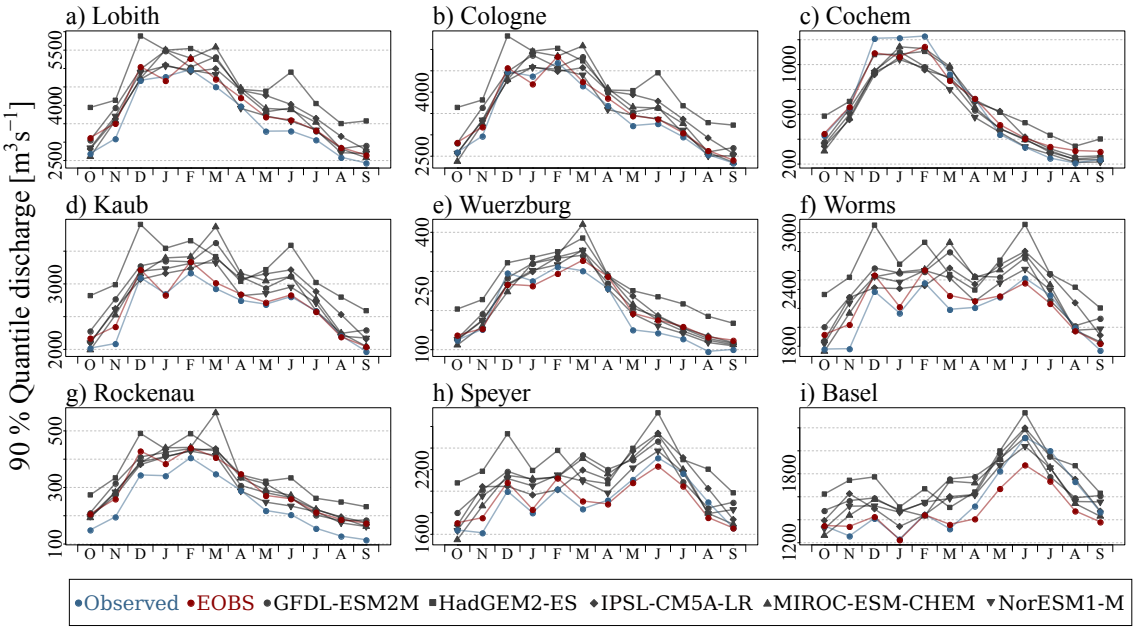


***Figure 5.12:*** *Streamflow quantiles (90 %) for every month of the year based on daily resolution observations and simulations using E-OBS-based meteorological forcing and climate model data from the ISI-MIP project for all validation gauges (Fig. 5.2). Time frame investigated: 1951–2000.*

# 6 Synthesis, conclusion and outlook

## 6.1 Synthesis and conclusion

River flooding poses a threat to riparian communities all over the world. The detection, quantification and attribution of changes in flood characteristics is key to assess possible changes in flood hazard and to help affected societies to timely mitigate and adapt to emerging risks. Within this thesis, some progress has been made in assessing historic and projected changes in flood characteristics in the Rhine River Basin. In the following, the main findings and conclusions for the specific and overarching research questions (Fig. 1.2) are summarised and discussed.

**RQ 1: What are the main drivers of changes in runoff timing and runoff seasonality?**

The construction and operation of large reservoirs strongly affect the runoff timing and runoff seasonality in the southern part of Rhine River Basin. The operation of high head hydropower stations with reservoir lakes redistributes water from summer to winter (Fig. 3.4). Signals emerging in the Alpine part of the Rhine Basin propagate downstream the Rhine River. Furthermore, a weekly pattern following the energy consumption and hydropower productions with high discharge during the week and low discharge on weekends shows up (Fig. 2.6). Changes in runoff seasonality imposed by hydropower production overlap with changes due to changes in seasonal snow covers. Rising temperatures reduce snow accumulation and snow covers are depleted earlier in the year already (Fig. 4.3 and 5.9 a and b). In addition, changes in precipitation characteristics affect changes in runoff timing and seasonality. The analysis of observational data hints at more (intense) rainfall in recent decades, particularly during winter, in turn increasing high runoff quantiles (Fig. 3.4). Hydrological simulations using an ensemble of climate

projections point a shift from solid to liquid precipitation, which enhances the overall increase in precipitation sums (Fig. 5.9 c–f). Mechanisms not specifically addressed in the framework of this thesis include the effect of lake regulations, land use changes and the retreat of Alpine glaciers.

**RQ 2: Which analytical and visualisation techniques are suitable to detect and present changes in river runoff?**

The developed interactive web application *Hydro Explorer* is a powerful tool to present, explore, learn and teach analytical and visualisation techniques related to streamflow changes (Chapter 2). A selection of commonly used analytical techniques, i.e., raster graphs, mean annual cycles, the timing of runoff fractions, quantile estimations and annual/monthly maxima, can be explored and more than 7000 runoff gauges all around the world investigated. The exploration and comparison of a great diversity of river gauges in the Rhine River Basin and beyond indicates that river systems around the world undergo fundamental changes. Results point out, that each analytical technique has its assets and drawbacks and that for the assessment of signal robustness, the ability to easily compare results of different methods, gauges, regions, and time frames is crucial. Next step in the development of the *Hydro Explorer* could be the incorporation of additional analytical tools and the application to other hydro-climatological data sets. The development and application of the analytical sequence, which combines quantile sampling with moving average trend statistics and empirical mode decomposition (Chapter 3), represents a further step in the scientific quest to disentangle natural variability, climate change signals and direct human impacts. In general, the usage of adequate analytical and visualisation techniques and the presentation of results in an easy accessible way is key in the communication of scientific insights. Future studies need to develop and improve visualisation techniques using newly available web-based infrastructures.

**RQ 3: How do higher temperatures affect snowmelt event characteristics?**

Alpine landscapes react particularly sensitive towards climatic changes. A thorough investigation of changes in seasonal snow packs is of great importance to anticipate future changes in flood hazard in the Rhine River Basin. The analysis of historic snow cover changes in the Rhine Basin upstream gauge Basel provides first insights on how changes in snowmelt translate into changes in river runoff (Fig. 4.3). Results obtained analysing snow observations are extended by simulations of the Alpine snow cover using a physically based snow model (Chapter 4) and hydrological simulations of the Rhine River Basin forcing the hydrological

model mHM with an ensemble of climate projections (Chapter 5). Results hint at strong decreases of both snow accumulation and snowmelt (Fig. 4.5 and 5.9 a and b). Rising temperatures do not just decrease maximum melt rates, a threefold effect can be identified: snowmelt becomes weaker, occurs earlier and forms at higher elevations (Fig. 4.7 and 5.7 e). Due to the wide range of elevations in the basin, snowmelt does not occur simultaneously at all elevations. Results indicate that elevation bands melt together in blocks (Fig. 4.8). The beginning and end of the release of meltwater seem to be determined by the passage of warm air masses, and the respective elevation range affected by accompanying temperatures and snow availability. Following those findings, a hypothesis describing elevation-dependent compensation effects in snowmelt is introduced: In a warmer world with similar sequences of weather conditions, snowmelt is moved upward to higher elevations, i.e. the block of elevation bands providing most water to the snowmelt-induced runoff is located at higher elevations. The movement upward the elevation range makes snowmelt in individual elevation bands occur earlier. The timing of the snowmelt-induced runoff, however, stays the same (Fig. 4.12). Meltwater from higher elevations, at least partly, replaces meltwater from elevations below. Future studies are required to further investigate the proposed hypothesis describing elevation-dependent compensation effects in snowmelt.

**RQ 4: Do precipitation events intensify?**

The analysis of long-term changes in hydro-climatic data hints more (intense) precipitation in recent decades, particularly during winter (Fig. 3.5). A trend of increasing precipitation amounts can also be detected in future climate projections. The analysis of 5-day precipitation sums in the Rhine Basin points at an increase in precipitation amounts with climate warming (Fig. 5.9 c–f). During winter, this overall increase is amplified by temperature-induced changes from solid to liquid precipitation (Fig. 5.7 c and d). Further research is required to improve the understanding of mechanisms causing changes in precipitation characteristics. These include the impact of changes in the frequency and persistence of large-scale circulation pattern, natural variations in sea-land moisture transport and temperature-moisture feedbacks in the atmosphere.

**RQ 5: What factors control future changes in Rhine River flood seasonality?**

To investigate transient changes in flood hazard in the Rhine River Basin in the 21st century, the spatially distributed hydrologic model mHM is forced with an ensemble of climate projection scenarios (Chapter 5). The analysis of streamflow, snowmelt, precipitation and evapotranspiration at 1.5, 2.0 and 3.0 °C global

warming levels extends the knowledge attained by the analysis of historic time frames. Simulation results suggest that future changes in flood characteristics in the Rhine River Basin are controlled by increased precipitation amounts on the one hand, and reduced snowmelt on the other hand. Rising temperatures deplete seasonal snowpacks. As a consequence, the importance of snowmelt as flood-generating process diminishes. At no time during the year, a warming climate results in an increase in the risk of snowmelt-driven flooding. Counterbalancing effects between snowmelt and precipitation can result in only little and transient changes in streamflow peaks (Fig. 5.8). In the Moselle catchment, the reduction in snowmelt-driven runoff during flood genesis seems to impede the increase in streamflow peaks due to increases in antecedent precipitation. In the Rhine River Basin upstream Basel, rising temperatures evoke changes from solid to liquid precipitation, which enhance the overall increase in precipitation sums, particularly in the cold season. At gauge Basel, the strongest increases in streamflow maxima show up during winter, when strong increases in liquid precipitation encounter almost unchanged snowmelt-driven runoff. However, the analysis conducted focuses on the magnitude and timing of annual maxima. When using annual maxima, not all peaks investigated represent flood events of relevant magnitude. A detailed analysis of very rare floods is still pending. The model set-up presented in chapter 5 seems to be predestined to form the basis for such a task.

**Overarching RQ: Does global warming cause the transient merging of nival and pluvial Rhine flow regimes and the creation of a new flood type with catastrophic consequences?**

Although investigations point at changes in both rainfall- and snowmelt-driven runoff, there are no indications of a transient merging of nival and pluvial Rhine flood regimes due to climate warming, as hypothesised at the beginning of this thesis (Fig. 1.1). The hypothesis bases on two assumptions: 1) Increased precipitation amounts cause more (intense) flood peaks in pluvial-type tributaries draining low mountain ranges and low land areas and 2) the earlier timing of snowmelt-driven runoff from the Alps shifts the risk of nival flooding forward in time. With regard to the first assumption, investigations indicate that the increase in streamflow peaks does not follow the increases in precipitation amounts. It seems that reduced snowmelt contributions to streamflow in pluvial-type tributaries result in only little and transient increases in streamflow peaks. The importance of snowmelt as runoff component in the pluvial-type tributaries of the Rhine River, such as the Moselle River, during winter must no be underestimated. Furthermore, analysis results hint that a distinct nival flood regime as illustrated in Fig. 1.1 with snowmelt-induced flooding occurring in spring and early summer

exists in the headwater catchments in the Alps, but starts to become increasingly blurry with increasing catchments size and variety and increasing complexity of the flow regime in the High Rhine. Hydrological simulation suggest that at no point in time during the snowmelt season, a warming climate results in an increase in the risk of snowmelt-driven flooding. The detected earlier timing of annual snowmelt maxima in the High Rhine (Fig. 5.6) is not due to an increase in snowmelt magnitudes earlier in the year. It rather seems that events early in the snowmelt season, even if weakened by rising temperatures, more often are the strongest of the year already, as snow packs are increasingly depleted within the course of the snowmelt season. In addition, snow simulations suggest that the wide elevation range enables elevation-dependent compensation effects in snowmelt. The presented hypothesis of elevation-dependent compensation effects suggests that despite the earlier timing of snowmelt in individual elevation bands, the timing of the snowmelt-induced runoff stays the same. Hydological simulations indicate that flooding in the large pluvial-type tributaries of the Rhine, such as the Moselle River, as well as the High Rhine is controlled by both precipitation and snowmelt. Caution has to be exercised labelling sub-basins such as the Moselle catchment as purely pluvial-type or the Rhine River Basin at Basel as purely nival-type. Results indicate that this (over-)simplifications can entail misleading assumptions with regard to flood-generating mechanisms and changes in flood hazard.

## 6.2 Outlook

This thesis represents a step forward in the scientific task to detect, quantify and attribute changes in historic and future flood characteristics in the Rhine River Basin. Some progress has been made, however, future investigations need to be conducted to ensure a comprehensive understanding of changes in future flood characteristics and underlying mechanisms.

**Interactive online tools**

In recent years, the potential of interactive web applications to share information is increasingly recognized. Particularly in hazard and risk research, the provision of background as well as real-time information to residents and decision-makers in an easy accessible way is of great importance. The *Hydro Explorer* represents another example that hints at the potential of scientifically engineered online tools. Future studies need to harness this potential and improve the communication of information related to hazards and risks. An interactive web application that allows

for a detailed investigation of the genesis of major historic and projected Rhine floods represents a possible next step in the investigation and communication of changing flood hazard in the Rhine Basin. This web application could include the analysis and visualization of the amount and spatial pattern of precipitation and snowmelt, flood extent and the superposition of flood waves originating from different sub-basins. In addition, the development and application of new analytical/visualization tools to investigate changes in flood generating processes due to (in-)direct anthropogenic impacts on river runoff can provide new insights.

**Hypothesis testing**

Further studies are required to investigate the proposed hypothesis describing elevation-dependent compensation effects in snowmelt. A systematic analysis using artificial catchments with varying elevation distributions to assess the degree of compensation effects resolved in space and time represents one possible next step.

**Improvement of input data and model set up**

Furthermore, investigations pursuing the improvement of meteorological input data and model set up are required. The snow volume distribution along the elevation range can be improved by implementing snow redistribution processes by wind and avalanches. The implementation and validation of a physically-based snow routine and a glacier module in mHM can substantiate results obtained from hydrological simulations. The usage of satellite-based snow cover maps in a multi-parameter calibration scheme might further improve the simulations of the snow cover dynamics. To ameliorate the understanding of snowmelt and rainfall as flood-generating processes at different Rhine gauges, a streamflow component model enabling the tracing of river flow originating processes can be coupled to mHM simulations. Furthermore, the representation of lakes and reservoirs and their management can improve streamflow simulations, particularly in the Alpine part of the Rhine River Basin.

# Bibliography


C. C. Abon, D. Kneis, I. Crisologo, A. Bronstert, C. P. C. David, and M. Heistermann. Evaluating the potential of radar-based rainfall estimates for streamflow and flood simulations in the philippines. *Geomatics, Natural Hazards and Risk*, 7 (4):1390–1405, 2016. DOI: 10.1080/19475705.2015.1058862.

N. Addor, O. Rössler, N. Köplin, M. Huss, R. Weingartner, and J. Seibert. Robust changes and sources of uncertainty in the projected hydrological regimes of swiss catchments. *Water Resources Research*, 50(10):7541–7562, 2014. DOI: 10.1002/2014WR015549.

L. Alfieri, P. Burek, L. Feyen, and G. Forzieri. Global warming increases the frequency of river floods in europe. *Hydrology and Earth System Sciences*, 19(5): 2247–2260, 2015. DOI: 10.5194/hess-19-2247-2015.

P. Allamano, P. Claps, and F. Laio. An analytical model of the effects of catchment elevation on the flood frequency distribution. *Water Resources Research*, 45(1), 2009a. DOI: 10.1029/2007WR006658.

P. Allamano, P. Claps, and F. Laio. Global warming increases flood risk in mountainous areas. *Geophysical Research Letters*, 36(24), 2009b. DOI: 10.1029/2009GL041395.

G. Ayzel, M. Heistermann, and T. Winterrath. Optical flow models as an open benchmark for radar-based precipitation nowcasting (rainymotion v0.1). *Geoscientific Model Development*, 12(4):1387–1402, 2019. DOI: 10.5194/gmd-12-1387-2019.

G. Ayzel, T. Scheffer, and M. Heistermann. Rainnet v1.0: a convolutional neural network for radar-based precipitation nowcasting. *Geoscientific Model Development*, 13(6):2631–2644, 2020. DOI: 10.5194/gmd-13-2631-2020.

A. Bárdossy and H. J. Caspary. Detection of climate change in Europe by analyzing European atmospheric circulation patterns from 1881 to 1989. *Theoretical and Applied Climatology*, 42(3):155–167, 1990. DOI: 10.1007/BF00866871.

T. P. Barnett, J. C. Adam, and D. P. Lettenmaier. Potential impacts of a warming climate on water availability in snow-dominated regions. *Nature*, 438(7066): 303–309, 2005. DOI: 10.1038/nature04141.

M. Bavay, M. Lehning, T. Jonas, and H. Löwe. Simulations of future snow cover and discharge in alpine headwater catchments. *Hydrological Processes*, 23(1): 95–108, 2009. DOI: 10.1002/hyp.7195.

V. Bačová-Mitková and M. Onderka. Analysis of extreme hydrological events on the Danube using the peak over threshold method. *Journal of Hydrology and Hydromechanics*, 58(2):88 – 101, 2010. DOI: https://doi.org/10.2478/v10098-010-0009-x.

M. Begert and C. Frei. Long-term area-mean temperature series for Switzerland—Combining homogenized station data and high resolution grid data. *International Journal of Climatology*, 38(6):2792–2807, 2018. DOI: 10.1002/joc.5460.

M. Begert, T. Schlegel, and W. Kirchhofer. Homogeneous temperature and precipitation series of Switzerland from 1864 to 2000. *International Journal of Climatology*, 25(1):65–80, 2005. DOI: 10.1002/joc.1118.

J. U. Belz, G. Brahmer, H. Buiteveld, H. Engel, R. Grabher, H. Hodel, P. Krahe, R. Lammersen, M. Larina, H.-G. Mendel, A. Meuser, G. Müller, B. Plonka, L. Pfister, and W. van Vuuren. Das Abflussregime des Rheins und seiner Nebenflüsse im 20. Jahrhundert. Analyse, Veränderungen und Trends. Technical Report Bericht Nr. I-22, Internationale Kommission fur die Hydrologie des Rheingebietes (KHR), Utrecht, Netherlands, 2007. URL https://www.chr-khr.org/sites/default/files/extended_abstract_i_22_d.pdf. (last access: 09/02/2021).

M. Beniston, D. Farinotti, M. Stoffel, L. M. Andreassen, E. Coppola, N. Eckert, A. Fantini, F. Giacona, C. Hauck, M. Huss, H. Huwald, M. Lehning, J.-I. López-Moreno, J. Magnusson, C. Marty, E. Morán-Tejéda, S. Morin, M. Naaim, A. Provenzale, A. Rabatel, D. Six, J. Stötter, U. Strasser, S. Terzago, and C. Vincent. The european mountain cryosphere: a review of its current state, trends, and future challenges. *The Cryosphere*, 12(2):759–794, 2018a. DOI: 10.5194/tc-12-759-2018.

M. Beniston. Impacts of climatic change on water and associated economic activities in the swiss alps. *Journal of Hydrology*, 412-413:291 – 296, 2012. DOI: 10.1016/j.jhydrol.2010.06.046.

M. Beniston, D. Farinotti, M. Stoffel, L. M. Andreassen, E. Coppola, N. Eckert, A. Fantini, F. Giacona, C. Hauck, M. Huss, H. Huwald, M. Lehning, J.-I. López-Moreno, J. Magnusson, C. Marty, E. Morán-Tejéda, S. Morin, M. Naaim, A. Provenzale, A. Rabatel, D. Six, J. Stötter, U. Strasser, S. Terzago, and C. Vincent. The European mountain cryosphere: a review of its current state, trends, and future challenges. *The Cryosphere*, 12(2):759–794, 2018b. DOI: 10.5194/tc-12-759-2018.

W. R. Berghuijs, S. Harrigan, P. Molnar, L. J. Slater, and J. W. Kirchner. The Relative Importance of Different Flood-Generating Mechanisms Across Europe. *Water Resources Research*, 55(6):4582–4593, 2019. DOI: 10.1029/2019WR024841.

M. Bertola, A. Viglione, D. Lun, J. Hall, and G. Blöschl. Flood trends in europe: are changes in small and big floods different? *Hydrology and Earth System Sciences*, 24(4):1805–1822, 2020. DOI: 10.5194/hess-24-1805-2020.

T. W. Biggs and T. M. Whitaker. Critical elevation zones of snowmelt during peak discharges in a mountain river basin. *Journal of Hydrology*, 438-439:52 – 65, 2012. DOI: 10.1016/j.jhydrol.2012.02.048.

M.-V. Birsan, P. Molnar, P. Burlando, and M. Pfaundler. Streamflow trends in Switzerland. *Journal of Hydrology*, 314(1):312–329, 2005. DOI: 10.1016/j.jhydrol.2005.06.008.

S. Blenkinsop and H. J. Fowler. Changes in european drought characteristics projected by the prudence regional climate models. *International Journal of Climatology*, 27(12):1595–1610, 2007. DOI: 10.1002/joc.1538.

G. Blöschl, T. Nester, J. Komma, J. Parajka, and R. A. P. Perdigão. The june 2013 flood in the upper danube basin, and comparisons with the 2002, 1954 and 1899 floods. *Hydrology and Earth System Sciences*, 17(12):5197–5212, 2013. DOI: 10.5194/hess-17-5197-2013.

G. Blöschl, J. Hall, J. Parajka, R. A. P. Perdigão, B. Merz, B. Arheimer, G. T. Aronica, A. Bilibashi, O. Bonacci, M. Borga, I. Čanjevac, A. Castellarin, G. B. Chirico, P. Claps, K. Fiala, N. Frolova, L. Gorbachova, A. Gül, J. Hannaford, S. Harrigan, M. Kireeva, A. Kiss, T. R. Kjeldsen, S. Kohnová, J. J. Koskela, O. Ledvinka, N. Macdonald, M. Mavrova-Guirguinova, L. Mediero, R. Merz, P. Molnar, A. Montanari, C. Murphy, M. Osuch, V. Ovcharuk, I. Radevski, M. Rogger, J. L. Salinas, E. Sauquet, M. Šraj, J. Szolgay, A. Viglione, E. Volpi, D. Wilson, K. Zaimi, and N. Živković. Changing climate shifts timing of European floods. *Science*, 357(6351):588–590, 2017. DOI: 10.1126/science.aan2506.

G. Blöschl, J. Hall, A. Viglione, R. A. P. Perdigão, J. Parajka, B. Merz, D. Lun, B. Arheimer, G. T. Aronica, A. Bilibashi, M. Boháč, O. Bonacci, M. Borga, I. Čanjevac, A. Castellarin, G. B. Chirico, P. Claps, N. Frolova, D. Ganora, L. Gorbachova, A. Gül, J. Hannaford, S. Harrigan, M. Kireeva, A. Kiss, T. R. Kjeldsen, S. Kohnová, J. J. Koskela, O. Ledvinka, N. Macdonald, M. Mavrova-Guirguinova, L. Mediero, R. Merz, P. Molnar, A. Montanari, C. Murphy, M. Osuch, V. Ovcharuk, I. Radevski, J. L. Salinas, E. Sauquet, M. Šraj, J. Szolgay, E. Volpi, D. Wilson, K. Zaimi, and N. Živković. Changing climate both increases and decreases European river floods. *Nature*, 573(7772):108–111, 2019. DOI: 10.1038/s41586-019-1495-6.

H. Bodemann and R. Pfammatter. Der Verband Aare-Rheinwerke 1915 bis 2015 – Rückblick auf ein Jahrhundert Wasserwirtschaft. *Wasser Energie Luft*, 2:85–97, 2015. URL https://www.swv.ch/fr/wp-content/uploads/sites/2/2018/03/R%C3%BCckblick-auf-ein-Jahrhundert-Wasserwirtschaft_WEL.pdf. (last access: 09/02/2021).

A. Bokwa. Natural hazard. In P. T. Bobrowsky, editor, *Encyclopedia of Natural Hazards*, pages 711–718. Springer Netherlands, Dordrecht, 2013. ISBN 978-1-4020-4399-4. DOI: 10.1007/978-1-4020-4399-4_248.

T. Bosshard, M. Carambia, K. Goergen, S. Kotlarski, P. Krahe, M. Zappa, and C. Schär. Quantifying uncertainty sources in an ensemble of hydrological climate-impact projections. *Water Resources Research*, 49(3):1523–1536, 2013. DOI: 10.1029/2011WR011533.

T. Bosshard, S. Kotlarski, M. Zappa, and C. Schär. Hydrological Climate-Impact Projections for the Rhine River: GCM–RCM Uncertainty and Separate Temperature and Precipitation Effects. *Journal of Hydrometeorology*, 15(2):697–713, 2014. DOI: 10.1175/JHM-D-12-098.1.

C. E. Brendel, R. L. Dymond, and M. F. Aguilar. An interactive web app for retrieval, visualization, and analysis of hydrologic and meteorological time series data. *Environmental Modelling & Software*, 117:14 – 28, 2019. DOI: 10.1016/j.envsoft.2019.03.003.

D. Bronaugh and A. Werner. *Zyp: Zhang + Yue-Pilon Trends Package*. R package version 0.10-1, Pacific Climate Impacts Consortium, University of Victoria, Victoria, Canada, 2013. URL https://CRAN.R-project.org/package=zyp. (last access: 09/02/2021).

A. Bronstert, A. Bárdossy, C. Bismuth, H. Buiteveld, M. Disse, H. Engel, U. Fritsch, Y. Hundecha, R. Lammersen, D. Niehoff, and N. Ritter. Multi-scale modelling

of land-use change and river training effects on floods in the Rhine basin. *River Research and Applications*, 23(10):1102–1125, 2007. DOI: 10.1002/rra.1036.

M. I. Brunner, D. Farinotti, H. Zekollari, M. Huss, and M. Zappa. Future shifts in extreme flow regimes in alpine regions. *Hydrology and Earth System Sciences*, 23 (11):4471–4489, 2019a. DOI: 10.5194/hess-23-4471-2019.

M. I. Brunner, L. A. Melsen, A. J. Newman, A. W. Wood, and M. P. Clark. Future streamflow regime changes in the United States: assessment using functional classification. *Hydrology and Earth System Sciences*, 24(8):3951–3966, 2020a. DOI: 10.5194/hess-24-3951-2020.

M. I. Brunner, D. Farinotti, H. Zekollari, M. Huss, and M. Zappa. Future shifts in extreme flow regimes in Alpine regions. *Hydrology and Earth System Sciences*, 23 (11):4471–4489, 2019b. DOI: 10.5194/hess-23-4471-2019.

M. I. Brunner, E. Gilleland, A. Wood, D. L. Swain, and M. Clark. Spatial dependence of floods shaped by spatiotemporal variations in meteorological and land-surface processes. *Geophysical Research Letters*, 47(13):e2020GL088000, 2020b. DOI: 10.1029/2020GL088000.

P. Bubeck, L. Berghäuser, P. Hudson, and A. H. Thieken. Using panel data to understand the dynamics of human behavior in response to flooding. *Risk Analysis*, 40(11):2340–2359, 2020. DOI: 10.1111/risa.13548.

G. Bürger, A. Pfister, and A. Bronstert. Temperature-Driven Rise in Extreme Sub-Hourly Rainfall. *Journal of Climate*, 32(22):7597–7609, 2019. DOI: 10.1175/JCLI-D-19-0136.1.

P. Ceppi, S. C. Scherrer, A. M. Fischer, and C. Appenzeller. Revisiting Swiss temperature trends 1959–2008. *International Journal of Climatology*, 32(2):203–213, 2012. DOI: 10.1002/joc.2260.

W. Chang, J. Cheng, J. Allaire, Y. Xie, and J. McPherson. *shiny: Web Application Framework for R*, 2019. URL https://CRAN.R-project.org/package=shiny. (last access: 09/02/2021).

D. W. Clow. Changes in the Timing of Snowmelt and Streamflow in Colorado: A Response to Recent Warming. *Journal of Climate*, 23(9):2293–2306, 2010. DOI: 10.1175/2009JCLI2951.1.

R. C. Cornes, G. van der Schrier, E. J. M. van den Besselaar, and P. D. Jones. An ensemble version of the e-obs temperature and precipitation data sets. *Journal*

*of Geophysical Research: Atmospheres*, 123(17):9391–9409, 2018. DOI: 10.1029/2017JD028200.

A. Costa Tomaz de Souza, G. Ayzel, and M. Heistermann. Quantifying the location error of precipitation nowcasts. *Advances in Meteorology*, 2020, 2020. DOI: 10.1155/2020/8841913.

D. Coumou and S. Rahmstorf. A decade of weather extremes. *Nature Climate Change*, 2(7):491–496, 2012. DOI: 10.1038/nclimate1452.

CRED & UNISDR. Economic losses, poverty & disasters: 1998-2017. Report, Center for Research on the Epidemiology of Disasters & United Nations Office for Disaster Risk Reduction, 2018. URL https://www.preventionweb.net/files/61119_credeconomiclosses.pdf. (last access: 09/02/2021).

D. Crichton. The risk triangle. *Natural disaster management*, pages 102–103, 1999. URL http://www.ilankelman.org/crichton/1999risktriangle.pdf. (last access: 09/02/2021).

M. J. Crozier. Deciphering the effect of climate change on landslide activity: A review. *Geomorphology*, 124(3):260–267, 2010. DOI: 10.1016/j.geomorph.2010.04.009.

R. Dankers and L. Feyen. Climate change impact on flood hazard in europe: An assessment based on high-resolution climate simulations. *Journal of Geophysical Research: Atmospheres*, 113(D19), 2008. DOI: 10.1029/2007JD009719.

F. V. Davenport, J. E. Herrera-Estrada, M. Burke, and N. S. Diffenbaugh. Flood size increases nonlinearly across the western united states in response to lower snow-precipitation ratios. *Water Resources Research*, 56(1):e2019WR025571, 2020. DOI: 10.1029/2019WR025571.

A. J. C. B. de Saint-Venant. Théorie du mouvement non permanent des eaux, avec application aux crues des rivières et a l'introduction de marées dans leurs lits. *Comptes Rendus des Séances de lAcadémie des Sciences, Gauthier-Villars, Paris, France*, 73:1–11, 1871.

P. M. Della-Marta, M. R. Haylock, J. Luterbacher, and H. Wanner. Doubled length of western european summer heat waves since 1880. *Journal of Geophysical Research: Atmospheres*, 112(D15), 2007. DOI: 10.1029/2007JD008510.

G. K. Devia, B. Ganasri, and G. Dwarakish. A review on hydrological models. *Aquatic Procedia*, 4:1001–1007, 2015. ISSN 2214-241X. DOI: https://doi.org/10.

1016/j.aqpro.2015.02.126. INTERNATIONAL CONFERENCE ON WATER RESOURCES, COASTAL AND OCEAN ENGINEERING (ICWRCOE'15).

F. Di Sante, E. Coppola, and F. Giorgi. Projections of river floods in europe using EURO-CORDEX, CMIP5 and CMIP6 simulations. *International Journal of Climatology*, pages 1–19, 2021. DOI: https://doi.org/10.1002/joc.7014.

I. Didovets, V. Krysanova, G. Bürger, S. Snizhko, V. Balabukh, and A. Bronstert. Climate change impact on regional floods in the carpathian region. *Journal of Hydrology: Regional Studies*, 22:100590, 2019. DOI: 10.1016/j.ejrh.2019.01.002.

J. Doi, G. Potter, J. Wong, I. Alcaraz, and P. Chi. Web application teaching tools for statistics using r and shiny. *Technology Innovations in Statistics Education*, 9(1), 2016. URL https://escholarship.org/uc/item/00d4q8cp. (last access: 09/02/2021).

D. Duethmann and G. Blöschl. Why has catchment evaporation increased in the past 40 years? a data-based study in austria. *Hydrology and Earth System Sciences*, 22(10):5143–5158, 2018. DOI: 10.5194/hess-22-5143-2018.

M. J. Dunning, S. L. Vowler, E. Lalonde, H. Ross-Adams, P. Boutros, I. G. Mills, A. G. Lynch, and A. D. Lamb. Mining human prostate cancer datasets: The "camcapp" shiny app. *EBioMedicine*, 17:5–6, 2017. DOI: 10.1016/j.ebiom.2017.02.022.

S. J. Déry, K. Stahl, R. D. Moore, P. H. Whitfield, B. Menounos, and J. E. Burford. Detection of runoff timing changes in pluvial, nival, and glacial rivers of western canada. *Water Resources Research*, 45(4), 2009. DOI: 10.1029/2008WR006975.

J. R. Eastman, S. Emani, S. Hulina, H. Jiang, A. Johnson, and M. Ramachandran. *Applications of geographic information systems (GIS) technology in environmental risk assessment and management*. Clark University. Clark Labs for Cartographic Technology and Geographic, 1997.

U. Ehret, E. Zehe, V. Wulfmeyer, K. Warrach-Sagi, and J. Liebert. Hess opinions "Should we apply bias correction to global and regional climate model data?". *Hydrology and Earth System Sciences*, 16(9):3391–3404, 2012. DOI: 10.5194/hess-16-3391-2012.

B. Elberling, A. Michelsen, C. Schädel, E. A. Schuur, H. H. Christiansen, L. Berg, M. P. Tamstorf, and C. Sigsgaard. Long-term $CO_2$ production following permafrost thaw. *Nature Climate Change*, 3(10):890–894, 2013.

D. Farinotti, A. Pistocchi, and M. Huss. From dwindling ice to headwater lakes: could dams replace glaciers in the European Alps? *Environmental Research Letters*, 11(5):054022, 2016. DOI: 10.1088/1748-9326/11/5/054022.

S. Fatichi, S. Rimkus, P. Burlando, and R. Bordoy. Does internal climate variability overwhelm climate change signals in streamflow? The upper Po and Rhone basin case studies. *Science of The Total Environment*, 493:1171–1182, 2014. DOI: 10.1016/j.scitotenv.2013.12.014.

R. A. Feddes, P. Kowalik, K. Kolinska-Malinka, and H. Zaradny. Simulation of field water uptake by plants using a soil water dependent root extraction function. *Journal of Hydrology*, 31(1):13 – 26, 1976. DOI: 10.1016/0022-1694(76)90017-2.

A. Fink, U. Ulbrich, and H. Engel. Aspects of the january 1995 flood in Germany. *Weather*, 51(2):34–39, 1996. DOI: 10.1002/j.1477-8696.1996.tb06182.x.

E. M. Fischer and C. Schär. Consistent geographical patterns of changes in high-impact european heatwaves. *Nature Geoscience*, 3(6):398–403, 2010. DOI: 10.1038/ngeo866.

M. Fischer, M. Huss, C. Barboux, and M. Hoelzle. The new swiss glacier inventory sgi2010: Relevance of using high-resolution source data in areas dominated by very small glaciers. *Arctic, Antarctic, and Alpine Research*, 46(4):933–945, 2014. DOI: 10.1657/1938-4246-46.4.933.

C. Frei and C. Schär. Detection Probability of Trends in Rare Events: Theory and Application to Heavy Precipitation in the Alpine Region. *Journal of Climate*, 14(7): 1568–1584, 2001. DOI: 10.1175/1520-0442(2001)014<1568:DPOTIR>2.0.CO;2.

C. Frei, H. C. Davies, J. Gurtz, and C. Schär. Climate dynamics and extreme precipitation and flood events in Central Europe. *Integrated Assessment*, 1(4): 281–300, 2000. DOI: 10.1023/A:1018983226334.

D. Freudiger, I. Kohn, K. Stahl, and M. Weiler. Large-scale analysis of changing frequencies of rain-on-snow events with flood-generation potential. *Hydrology and Earth System Sciences*, 18(7):2695–2709, 2014. DOI: 10.5194/hess-18-2695-2014.

D. Freudiger, B. Frielingsdorf, K. Stahl, A. Steinbrich, M. Weiler, N. Griessinger, and J. Seibert. Das Potential meteorologischer Rasterdatensätze für die Modellierung der Schneedecke alpiner Einzugsgebiete – Potential of meteorological gridded datasets for hydrological modeling in alpine basins. *Hydrologie & Wasserbewirtschaftung*, 60(6), 2016. DOI: 10.5675/HyWa_2016,6_1.

D. Freudiger, I. Kohn, J. Seibert, K. Stahl, and M. Weiler. Snow redistribution for the hydrological modeling of alpine catchments. *WIREs Water*, 4(5):e1232, 2017. DOI: 10.1002/wat2.1232.

P. Froidevaux, J. Schwanbeck, R. Weingartner, C. Chevalier, and O. Martius. Flood triggering in switzerland: the role of daily to monthly preceding precipitation. *Hydrology and Earth System Sciences*, 19(9):3903–3924, 2015. DOI: 10.5194/hess-19-3903-2015.

J. Gehrig-Fasel, A. Guisan, and N. E. Zimmermann. Tree line shifts in the swiss alps: Climate change or land abandonment? *Journal of Vegetation Science*, 18(4): 571–582, 2007. DOI: 10.1111/j.1654-1103.2007.tb02571.x.

B. J. Gillan, J. T. Harper, and J. N. Moore. Timing of present and future snowmelt from high elevations in northwest montana. *Water Resources Research*, 46(1), 2010. DOI: 10.1029/2009WR007861.

A. Gobiet, S. Kotlarski, M. Beniston, G. Heinrich, J. Rajczak, and M. Stoffel. 21st century climate change in the european alps—a review. *Science of The Total Environment*, 493:1138 – 1151, 2014. DOI: 10.1016/j.scitotenv.2013.07.050.

M. G. Grillakis. Increase in severe and extreme soil moisture droughts for europe under climate change. *Science of The Total Environment*, 660:1245 – 1255, 2019. DOI: 10.1016/j.scitotenv.2019.01.001.

H. V. Gupta, H. Kling, K. K. Yilmaz, and G. F. Martinez. Decomposition of the mean squared error and nse performance criteria: Implications for improving hydrological modelling. *Journal of Hydrology*, 377(1):80 – 91, 2009. DOI: 10.1016/j.jhydrol.2009.08.003.

S. Häkkinen, P. B. Rhines, and D. L. Worthen. Atmospheric Blocking and Atlantic Multidecadal Ocean Variability. *Science*, 334(6056):655–659, 2011. DOI: 10.1126/science.1205683.

J. Hall and G. Blöschl. Spatial patterns and characteristics of flood seasonality in europe. *Hydrology and Earth System Sciences*, 22(7):3883–3901, 2018. DOI: 10.5194/hess-22-3883-2018.

R. T. Hanson, M. D. Dettinger, and M. W. Newhouse. Relations between climatic variability and hydrologic time series from four alluvial basins across the southwestern United States. *Hydrogeology Journal*, 14(7):1122–1146, 2006. DOI: 10.1007/s10040-006-0067-7.

F. Hanzer, K. Förster, J. Nemec, and U. Strasser. Projected cryospheric and hydrological impacts of 21st century climate change in the Ötztal Alps (Austria) simulated using a physically based approach. *Hydrology and Earth System Sciences*, 22(2):1593–1614, 2018. DOI: 10.5194/hess-22-1593-2018.

G. H. Hargreaves and Z. A. Samani. Reference crop evapotranspiration from temperature. *Applied engineering in agriculture*, 1(2):96–99, 1985. DOI: 10.13031/2013.26773.

M. R. Haylock, N. Hofstra, A. M. G. Klein Tank, E. J. Klok, P. D. Jones, and M. New. A european daily high-resolution gridded data set of surface temperature and precipitation for 1950–2006. *Journal of Geophysical Research: Atmospheres*, 113 (D20), 2008.

I. M. Held and B. J. Soden. Water Vapor Feedback and Global Warming. *Annual Review of Energy and the Environment*, 25(1):441–475, 2000. DOI: 10.1146/annurev.energy.25.1.441.

S. Hempel, K. Frieler, L. Warszawski, and J. Schewe. Bias corrected GCM input data for ISIMIP Fast Track. Fact sheet, The Inter-Sectoral Impact Model Intercomparison Project, 2013a. URL https://www.isimip.org/gettingstarted/fast-track-bias-correction/. (last access: 22/06/2020).

S. Hempel, K. Frieler, L. Warszawski, J. Schewe, and F. Piontek. A trend-preserving bias correction - the ISI-MIP approach. *Earth System Dynamics*, 4(2):219–236, 2013b. DOI: 10.5194/esd-4-219-2013.

T. Hengl, J. Mendes de Jesus, G. B. Heuvelink, M. Ruiperez Gonzalez, M. Kilibarda, A. Blagotić, W. Shangguan, M. N. Wright, X. Geng, B. Bauer-Marschallinger, et al. Soilgrids250m: Global gridded soil information based on machine learning. *PLoS one*, 12(2):e0169748, 2017. DOI: 10.1371/journal.pone.0169748.

R. Hock, G. Rasul, C. Adler, B. Cáceres, Y. Gruber, Hirabayashi, M. Jackson, A. Kääb, S. Kang, S. Kutuzov, A. Milner, U. Molau, S. Morin, B. Orlove, and H. Steltzer. High mountain areas. In H. O. Pörtner, D. C. Roberts, V. Masson-Delmotte, P. Zhai, M. Tignor, E. Poloczanska, K. Mintenbeck, A. Alegria, M. Nicolai, A. Okem, J. Petzold, B. Rama, and N. M. Weyer, editors, *IPCC Special Report on the Ocean and Cryosphere in a Changing Climate*. In press, 2019. URL https://www.ipcc.ch/srocc/chapter/chapter-2/. (last access: 09/02/2021).

N. Hofstra, M. Haylock, M. New, P. Jones, and C. Frei. Comparison of six methods for the interpolation of daily, european climate data. *Journal of Geophysical Research: Atmospheres*, 113(D21), 2008. DOI: 10.1029/2008JD010100.

P. Horton, B. Schaefli, A. Mezghani, B. Hingray, and A. Musy. Assessment of climate-change impacts on alpine discharge regimes with climate model uncertainty. *Hydrological Processes*, 20(10):2091–2109, 2006. DOI: 10.1002/hyp.6197.

N. E. Huang, Z. Shen, S. R. Long, M. C. Wu, H. H. Shih, Q. Zheng, N.-C. Yen, C. C. Tung, and H. H. Liu. The empirical mode decomposition and the Hilbert spectrum for nonlinear and non-stationary time series analysis. *Proceedings of the Royal Society A: Mathematical, Physical and Engineering Sciences*, 454(1971): 903–995, 1998. DOI: 10.1098/rspa.1998.0193.

N. E. Huang, Z. Shen, and S. R. Long. A NEW VIEW OF NONLINEAR WATER WAVES: The Hilbert Spectrum. *Annual Review of Fluid Mechanics*, 31(1):417–457, 1999. DOI: 10.1146/annurev.fluid.31.1.417.

S. Huang, F. F. Hattermann, V. Krysanova, and A. Bronstert. Projections of climate change impacts on river flood conditions in germany by combining three different rcms with a regional eco-hydrological model. *Climatic change*, 116(3-4):631–663, 2013. DOI: 10.1007/s10584-012-0586-2.

S. Huang, R. Kumar, O. Rakovec, V. Aich, X. Wang, L. Samaniego, S. Liersch, and V. Krysanova. Multimodel assessment of flood characteristics in four large river basins at global warming of 1.5, 2.0 and 3.0 k above the pre-industrial level. *Environmental Research Letters*, 13(12):124005, 2018. DOI: 10.1088/1748-9326/aae94b.

C. Huggel, J. J. Clague, and O. Korup. Is climate change responsible for changing landslide activity in high mountains? *Earth Surface Processes and Landforms*, 37 (1):77–91, 2012. DOI: 10.1002/esp.2223.

C. T. Hunsaker, T. W. Whitaker, and R. C. Bales. Snowmelt runoff and water yield along elevation and temperature gradients in california's southern sierra nevada. *JAWRA Journal of the American Water Resources Association*, 48(4):667–678, 2012. DOI: 10.1111/j.1752-1688.2012.00641.x.

T. G. Huntington. Evidence for intensification of the global water cycle: Review and synthesis. *Journal of Hydrology*, 319(1):83–95, 2006. DOI: 10.1016/j.jhydrol.2005.07.003.

R. Hurkmans, W. Terink, R. Uijlenhoet, P. Torfs, D. Jacob, and P. A. Troch. Changes in Streamflow Dynamics in the Rhine Basin under Three High-Resolution Regional Climate Scenarios. *Journal of Climate*, 23(3):679–699, 2010. DOI: 10.1175/2009JCLI3066.1.

M. Huss. Present and future contribution of glacier storage change to runoff from macroscale drainage basins in europe. *Water Resources Research*, 47(7), 2011. DOI: 10.1029/2010WR010299.

M. Huss and D. Farinotti. Distributed ice thickness and volume of all glaciers around the globe. *Journal of Geophysical Research: Earth Surface*, 117(F4), 2012. DOI: 10.1029/2012JF002523.

M. Huss, D. Farinotti, A. Bauder, and M. Funk. Modelling runoff from highly glacierized alpine drainage basins in a changing climate. *Hydrological processes*, 22(19):3888–3902, 2008. DOI: 10.1002/hyp.7055.

R. J. Hyndman and Y. Fan. Sample Quantiles in Statistical Packages. *The American Statistician*, 50(4):361–365, 1996. DOI: 10.2307/2684934.

R. O. Imhoff, W. J. van Verseveld, B. van Osnabrugge, and A. H. Weerts. Scaling point-scale (pedo)transfer functions to seamless large-domain parameter estimates for high-resolution distributed hydrologic modeling: An example for the rhine river. *Water Resources Research*, 56(4):e2019WR026807, 2020. DOI: 10.1029/2019WR026807.

M. Jajarmizadeh, S. Harun, and M. Salarpour. A review on theoretical consideration and types of models in hydrology. *Journal of Environmental Science and Technology*, 5(5):249–261, 2012. DOI: 10.3923/jest.2012.249.261.

N. Junghans, J. Cullmann, and M. Huss. Evaluating the effect of snow and ice melt in an alpine headwater catchment and further downstream in the river rhine. *Hydrological Sciences Journal*, 56(6):981–993, 2011. DOI: 10.1080/02626667.2011.595372.

D. A. Keim. Designing pixel-oriented visualization techniques: Theory and applications. *IEEE Transactions on visualization and computer graphics*, 6(1):59–78, 2000. DOI: 10.1109/2945.841121.

M. Kemter, B. Merz, N. Marwan, S. Vorogushyn, and G. Blöschl. Joint trends in flood magnitudes and spatial extents across europe. *Geophysical Research Letters*, 47, 2020. DOI: 10.1029/2020GL087464.

M. Kendall. *Rank correlation methods*. Griffin, Charles, London, 4 edition, 1975.

R. A. Kerr. A North Atlantic Climate Pacemaker for the Centuries. *Science*, 288 (5473):1984–1985, 2000. DOI: 10.1126/science.288.5473.1984.

T. Kerr, M. Clark, J. Hendrikx, and B. Anderson. Snow distribution in a steep mid-latitude alpine catchment. *Advances in Water Resources*, 55:17–24, 2013. DOI: 10.1016/j.advwatres.2012.12.010.

A. D. King and D. J. Karoly. Climate extremes in europe at 1.5 and 2 degrees of global warming. *Environmental Research Letters*, 12(11):114031, 2017. DOI: 10.1088/1748-9326/aa8e2c.

G. Klein, Y. Vitasse, C. Rixen, C. Marty, and M. Rebetez. Shorter snow cover duration since 1970 in the Swiss Alps due to earlier snowmelt more than to later snow onset. *Climatic Change*, 139(3):637–649, 2016. DOI: 10.1007/s10584-016-1806-y.

D. Kneis. Eco-Hydrological Simulation Environment (echse) - Documentation of model engines. Technical report, University of Potsdam, 2014. URL http://echse.github.io/downloads/documentation/echse_engines_doc.pdf. (last access: 08/02/2021).

D. Kneis. A lightweight framework for rapid development of object-based hydrological model engines. *Environmental Modelling & Software*, 68:110–121, 2015. DOI: 10.1016/j.envsoft.2015.02.009.

D. Kneis, C. Abon, A. Bronstert, and M. Heistermann. Verification of short-term runoff forecasts for a small philippine basin (marikina). *Hydrological Sciences Journal*, 62(2):205–216, 2017. DOI: 10.1080/02626667.2016.1183773.

R. Koehler. *Raster Based Analysis and Visualization of Hydrologic Time Series*. Phd dissertation, University of Arizona. Tucson, AZ, 2004. URL https://repository.arizona.edu/handle/10150/280516. (last access: 25/06/2020).

C. Kormann, T. Francke, M. Renner, and A. Bronstert. Attribution of high resolution streamflow trends in Western Austria: An approach based on climate and discharge station data. *Hydrology and Earth System Sciences*, 19(3):1225–1245, 2015. DOI: 10.5194/hess-19-1225-2015.

C. Kormann, A. Bronstert, T. Francke, T. Recknagel, and T. Graeff. Model-based attribution of high-resolution streamflow trends in two alpine basins of Western Austria. *Hydrology*, 3(1):7, 2016. DOI: 10.3390/hydrology3010007.

H. Kreibich, A. H. Thieken, T. Petrow, M. Müller, and B. Merz. Flood loss reduction of private households due to building precautionary measures – lessons learned from the Elbe flood in August 2002. *Natural Hazards and Earth System Sciences*, 5 (1):117–126, 2005. DOI: 10.5194/nhess-5-117-2005.

J. Kreyling and H. A. L. Henry. Vanishing winters in Germany: soil frost dynamics and snow cover trends, and ecological implications. *Climate Research*, 46(3): 269–276, 2011. DOI: 10.3354/cr00996.

W. Kron. Flood Risk = Hazard • Values • Vulnerability. *Water International*, 30(1): 58–68, 2005. DOI: 10.1080/02508060508691837.

R. Kumar, L. Samaniego, and S. Attinger. Implications of distributed hydrologic model parameterization on water fluxes at multiple scales and locations. *Water Resources Research*, 49(1):360–379, 2013. DOI: 10.1029/2012WR012195.

Z. W. Kundzewicz, U. Ulbrich, T. Brücher, D. Graczyk, A. Krüger, G. C. Leckebusch, L. Menzel, I. Pińskwar, M. Radziejewski, and M. Szwed. Summer Floods in Central Europe – Climate Change Track? *Natural Hazards*, 36(1):165–189, 2005. DOI: 10.1007/s11069-004-4547-6.

Z. W. Kundzewicz, I. Pińskwar, and G. R. Brakenridge. Large floods in Europe, 1985–2009. *Hydrological Sciences Journal*, 58(1):1–7, 2013. DOI: 10.1080/02626667.2012.745082.

Z. W. Kundzewicz, I. Pińskwar, and G. R. Brakenridge. Changes in river flood hazard in Europe: a review. *Hydrology research*, 49(2):294–302, 2018. DOI: 10.2166/nh.2017.016.

D. Labat, Y. Goddéris, J. L. Probst, and J. L. Guyot. Evidence for global runoff increase related to climate warming. *Advances in Water Resources*, 27(6):631–642, 2004. DOI: 10.1016/j.advwatres.2004.02.020.

A. N. Laghari, D. Vanham, and W. Rauch. To what extent does climate change result in a shift in Alpine hydrology? A case study in the Austrian Alps. *Hydrological Sciences Journal*, 57(1):103–117, 2012. DOI: 10.1080/02626667.2011.637040.

M. Laternser and M. Schneebeli. Long-term snow climate trends of the Swiss Alps (1931–99). *International Journal of Climatology*, 23(7):733–750, 2003. DOI: 10.1002/joc.912.

D. Lavers, C. Prudhomme, and D. M. Hannah. European precipitation connections with large-scale mean sea-level pressure (MSLP) fields. *Hydrological Sciences Journal*, 58(2):310–327, 2013. DOI: 10.1080/02626667.2012.754545.

J. Lehmann, D. Coumou, and K. Frieler. Increased record-breaking precipitation events under global warming. *Climatic Change*, 132(4):501–515, 2015. DOI: 10.1007/s10584-015-1434-y.

B. Lehner. Derivation of watershed boundaries for GRDC gauging stations based on the HydroSHEDS drainage network. GRDC Report Series 41, Global Runoff Data Centre GRDC, Koblenz, 2012. URL https://www.bafg.de/GRDC/EN/02_srvcs/24_rprtsrs/report_41.pdf?__blob=publicationFile. (last access: 09/02/2021).

C. Li-Juan and Y. Zhong-Wei. Progress in research on homogenization of climate data. *Advances in Climate Change Research*, 3(2):59–67, 2012. ISSN 1674-9278. DOI: https://doi.org/10.3724/SP.J.1248.2012.00059.

M. J. Lighthill and G. B. Whitham. On kinematic waves i. flood movement in long rivers. *Proceedings of the Royal Society of London. Series A. Mathematical and Physical Sciences*, 229(1178):281–316, 1955. DOI: 10.1098/rspa.1955.0088.

H. F. Lins and J. R. Slack. Streamflow trends in the United States. *Geophysical Research Letters*, 26(2):227–230, 1999. DOI: 10.1029/1998GL900291.

B. Livneh, R. Kumar, and L. Samaniego. Influence of soil textural properties on hydrologic fluxes in the Mississippi river basin. *Hydrological Processes*, 29(21): 4638–4655, 2015. DOI: 10.1002/hyp.10601.

P. J. J. Luukko, J. Helske, and E. Räsänen. Introducing libeemd: a program package for performing the ensemble empirical mode decomposition. *Computational Statistics*, 31(2):545–557, 2016. DOI: 10.1007/s00180-015-0603-9.

U. Maniak. Einführung Hydrologie und Wasserwirtschaft. In U. Maniak, editor, *Hydrologie und Wasserwirtschaft: Eine Einführung für Ingenieure*, pages 1–19. Springer Berlin Heidelberg, Berlin, Heidelberg, 2016. ISBN 978-3-662-49087-7. DOI: 10.1007/978-3-662-49087-7_1.

H. B. Mann. Nonparametric Tests Against Trend. *Econometrica*, 13(3):245–259, 1945. DOI: 10.2307/1907187.

J. Mao and B. Yan. Global monthly mean leaf area index climatology, 1981-2015. *ORNL Distributed Active Archive Center*, 2019. DOI: 10.3334/ORNLDAAC/1653.

C. Marty. Regime shift of snow days in Switzerland. *Geophysical Research Letters*, 35(12):L12501, 2008. DOI: 10.1029/2008GL033998.

C. Marty and J. Blanchet. Long-term changes in annual maximum snow depth and snowfall in Switzerland based on extreme value statistics. *Climatic Change*, 111(3-4):705–721, 2012. DOI: 10.1007/s10584-011-0159-9.

C. Marty, S. Schlögl, M. Bavay, and M. Lehning. How much can we save? Impact of different emission scenarios on future snow cover in the Alps. *The Cryosphere*, 11(1):517–529, 2017. DOI: 10.5194/tc-11-517-2017.

A. Marx, R. Kumar, S. Thober, O. Rakovec, N. Wanders, M. Zink, E. F. Wood, M. Pan, J. Sheffield, and L. Samaniego. Climate change alters low flows in europe under global warming of 1.5, 2, and 3 °C. *Hydrology and Earth System Sciences*, 22(2):1017–1032, 2018. DOI: 10.5194/hess-22-1017-2018.

M. Matiu, A. Jacob, and C. Notarnicola. Daily MODIS snow cover maps for the European Alps from 2002 onwards at 250m horizontal resolution along with a nearly cloud-free version (version v1.0.2) [data set]. *Zenodo*, 2019. DOI: 10.5281/zenodo.3601891.

M. Matiu, A. Jacob, and C. Notarnicola. Daily MODIS Snow Cover Maps for the European Alps from 2002 onwards at 250 m Horizontal Resolution Along with a Nearly Cloud-Free Version. *Data*, 5(1):1, 2020. DOI: 10.3390/data5010001.

E. P. Maurer, I. T. Stewart, C. Bonfils, P. B. Duffy, and D. Cayan. Detection, attribution, and sensitivity of trends toward earlier streamflow in the sierra nevada. *Journal of Geophysical Research: Atmospheres*, 112(D11), 2007. DOI: 10.1029/2006JD008088.

R. McGill, J. W. Tukey, and W. A. Larsen. Variations of box plots. *The American Statistician*, 32(1):12–16, 1978. DOI: 10.2307/2683468.

P. J. McMurdie and S. Holmes. Shiny-phyloseq: Web application for interactive microbiome analysis with provenance tracking. *Bioinformatics*, 31(2):282–283, 2014. DOI: 10.1093/bioinformatics/btu616.

R. Mechler and J. Weichselgartner. Disaster loss financing in germany - the case of the elbe river floods 2002. IIASA interim report, IIASA, Laxenburg, Austria, 2003. URL http://pure.iiasa.ac.at/id/eprint/7060/. (last access: 09/02/2021).

G. A. Meehl and C. Tebaldi. More intense, more frequent, and longer lasting heat waves in the 21st century. *Science*, 305(5686):994–997, 2004. DOI: 10.1126/science.1098704.

T. Meile, J.-L. Boillat, and A. J. Schleiss. Hydropeaking indicators for characterization of the Upper-Rhone River in Switzerland. *Aquatic Sciences*, 73(1):171–182, 2011. DOI: 10.1007/s00027-010-0154-7.

L. Menzel, A. H. Thieken, D. Schwandt, and G. Bürger. Impact of climate change on the regional hydrology–scenario-based modelling studies in the german rhine catchment. *Natural Hazards*, 38(1-2):45–61, 2006. DOI: 0.1007/s11069-005-8599-z.

B. Merz, J. Hall, M. Disse, and A. Schumann. Fluvial flood risk management in a changing world. *Natural Hazards and Earth System Sciences*, 10(3):509–527, 2010. DOI: 10.5194/nhess-10-509-2010.

R. Merz and G. Blöschl. A process typology of regional floods. *Water Resources Research*, 39(12):1340, 2003. DOI: 10.1029/2002WR001952.

H. Middelkoop, K. Daamen, D. Gellens, W. Grabs, J. C. Kwadijk, H. Lang, B. W. Parmet, B. Schädler, J. Schulla, and K. Wilke. Impact of climate change on hydrological regimes and water resources management in the rhine basin. *Climatic change*, 49(1-2):105–128, 2001. DOI: 10.1023/A:1010784727448.

N. Mietkiewicz, D. Kulakowski, J. Rogan, and P. Bebi. Long-term change in sub-alpine forest cover, tree line and species composition in the Swiss Alps. *Journal of Vegetation Science*, 28(5):951–964, 2017. DOI: 10.1111/jvs.12561.

A. Moberg, P. D. Jones, D. Lister, A. Walther, M. Brunet, J. Jacobeit, L. V. Alexander, P. M. Della-Marta, J. Luterbacher, P. Yiou, D. Chen, A. M. G. K. Tank, O. Saladié, J. Sigró, E. Aguilar, H. Alexandersson, C. Almarza, I. Auer, M. Barriendos, M. Begert, H. Bergström, R. Böhm, C. J. Butler, J. Caesar, A. Drebs, D. Founda, F.-W. Gerstengarbe, G. Micela, M. Maugeri, H. Österle, K. Pandzic, M. Petrakis, L. Srnec, R. Tolasz, H. Tuomenvirta, P. C. Werner, H. Linderholm, A. Philipp, H. Wanner, and E. Xoplaki. Indices for daily temperature and precipitation extremes in Europe analyzed for the period 1901–2000. *Journal of Geophysical Research: Atmospheres*, 111(D22):D22106, 2006. DOI: 10.1029/2006JD007103.

D. Moghadas, W. Schaaf, W. Gerwin, A. Badorreck, and R. F. Hüttl. A web-based platform for terrestrial data repository from chicken creek catchment. *Earth Science Informatics*, 12(4):671–684, 2019. DOI: 10.1007/s12145-019-00385-0.

L. Mtilatila, A. Bronstert, P. Shrestha, P. Kadewere, and K. Vormoor. Susceptibility of water resources and hydropower production to climate change in the tropics: The case of lake malawi and shire river basins, se africa. *Hydrology*, 7(3), 2020. DOI: 10.3390/hydrology7030054.

R. Muelchi, O. Rössler, J. Schwanbeck, R. Weingartner, and O. Martius. Future runoff regime changes and their time of emergence for 93 catchments in

Switzerland. *Hydrology and Earth System Sciences Discussions*, 2020:1–25, 2020. DOI: 10.5194/hess-2020-516.

E. N. Mueller and A. Pfister. Increasing occurrence of high-intensity rainstorm events relevant for the generation of soil erosion in a temperate lowland region in Central Europe. *Journal of Hydrology*, 411(3):266–278, 2011. DOI: 10.1016/j.jhydrol.2011.10.005.

A. Murawski, S. Vorogushyn, G. Bürger, L. Gerlitz, and B. Merz. Do Changing Weather Types Explain Observed Climatic Trends in the Rhine Basin? An Analysis of Within- and Between-Type Changes. *Journal of Geophysical Research: Atmospheres*, 123(3):1562–1584, 2018. DOI: 10.1002/2017JD026654.

K. N. Musselman, J. W. Pomeroy, R. L. H. Essery, and N. Leroux. Impact of windflow calculations on simulations of alpine snow accumulation, redistribution and ablation. *Hydrological Processes*, 29(18):3983–3999, 2015. DOI: 10.1002/hyp.10595.

K. N. Musselman, M. P. Clark, C. Liu, K. Ikeda, and R. Rasmussen. Slower snowmelt in a warmer world. *Nature Climate Change*, 7(3):214–219, 2017. DOI: 10.1038/nclimate3225.

J. E. Nash and J. V. Sutcliffe. River flow forecasting through conceptual models part i — a discussion of principles. *Journal of Hydrology*, 10(3):282 – 290, 1970. DOI: 10.1016/0022-1694(70)90255-6.

J. R. Norris and M. Wild. Trends in aerosol radiative effects over Europe inferred from observed cloud cover, solar "dimming," and solar "brightening". *Journal of Geophysical Research: Atmospheres*, 112(D8):D08214, 2007. DOI: 10.1029/2006JD007794.

U. Ozturk, N. Marwan, O. Korup, H. Saito, A. Agarwal, M. J. Grossman, M. Zaiki, and J. Kurths. Complex networks for tracking extreme rainfall during typhoons. *Chaos: An Interdisciplinary Journal of Nonlinear Science*, 28(7):075301, 2018. DOI: 10.1063/1.5004480.

J. Parajka, N. Bezak, J. Burkhart, B. Hauksson, L. Holko, Y. Hundecha, M. Jenicek, P. Krajčí, W. Mangini, P. Molnar, P. Riboust, J. Rizzi, A. Sensoy, G. Thirel, and A. Viglione. Modis snowline elevation changes during snowmelt runoff events in europe. *Journal of Hydrology and Hydromechanics*, 67(1):101 – 109, 2019. DOI: 10.2478/johh-2018-0011.

K. M. Parding, A. Dobler, C. F. McSweeney, O. A. Landgren, R. Benestad, H. B. Erlandsen, A. Mezghani, H. Gregow, O. Räty, E. Viktor, J. El Zohbi, O. B. Christensen, and H. Loukos. Gcmeval – an interactive tool for evaluation and selection of climate model ensembles. *Climate Services*, 18:100167, 2020. DOI: 10.1016/j.cliser.2020.100167.

M. Pardé. Fleuves et rivières. *Armand Colin.Paris*, 1933.

D. Parker, C. Folland, A. Scaife, J. Knight, A. Colman, P. Baines, and B. Dong. Decadal to multidecadal variability and the climate change background. *Journal of Geophysical Research: Atmospheres*, 112(D18):D18115, 2007. DOI: 10.1029/2007JD008411.

V. Pavan, S. Tibaldi, and Č. Branković. Seasonal prediction of blocking frequency: Results from winter ensemble experiments. *Quarterly Journal of the Royal Meteorological Society*, 126(567):2125–2142, 2000. DOI: 10.1002/qj.49712656708.

P. Peduzzi, Q.-H. Dao, C. Herold, D. S. Rochette, and H. Sanahuja. Feasibility study report on global risk and vulnerability index–trends per year (GRAVITY). Technical report, United Nations Development Programme, 2001. URL https://archive-ouverte.unige.ch/unige:32337/ATTACHMENT01. (last access: 08/02/2021).

Y. Peings and G. Magnusdottir. Forcing of the wintertime atmospheric circulation by the multidecadal fluctuations of the North Atlantic ocean. *Environmental Research Letters*, 9(3):034018, 2014. DOI: 10.1088/1748-9326/9/3/034018.

T. Petrow and B. Merz. Trends in flood magnitude, frequency and seasonality in germany in the period 1951–2002. *Journal of Hydrology*, 371(1):129 – 141, 2009. DOI: 10.1016/j.jhydrol.2009.03.024.

C. Pfister, R. Weingartner, and J. Luterbacher. Hydrological winter droughts over the last 450 years in the Upper Rhine basin: a methodological approach. *Hydrological Sciences Journal*, 51(5):966–985, 2006. DOI: 10.1623/hysj.51.5.966.

L. Pfister, J. Kwadijk, A. Musy, A. Bronstert, and L. Hoffmann. Climate change, land use change and runoff prediction in the Rhine–Meuse basins. *River Research and Applications*, 20(3):229–241, 2004. DOI: 10.1002/rra.775.

R. Philipona, K. Behrens, and C. Ruckstuhl. How declining aerosols and rising greenhouse gases forced rapid warming in Europe since the 1980s. *Geophysical Research Letters*, 36(2), 2009. DOI: 10.1029/2008GL036350.

T. Pilz, T. Francke, G. Baroni, and A. Bronstert. How to tailor my process-based hydrological model? dynamic identifiability analysis of flexible model structures. *Water Resources Research*, 56(8):e2020WR028042, 2020. DOI: 10.1029/2020WR028042.

T. Pérez Ciria, D. Labat, and G. Chiogna. Detection and interpretation of recent and historical streamflow alterations caused by river damming and hydropower production in the Adige and Inn river basins using continuous, discrete and multiresolution wavelet analysis. *Journal of Hydrology*, 578:124021, 2019. DOI: 10.1016/j.jhydrol.2019.124021.

R Core Team. *R: A Language and Environment for Statistical Computing*. R Foundation for Statistical Computing, Vienna, Austria, 2019. URL https://www.R-project.org/. (last access: 09/02/2021).

V. Radić and R. Hock. Glaciers in the Earth's Hydrological Cycle: Assessments of Glacier Mass and Runoff Changes on Global and Regional Scales. *Surveys in Geophysics*, 35(3):813–837, 2014. DOI: 10.1007/s10712-013-9262-y.

O. Rakovec, R. Kumar, J. Mai, M. Cuntz, S. Thober, M. Zink, S. Attinger, D. Schäfer, M. Schrön, and L. Samaniego. Multiscale and multivariate evaluation of water fluxes and states over european river basins. *Journal of Hydrometeorology*, 17(1):287–307, 2016. DOI: 10.1175/JHM-D-15-0054.1.

R. Rojas, L. Feyen, A. Bianchi, and A. Dosio. Assessment of future flood hazard in europe using a large ensemble of bias-corrected regional climate simulations. *Journal of Geophysical Research: Atmospheres*, 117(D17), 2012. DOI: 10.1029/2012JD017461.

O. Rössler, P. Froidevaux, U. Börst, R. Rickli, O. Martius, and R. Weingartner. Retrospective analysis of a nonforecasted rain-on-snow flood in the Alps – a matter of model limitations or unpredictable nature? *Hydrology and Earth System Sciences*, 18(6):2265–2285, 2014. DOI: 10.5194/hess-18-2265-2014.

E. Rottler, T. Francke, G. Bürger, and A. Bronstert. Long-term changes in central European river discharge for 1869–2016: impact of changing snow covers, reservoir constructions and an intensified hydrological cycle. *Hydrology and Earth System Sciences*, 24(4):1721–1740, 2020. DOI: 10.5194/hess-24-1721-2020.

E. Rottler, C. Kormann, T. Francke, and A. Bronstert. Elevation-dependent warming in the Swiss Alps 1981–2017: Features, forcings and feedbacks. *International Journal of Climatology*, 39(5):2556–2568, 2019. DOI: 10.1002/joc.5970.

E. Rottler, K. Vormoor, T. Francke, M. Warscher, U. Strasser, and A. Bronstert. Elevation-dependent compensation effects in snowmelt in the Rhine River Basin upstream gauge basel. *Hydrology Research*, 2021. DOI: 10.2166/nh.2021.092.

M. Rousselot, Y. Durand, G. Giraud, L. Mérindol, I. Dombrowski-Etchevers, M. Déqué, and H. Castebrunet. Statistical adaptation of aladin rcm outputs over the french alps – application to future climate and snow cover. *The Cryosphere*, 6 (4):785–805, 2012. DOI: 10.5194/tc-6-785-2012.

C. Ruckstuhl and J. R. Norris. How do aerosol histories affect solar "dimming" and "brightening" over Europe?: IPCC-AR4 models versus observations. *Journal of Geophysical Research: Atmospheres*, 114(D10):D00D04, 2009. DOI: 10.1029/2008JD011066.

C. Ruckstuhl, R. Philipona, K. Behrens, M. C. Coen, B. Dürr, A. Heimo, C. Mätzler, S. Nyeki, A. Ohmura, L. Vuilleumier, M. Weller, C. Wehrli, and A. Zelenka. Aerosol and cloud effects on solar brightening and the recent rapid warming. *Geophysical Research Letters*, 35(12):L12708, 2008. DOI: 10.1029/2008GL034228.

Z. Samani. Estimating solar radiation and evapotranspiration using minimum climatological data. *Journal of Irrigation and Drainage Engineering*, 126(4):265–267, 2000. DOI: 10.1061/(ASCE)0733-9437(2000)126:4(265).

L. Samaniego, R. Kumar, S. Thober, O. Rakovec, M. Zink, N. Wanders, S. Eisner, H. Müller Schmied, E. H. Sutanudjaja, K. Warrach-Sagi, and S. Attinger. Toward seamless hydrologic predictions across spatial scales. *Hydrology and Earth System Sciences*, 21(9):4323–4346, 2017. DOI: 10.5194/hess-21-4323-2017.

L. Samaniego, S. Thober, R. Kumar, N. Wanders, O. Rakovec, M. Pan, M. Zink, J. Sheffield, E. F. Wood, and A. Marx. Anthropogenic warming exacerbates European soil moisture droughts. *Nature Climate Change*, 8(5):421, 2018a. DOI: 10.1038/s41558-018-0138-5.

L. Samaniego, R. Kumar, and S. Attinger. Multiscale parameter regionalization of a grid-based hydrologic model at the mesoscale. *Water Resources Research*, 46(5), 2010. DOI: 10.1029/2008WR007327.

L. Samaniego, R. Kumar, S. Thober, O. Rakovec, R. Schweppe, D. Schäfer, M. Schrön, J. Brenner, C. M. Demirel, M. Kaluza, M. Jing, B. Langenberg, and S. Attinger. mesoscale Hydrologic Model [software]. *Zenodo*, 2018b. DOI: 10.5281/zenodo.1299584.

L. Samaniego, S. Thober, N. Wanders, M. Pan, O. Rakovec, J. Sheffield, E. F. Wood, C. Prudhomme, G. Rees, H. Houghton-Carr, M. Fry, K. Smith, G. Watts, H. Hisdal, T. Estrela, C. Buontempo, A. Marx, and R. Kumar. Hydrological forecasts and projections for improved decision-making in the water sector in europe. *Bulletin of the American Meteorological Society*, 100(12):2451–2471, 2019. DOI: 10.1175/BAMS-D-17-0274.1.

M. Savina, B. Schäppi, P. Molnar, P. Burlando, and B. Sevruk. Comparison of a tipping-bucket and electronic weighing precipitation gage for snowfall. *Atmospheric Research*, 103:45 – 51, 2012. DOI: 10.1016/j.atmosres.2011.06.010.

B. Schädler and R. Weingartner. Impact of Climate Change on Water Resources in the Alpine Regions of Switzerland. In U. Bundi, editor, *Alpine Waters*, The Handbook of Environmental Chemistry, pages 59–69. Springer Berlin Heidelberg, Berlin, Heidelberg, 2010. ISBN 978-3-540-88275-6. DOI: 10.1007/978-3-540-88275-6_3.

H. Scheifinger, A. Menzel, E. Koch, and C. Peter. Trends of spring time frost events and phenological dates in Central Europe. *Theoretical and Applied Climatology*, 74(1):41–51, 2003. DOI: 10.1007/s00704-002-0704-6.

S. C. Scherrer and C. Appenzeller. Swiss Alpine snow pack variability: major patterns and links to local climate and large-scale flow. *Climate Research*, 32(3): 187–199, 2006. DOI: 10.3354/cr032187.

S. C. Scherrer, C. Appenzeller, and M. Laternser. Trends in Swiss Alpine snow days: The role of local- and large-scale climate variability. *Geophysical Research Letters*, 31(13):L13215, 2004. DOI: 10.1029/2004GL020255.

S. C. Scherrer, M. Croci-Maspoli, C. Schwierz, and C. Appenzeller. Two-dimensional indices of atmospheric blocking and their statistical relationship with winter climate patterns in the Euro-Atlantic region. *International Journal of Climatology*, 26(2):233–249, 2006. DOI: 10.1002/joc.1250.

S. C. Scherrer, M. Begert, M. Croci-Maspoli, and C. Appenzeller. Long series of Swiss seasonal precipitation: regionalization, trends and influence of large-scale flow. *International Journal of Climatology*, 36(11):3673–3689, 2016. DOI: 10.1002/joc.4584.

J. Schmidli and C. Frei. Trends of heavy precipitation and wet and dry spells in Switzerland during the 20th century. *International Journal of Climatology*, 25(6): 753–771, 2005. DOI: 10.1002/joc.1179.

P. Schmocker-Fackel and F. Naef. Changes in flood frequencies in Switzerland since 1500. *Hydrology and Earth System Sciences*, 14(8):1581–1594, 2010. DOI: 10.5194/hess-14-1581-2010.

E. Schmucki, C. Marty, C. Fierz, and M. Lehning. Simulations of 21st century snow response to climate change in switzerland from a set of rcms. *International Journal of Climatology*, 35(11):3262–3273, 2015. DOI: 10.1002/joc.4205.

S. Schneiderbauer and D. Ehrlich. Risk, hazard and people's vulnerability to natural hazards: a review of definitions, concepts and data. Technical report EUR 21410 EN, European Commission Joint Research Centre, 2004.

C.-D. Schönwiese and J. Rapp. *Climate trend atlas of Europe based on observations 1891–1990*. Springer Science & Business Media, Dordrecht, Netherlands, 1997. DOI: 10.1007/978-94-015-8818-8.

L. Schoppa, T. Sieg, K. Vogel, G. Zöller, and H. Kreibich. Probabilistic flood loss models for companies. *Water Resources Research*, 56(9):e2020WR027649, 2020. DOI: 10.1029/2020WR027649.

E. A. G. Schuur, A. D. McGuire, C. Schädel, G. Grosse, J. W. Harden, D. J. Hayes, G. Hugelius, C. D. Koven, P. Kuhry, D. M. Lawrence, et al. Climate change and the permafrost carbon feedback. *Nature*, 520(7546):171–179, 2015. DOI: 10.1038/nature14338.

M. Schwartz, A. Hall, F. Sun, D. Walton, and N. Berg. Significant and Inevitable End-of-Twenty-First-Century Advances in Surface Runoff Timing in California's Sierra Nevada. *Journal of Hydrometeorology*, 18(12):3181–3197, 2017. DOI: 10.1175/JHM-D-16-0257.1.

P. K. Sen. Estimates of the Regression Coefficient Based on Kendall's Tau. *Journal of the American Statistical Association*, 63(324):1379–1389, 1968. DOI: 10.1080/01621459.1968.10480934.

M. C. Serreze, J. E. Walsh, F. S. Chapin, T. Osterkamp, M. Dyurgerov, V. Romanovsky, W. C. Oechel, J. Morison, T. Zhang, and R. G. Barry. Observational evidence of recent change in the northern high-latitude environment. *Climatic change*, 46(1-2):159–207, 2000. DOI: 10.1023/A:1005504031923.

T. Sieg, K. Vogel, B. Merz, and H. Kreibich. Seamless estimation of hydrometeorological risk across spatial scales. *Earth's Future*, 7(5):574–581, 2019. DOI: 10.1029/2018EF001122.

G. Simpkins. Snow-related water woes. *Nature Climate Change*, 8(11):945, 2018. DOI: 10.1038/s41558-018-0330-7.

A. Skålevåg and K. Vormoor. Daily streamflow trends in western vs. eastern Norway and their attribution to hydro-meteorological drivers. *Authorea Preprints*, 2021. DOI: 10.22541/au.161319077.75813136/v1.

L. J. Slater, G. Thirel, S. Harrigan, O. Delaigue, A. Hurley, A. Khouakhi, I. Prosdocimi, C. Vitolo, and K. Smith. Using r in hydrology: a review of recent developments and future directions. *Hydrology and Earth System Sciences*, 23(7): 2939–2963, 2019. DOI: 10.5194/hess-23-2939-2019.

H. Sodemann and E. Zubler. Seasonal and inter-annual variability of the moisture sources for Alpine precipitation during 1995–2002. *International Journal of Climatology*, 30(7):947–961, 2010. DOI: 10.1002/joc.1932.

S. Sorooshian, Q. Duan, and V. K. Gupta. Calibration of rainfall-runoff models: Application of global optimization to the sacramento soil moisture accounting model. *Water Resources Research*, 29(4):1185–1194, 1993. DOI: 10.1029/92WR02617.

M. J. R. Speich, L. Bernhard, A. J. Teuling, and M. Zappa. Application of bivariate mapping for hydrological classification and analysis of temporal change and scale effects in switzerland. *Journal of Hydrology*, 523:804 – 821, 2015. DOI: 10.1016/j.jhydrol.2015.01.086.

M. Spreafico and R. Weingartner. *The Hydrology of Switzerland - Selected aspects and results*. Water Series no. 7. FOWG Reports, Berne, 2005. URL https://www.bafu.admin.ch/dam/bafu/en/dokumente/hydrologie/uw-umwelt-wissen/hydrologie_der_schweizausgewaehlteaspekteundresultate.pdf.download.pdf/the_hydrology_inswitzerlandselectedaspectsandresults.pdf. (last access: 09/02/2021).

K. Stahl, M. Weiler, I. Kohn, D. Freudiger, J. Seibert, M. Vis, K. Gerlinger, and M. Böhm. The snow and glacier melt components of streamflow of the river Rhine and its tributaries considering the influence of climate change. Synthesis report I-25, International Commission for the Hydrology of the Rhine Basin, Lelystad, Netherlands, 2016. URL https://chr-khr.org/en/file/1057/download?token=Zg6SY04i. (last access: 08/02/2020).

C. Steger, S. Kotlarski, T. Jonas, and C. Schär. Alpine snow cover in a changing climate: a regional climate model perspective. *Climate dynamics*, 41(3-4):735–754, 2013. DOI: 10.1007/s00382-012-1545-3.

O. Stein. The variability of Atlantic–European blocking as derived from long SLP time series. *Tellus A*, 52(3):225–236, 2000. DOI: 10.3402/tellusa.v52i3.12263.

I. T. Stewart. Changes in snowpack and snowmelt runoff for key mountain regions. *Hydrological Processes*, 23(1):78–94, 2009. DOI: 10.1002/hyp.7128.

I. T. Stewart, D. R. Cayan, and M. D. Dettinger. Changes in snowmelt runoff timing in western north america under a business as usual'climate change scenario. *Climatic Change*, 62(1-3):217–232, 2004. DOI: 10.1023/B:CLIM.0000013702.22656.e8.

I. T. Stewart, D. R. Cayan, and M. D. Dettinger. Changes toward Earlier Streamflow Timing across Western North America. *Journal of Climate*, 18(8):1136–1155, 2005. DOI: 10.1175/JCLI3321.1.

E. Strandhagen, W. A. Marcus, and J. E. Meacham. *Views of the rivers: representing streamflow of the greater Yellowstone ecosystem*. Cartographic perspectives, no. 55, fall, University of Oregon, 2006. URL http://geography.uoregon.edu/amarcus/Publications/Strandhagen-et-al_2006_Cart_Pers.pdf. (last access: 09/02/2021).

J. Sui and G. Koehler. Rain-on-snow induced flood events in Southern Germany. *Journal of Hydrology*, 252(1):205–220, 2001. DOI: 10.1016/S0022-1694(01)00460-7.

K. E. Taylor, R. J. Stouffer, and G. A. Meehl. An overview of cmip5 and the experiment design. *Bulletin of the American Meteorological Society*, 93(4):485 – 498, 2012. DOI: 10.1175/BAMS-D-11-00094.1.

H. Theil. A rank-invariant method of linear and polynomial regression analysis. *Proceedings of the National Academy of Sciences*, 53:Part I: 386–392, Part II: 521–525, Part III: 1397–1412, 1950.

A. H. Thieken, T. Bessel, S. Kienzler, H. Kreibich, M. Müller, S. Pisi, and K. Schröter. The flood of june 2013 in germany: how much do we know about its impacts? *Natural Hazards and Earth System Sciences*, 16(6):1519–1540, 2016. DOI: 10.5194/nhess-16-1519-2016.

S. Thober, M. Cuntz, M. Kelbling, R. Kumar, J. Mai, and L. Samaniego. The multiscale routing model mrm v1.0: simple river routing at resolutions from 1 to 50 km. *Geoscientific Model Development*, 12(6):2501–2521, 2019. DOI: 10.5194/gmd-12-2501-2019.

S. Thober, R. Kumar, N. Wanders, A. Marx, M. Pan, O. Rakovec, L. Samaniego, J. Sheffield, E. F. Wood, and M. Zink. Multi-model ensemble projections of european river floods and high flows at 1.5, 2, and 3 degrees global warming. *Environmental Research Letters*, 13(1):014003, 2018. DOI: 10.1088/1748-9326/aa9e35.

B. A. Tolson and C. A. Shoemaker. Dynamically dimensioned search algorithm for computationally efficient watershed model calibration. *Water Resources Research*, 43(1), 2007. DOI: 10.1029/2005WR004723.

M. E. Torres, M. A. Colominas, G. Schlotthauer, and P. Flandrin. A complete ensemble empirical mode decomposition with adaptive noise. In *2011 IEEE International Conference on Acoustics, Speech and Signal Processing (ICASSP)*, pages 4144–4147, Prague, Czech Republic, 2011. IEEE. ISBN 978-1-4577-0538-0. DOI: 10.1109/ICASSP.2011.5947265.

B. Truffer, J. Markard, C. Bratrich, and B. Wehrli. Green Electricity from Alpine Hydropower Plants. *Mountain Research and Development*, 21(1):19–25, 2001. ISSN 0276-4741, 1994-7151. DOI: 10.1659/0276-4741(2001)021[0019:GEFAHP]2.0.CO;2.

U. Ulbrich and A. Fink. The January 1995 flood in Germany: Meteorological versus hydrological causes. *Physics and Chemistry of the Earth*, 20(5):439 – 444, 1995. DOI: 10.1016/S0079-1946(96)00002-X.

U. Ulbrich, T. Brücher, A. H. Fink, G. C. Leckebusch, A. Krüger, and J. G. Pinto. The central European floods of August 2002: Part 1 – rainfall periods and flood development. *Weather*, 58(10):371–377, 2003. DOI: 10.1256/wea.61.03A.

J. Ulrich, O. E. Jurado, M. Peter, M. Scheibel, and H. W. Rust. Estimating IDF curves consistently over durations with spatial covariates. *Water*, 12(11), 2020. DOI: 10.3390/w12113119.

UNDRR. Global assessment report on disaster risk reduction 2019. Assessment report, United Nations Office for Disaster Risk Reduction, Geneva, Switzerland, 2019. URL https://www.undrr.org/publication/global-assessment-report-disaster-risk-reduction-2019. (last access: 09/02/2021).

R. Vautard, A. Gobiet, S. Sobolowski, E. Kjellström, A. Stegehuis, P. Watkiss, T. Mendlik, O. Landgren, G. Nikulin, C. Teichmann, and D. Jacob. The european climate under a 2 °C global warming. *Environmental Research Letters*, 9(3):034006, 2014. DOI: 10.1088/1748-9326/9/3/034006.

G. Veh, O. Korup, S. Roessner, and A. Walz. Detecting himalayan glacial lake outburst floods from landsat time series. *Remote Sensing of Environment*, 207:84 – 97, 2018. DOI: 10.1016/j.rse.2017.12.025.

G. Veh, O. Korup, S. Specht, S. Roessner, and A. Walz. Unchanged frequency of moraine-dammed glacial lake outburst floods in the himalaya. *Nature Climate Change*, 9:379–383, 2019. DOI: 10.1038/s41558-019-0437-5.

M. Verbunt, M. G. Zwaaftink, and J. Gurtz. The hydrologic impact of land cover changes and hydropower stations in the Alpine Rhine basin. *Ecological Modelling*, 187(1):71–84, 2005. DOI: 10.1016/j.ecolmodel.2005.01.027.

G. Villarini and J. A. Smith. Flood peak distributions for the eastern United States. *Water Resources Research*, 46(6), 2010. DOI: 10.1029/2009WR008395.

L. A. Vincent, X. Zhang, B. R. Bonsal, and W. D. Hogg. Homogenization of Daily Temperatures over Canada. *Journal of Climate*, 15(11):1322–1334, 2002. DOI: 10.1175/1520-0442(2002)015<1322:HODTOC>2.0.CO;2.

D. Viviroli, D. R. Archer, W. Buytaert, H. J. Fowler, G. B. Greenwood, A. F. Hamlet, Y. Huang, G. Koboltschnig, M. I. Litaor, J. I. López-Moreno, S. Lorentz, B. Schädler, H. Schreier, K. Schwaiger, M. Vuille, and R. Woods. Climate change and mountain water resources: overview and recommendations for research, management and policy. *Hydrology and Earth System Sciences*, 15(2):471–504, 2011. DOI: 10.5194/hess-15-471-2011.

D. Viviroli, H. H. Dürr, B. Messerli, M. Meybeck, and R. Weingartner. Mountains of the world, water towers for humanity: Typology, mapping, and global significance. *Water Resources Research*, 43(7), 2007. DOI: 10.1029/2006WR005653.

K. Vormoor, D. Lawrence, M. Heistermann, and A. Bronstert. Climate change impacts on the seasonality and generation processes of floods: projections and uncertainties for catchments with mixed snowmelt/rainfall regimes. *Hydrology and Earth System Sciences*, 19(2):913–931, 2015. DOI: 10.5194/hess-19-913-2015.

K. Vormoor, D. Lawrence, L. Schlichting, D. Wilson, and W. K. Wong. Evidence for changes in the magnitude and frequency of observed rainfall vs. snowmelt driven floods in norway. *Journal of Hydrology*, 538:33 – 48, 2016. DOI: 10.1016/j.jhydrol.2016.03.066.

B. Wagner, C. Hauer, A. Schoder, and H. Habersack. A review of hydropower in Austria: Past, present and future development. *Renewable and Sustainable Energy Reviews*, 50:304–314, 2015. DOI: 10.1016/j.rser.2015.04.169.

G.-R. Walther, S. Beißner, and C. A. Burga. Trends in the upward shift of alpine plants. *Journal of Vegetation Science*, 16(5):541–548, 2005. DOI: 10.1111/j.1654-1103.2005.tb02394.x.

M. Warscher, U. Strasser, G. Kraller, T. Marke, H. Franz, and H. Kunstmann. Performance of complex snow cover descriptions in a distributed hydrological model system: A case study for the high alpine terrain of the berchtesgaden alps. *Water Resources Research*, 49(5):2619–2637, 2013. DOI: 10.1002/wrcr.20219.

L. Warszawski, K. Frieler, V. Huber, F. Piontek, O. Serdeczny, and J. Schewe. The inter-sectoral impact model intercomparison project (isi–mip): Project framework. *Proceedings of the National Academy of Sciences*, 111(9):3228–3232, 2014. DOI: 10.1073/pnas.1312330110.

R. Weingartner and H. Aschwanden. Abflussregimes als grundlage zur abschätzung von mittelwerten des abflusses. *Hydrologischer Atlas der Schweiz – Tafel 5.2, Federal Office for the Environment, Bern*, 1992. URL https://hydrologischeratlas.ch/downloads/01/content/Tafel_52.pdf. (last access: 09/02/2021).

D. Wendi, B. Merz, and N. Marwan. Assessing hydrograph similarity and rare runoff dynamics by cross recurrence plots. *Water Resources Research*, 55(6): 4704–4726, 2019. DOI: 10.1029/2018WR024111.

J. Wesemann, H. Holzmann, K. Schulz, and M. Herrnegger. Behandlung künstlicher Speicher und Überleitungen in der alpinen Niederschlags-Abfluss-Vorhersage. *Österreichische Wasser- und Abfallwirtschaft*, 70(9-10):485–496, 2018. DOI: 10.1007/s00506-018-0501-9.

O. Wetter, C. Pfister, R. Weingartner, J. Luterbacher, T. Reist, and J. Trösch. The largest floods in the High Rhine basin since 1268 assessed from documentary and instrumental evidence. *Hydrological Sciences Journal*, 56(5):733–758, 2011. DOI: 10.1080/02626667.2011.583613.

T. Weusthoff. Weather Type Classification at MeteoSwiss - Introduction of new automatic classification schemes. Arbeitsbericht MeteoSchweiz Nr. 235, Bundesamt für Meteorologie und Klimatologie MeteoSchweiz, Zurich, 2011. URL https://www.meteoschweiz.admin.ch/content/dam/meteoswiss/en/Ungebundene-Seiten/Publikationen/Fachberichte/doc/ab235.pdf. (last access: 09/02/2021).

P. H. Whitfield. Is 'centre of volume' a robust indicator of changes in snowmelt timing? *Hydrological Processes*, 27(18):2691–2698, 2013. DOI: 10.1002/hyp.9817.

L.-M. Wielke, L. Haimberger, and M. Hantel. Snow cover duration in Switzerland compared to Austria. *Meteorologische Zeitschrift*, pages 13–17, 2004. DOI: 10.1127/0941-2948/2004/0013-0013.

M. Wild, A. Ohmura, and K. Makowski. Impact of global dimming and brightening on global warming. *Geophysical Research Letters*, 34(4):L04702, 2007. DOI: 10.1029/2006GL028031.

E. Wildenhahn and U. Klaholz. Große Speicherseen im Einzugsgebiet des Rheins. Technical Report Bericht Nr. II-10, Internationale Kommission fur die Hydrologie des Rheingebietes (KHR), Koblenz, 1996. URL https://www.chr-khr.org/de/veroffentlichung/grosse-speicherseen-im-einzugsgebiet-des-rheins?position=16&list=acQNUZbSQEZRiCQcJ8XBIECvRNv2_T0jZhOmtoN8l5A. (last access: 09/02/2021).

W. Wildi, J. Dominik, J.-L. Loizeau, R. L. Thomas, P.-Y. Favarger, L. Haller, A. Perroud, and C. Peytremann. River, reservoir and lake sediment contamination by heavy metals d downstream from urban areas of Switzerland. *Lakes & Reservoirs: Science, Policy and Management for Sustainable Use*, 9(1):75–87, 2004. DOI: 10.1111/j.1440-1770.2004.00236.x.

E. Wirth. Die Großschiffahrtsstraße Rhein-Main-Donau. Ein Weg für Südosteuropa? - Kritische Bestandsaufnahme und Zukunftsperspektiven. *Mitteilungen der Fränkischen Geographischen Gesellschaft Bd. 42, Erlangen-Nürnberg*, pages 33–102, 1995.

M. Wolf. Hochwasser im mittleren neckarraum - charakterisierung unter berücksichtigungregionaler klimaszenariensowie dessen wahrnehmungdurch befragte anwohner. PIK Report 87, Potsdam Institute for Climate Impact Research, Potsdam, Germany, 2003. URL https://www.pik-potsdam.de/en/output/publications/pikreports/.files/pr87.pdf. (last access: 09/02/2021).

Word Commision on Dams. *Dams and Development: A New Framework for Decision-Making : The Report of the World Commission on Dams*. Earthscan, London, 2000. ISBN 978-1-85383-798-2.

X. Wu, T. Che, X. Li, N. Wang, and X. Yang. Slower Snowmelt in Spring Along With Climate Warming Across the Northern Hemisphere. *Geophysical Research Letters*, 45(22):12,331–12,339, 2018. DOI: 10.1029/2018GL079511.

Z. Wu, N. E. Huang, S. R. Long, and C.-K. Peng. On the trend, detrending, and variability of nonlinear and nonstationary time series. *Proceedings of the National Academy of Sciences*, 104(38):14889–14894, 2007. DOI: 10.1073/pnas.0701020104.

Z. Wu and N. E. Huang. Ensemble Empirical Mode Decomposition: A noise-assisted data analysis method. *Advances in Adaptive Data Analysis*, 01(01):1–41, 2009. DOI: 10.1142/S1793536909000047.

M. Zambrano-Bigiarini. *hydroGOF: Goodness-of-fit functions for comparison of simulated and observed hydrological time series*, 2017. URL http://hzambran.github.io/hydroGOF/. (last access: 09/02/2021).

M. Zemp, W. Haeberli, M. Hoelzle, and F. Paul. Alpine glaciers to disappear within decades? *Geophysical Research Letters*, 33(13), 2006. DOI: 10.1029/2006GL026319.

M. Zink, L. Samaniego, R. Kumar, S. Thober, J. Mai, D. Schäfer, and A. Marx. The german drought monitor. *Environmental Research Letters*, 11(7):074002, 2016. DOI: 10.1088/1748-9326/11/7/074002.

M. Zink, R. Kumar, M. Cuntz, and L. Samaniego. A high-resolution dataset of water fluxes and states for Germany accounting for parametric uncertainty. *Hydrology and Earth System Sciences*, 21(3):1769–1790, 2017. DOI: 10.5194/hess-21-1769-2017.

E. M. Zubler, S. C. Scherrer, M. Croci-Maspoli, M. A. Liniger, and C. Appenzeller. Key climate indices in Switzerland; expected changes in a future climate. *Climatic Change*, 123(2):255–271, 2014. DOI: 10.1007/s10584-013-1041-8.